2009

Hydrodynamic response to cold fronts along the Louisiana coast

Zhixuan Feng
Louisiana State University and Agricultural and Mechanical College

HYDRODYNAMIC RESPONSE TO COLD FRONTS ALONG THE LOUISIANA COAST

A Thesis

Submitted to the Graduate Faculty of the
Louisiana State University and
Agricultural and Mechanical College
in partial fulfillment of the
requirements for the degree of
Master of Science

in

The Department of Oceanography and Coastal Sciences

by
Zhixuan Feng
B.S., Nanjing University, 2007
August, 2009

ACKNOWLEDGEMENTS

I wish to express my sincere gratitude to my major advisor, Dr. Chunyan Li, for his encouragement, guidance and support during my graduate study and thesis research. I would also like to thank my committee members, Drs. Nan D. Walker and Kam-Biu Liu for their comments and suggestions. I want to acknowledge Dr. Gregory W. Stone and Yixin Luo for the access of WAVCIS data. Additional thanks to Brenda Babin and Holly Hebert at LUMCON for sharing water level data, Quan Tang and Yuliang Chen for their technical support in ArcGIS, and Joao L. Rego and Felix Jose for their help in my thesis writing and defense. Finally, I wish to recognize my mother, who is always supporting me throughout my study and life abroad.

TABLE OF CONTENTS

LIST OF SYMBOLS

ω Angular velocity

Θ Initial phase

τ Wind stress

τ_x Cross-shore wind stress

τ_y Alongshore wind stress

i Imaginary unit

t Time

x Distance to the mouth of the estuary

l Length of the estuary

b Width of the estuary

η Subtidal sea level

E Cross-shelf component of the Ekman flux

α Remote wind coefficient

f Coriolis parameter

u Subtidal current velocity in the along-estuary direction

g Gravitational acceleration

$\tau_b^{(x)}$ Bottom friction in the along-estuary direction

ρ Sea water density

h Constant water depth of the estuary

C_D Bottom drag coefficient

u_T Root mean squared subtidal current velocity

U Dimensionless subtidal velocity

T Dimensionless time

H Dimensionless subtidal sea level

X Dimensionless distance to the mouth of the estuary

λ Dimensionless bottom friction parameter

W Dimensionless local wind parameter

c Long wave phase speed

σ Standard deviation of the subtidal sea level variation

A(0) Scaled sea level amplitude at the mouth of the estuary

L Scaled length of the estuary

K Complex wave number

ABSTRACT

Cold fronts play important roles in flushing water out of the Louisiana estuaries. This study is aimed at examining the impact of cold front passages on the hydrodynamics in autumn-winter-spring of 2006-2007, and tries to determine the geographic difference, correlation and relative importance of winds, tides, and river discharge on water level variability and flow field.

The amplitude spectra of water level reveal that diurnal tides dominate most stations. Areas west of 91°W have relatively high semidiurnal tides. The subtidal fluctuations are mainly wind-driven. Only the station in the Atchafalaya River shows obvious response to the spring flood of the Mississippi/Atchafalaya Rivers.

Coastal bays have different water exchange rates depending on their water body area and geomorphology. Five largest flushing events correspond to migrating extratropical cyclones with frontal orientation perpendicular to the coastline, suggesting that wind direction is one of the controlling factors in the flushing rate and total transport. Both alongshore and cross-shore winds may effectively induce bay-shelf exchange. Northwest/north winds appear to be the most effective wind forcing in driving water movement from bay to shelf. Strong cold fronts may flush more than 40% of the bay waters onto the shelf within a period less than 40 hours.

The near-surface current on the Louisiana inner shelf is mainly wind-driven, but tidal forcing becomes more important in the sub-surface layers or in the vicinity of the coastline of shallow waters. A prevailing down-coast flow occurs 81% and 70% of the time at CSI-6 and CSI-3, respectively. Strong cold front events may disturb this down-coast flow system by inducing a 1- to 3-day up-coast flow. At CSI-6, the Mississippi river discharge has little influence in non-flood seasons. During the period of spring flood, however, the large amount of freshwater exerts significant barotropic and baroclinic forcings on the current field and reinforces the down-coast flow.

The analytical model reveals that the amplitudes of water level variations induced by alongshore and cross-shore wind forcings have the same order of magnitude (i.e., 10^{-1} m), indicating that they play almost equally important roles in driving the subtidal water level variability inside the bays.

CHAPTER 1 INTRODUCTION

1.1 Background

The Louisiana coastal zone, including the lower deltaic plain, wetlands, estuaries, bays, barrier islands and inner continental shelf, contains 40% of the U.S. coastal and estuarine wetlands (Craig et al., 1979; Penland, et al, 1990; Stone et al., 1997a). It serves as an important renewable natural resource with an estimated annual value of more than $1 billion (Williams, et al., 1997). However, these systems are suffering 80% of the nation's coastal erosion and wetland loss due to the combined effects of natural processes and anthropogenic activities (Craig, et al., 1979; Penland, et al, 1990). The coastal wetlands and adjacent shelf, supplied by a large amount of sediments and nutrients from the Mississippi and Atchafalaya Rivers, form a complex and productive marine ecosystem, which support abundant and diverse living resources with annual fishery landings of more than 1 billion pounds (Chesney, et al., 2000). Nevertheless, all kinds of coastal developments have been carried out on this ecosystem over the last few decades, which have induced some ecological problems (Chesney, et al., 2000). The world's second largest zone of coastal hypoxia (oxygen-depleted bottom waters, which are defined as dissolved oxygen levels less than 2 mg/L) is located on the Louisiana-Texas continental shelf of the northern Gulf of Mexico, referred to as the "Dead Zone" (Rabalais, et al, 2001; Rabalais, et al, 2002). Although located in a relatively low wave and tidal energy environment in the northern Gulf of Mexico, the erosional and depositional trends of the low-lying Louisiana deltaic plain are strongly influenced by various coastal processes, of which the subsidence and combined impacts of occasional tropical cyclones and frequent winter-spring cold fronts are most significant (Georgiou, et al., 2005).

A cold front is the interface or transition zone (25-250 km) between heterogeneous air masses

where colder, drier and denser air is advancing towards warmer, moister and lighter air (Grenci and Nese, 2006; Hsu, 1988). Cold front passages are the dominant local weather patterns, with a 3- to 7-day cycle, along the Gulf coast of the United States between October and April (Chuang and Wiseman, 1983; Hsu, 1988). In the literature, weather systems related to strong cold fronts are also called winter storms, extratropical storms, or extratropical cyclones (Walker and Hammack, 2000; Pepper and Stone, 2002; Keen, 2002). Compared with occasional but more violent tropical cyclones, the lower energy but more frequent cold fronts appear to drive greater cumulative coastal changes (Roberts, et al., 1987; Moeller, et al., 1993). Numerous meteorological and oceanic phenomena are associated with cold front passages, such as wind and current veering, significant temperature and humidity decrease, sediment resuspension and transport, and water level variation (Mossa and Roberts, 1990; Walker and Hammack, 2000; Walker et al., 2005a; Li et al., 2009). The impacts of cold fronts on Louisiana coastal environments are considered very important and they are thus widely studied (e.g. Roberts, 1987; Reed, 1989; Moeller, et al., 1993; Perez, et al., 2000; Walker and Hammack, 2000; Kineke et al., 2006). The intensities of the pressure system, the speed of advance, and frontal orientation relative to the coastline, all exhibit controls on coastal processes (Roberts, et al., 1987). In situ observations and measurements, coupled with numerical models and remote sensing, provide essential and powerful methods and tools for studying, predicting and managing coastal environments. High-resolution data sets, including bathymetric and topographic surveys, hydrodynamic and sediment measurements, satellite imagery, and aerial photographs, during and after high-energy events, have been used in recent research of cold-front related coastal processes (e.g. List et al., 1997; Walker and Hammack, 2000; Walker, 2001a; Stone and Orford, 2004; Pepper and Stone, 2004; Draut et al., 2005).

1.2 Motivation

Louisiana is experiencing severe wetland loss and deterioration and associated ecological problems (Williams et al., 1997; Barras, et al., 2003; Barras, et al., 2004). For wetland restoration, barrier island protection and coastal management, it is essential and critical to understand how meteorological conditions, hydrodynamic processes, and sediment and nutrient transport are functioning and interacting with each other in such a coastal setting with unique coastal hydrological, geomorphologic, and biological features.

1.3 Objectives

The goal of this study is to use in situ observational data and synoptic weather maps from September 2006 to April 2007, as well as an analytical model, to obtain a better understanding of coastal circulation associated with cold front passages along the Louisiana coast and the primary forcing processes and mechanisms on the inner shelf, and in bays, estuaries and bayous. The primary objectives of this study are:

1. To determine the hydrodynamic responses to different types of cold fronts with respect to coastline orientation, focusing on the relationship between water level, current and winds.

2. To determine the geographic differences, correlations, and time lags of hydrodynamic responses to cold fronts in different bays and estuaries along the Louisiana coast.

3. To determine the relative importance of cross-shore and alongshore wind effects in driving subtidal sea level variability and current fluctuations in the Louisiana estuaries.

1.4 Organization of Thesis

Chapter 1 presents the background information, motivation and objectives of this study. In chapter 2, past research related to the Louisiana coastal environments is reviewed, including the Mississippi and Atchafalaya watershed, evolution of the Mississippi deltaic plain, general circulation over the Louisiana-Texas continental shelf, barrier islands, bays and wetlands. A

thorough literature review is also conducted on the responses of coastal environments to cold front passages, focusing on the meteorological characteristics of cold fronts, air-sea interactions, cold-front-related sea level variations, geomorphic changes, larval transport and recruitment, and river plume variability. I address two important techniques (i.e., numerical modeling and remote sensing) and some of their applications to the Louisiana coast. Finally, I emphasize some important studies (most are conducted along the middle Atlantic coast of the United States), which provide insights on the processes and mechanisms of wind-induced barotropic estuarine circulation. Chapter 3 describes all data sets and methods used in this study.

In chapter 4, the characteristics of all cold front events impacting the study area between September 2006 and April 2007 are examined. Then, water level data from stations across the coast are analyzed to determine the geographic correlations and differences and relative importance of different forcings on water level variability. Furthermore, the cold-front-induced estuary-shelf volume exchange for three major Louisiana bay systems are quantified and the five largest flushing events are also isolated for more in-depth investigation. In the final part of this chapter, wind data are complied to plot monthly wind roses, providing frequencies of occurrence of the eight principle winds. Time-series ADCP data are also analyzed to depict the eight-month synoptic characteristics of flow field on the Louisiana inner shelf. Then, rotary spectra of winds and currents are calculated and compared to determine the relationships between wind forcing and current variability at different geographic locations and vertical depths in the water column. By combining the wind and current data with daily mean Mississippi and Atchafalaya River discharge data, five one-month periods are selected as case studies to examine and compare the responses of the flow field to cold front passages within different river discharge regimes.

In chapter 5, a one-dimensional analytical model, modified from Garvine's paper (1985), is applied to examine the relative importance of cross-shore and alongshore winds on the subtidal

water level variability of the Louisiana estuaries. Chapter 6 summarizes all important findings and conclusions in this study.

CHAPTER 2 LITERATURE REVIEW

2.1 The Mississippi and Atchafalaya River Basin and Delta

The Mississippi and Atchafalaya River is one of the world's largest rivers, discharging the largest amount of sediment into the Gulf of Mexico in the conterminous United States. It also has a drainage basin of approximately 3.27×10^6 km^2, and average water and sediment discharge of 580 km^3/yr and 210×10^6 t/yr, respectively (Milliman and Meade, 1983). More than half of the present Mississippi River basin is cropland, within which a large amount of fertilizers and pesticides are applied by intensive agricultural activities (Goolsby, et al., 1999) (Figure 2.1).

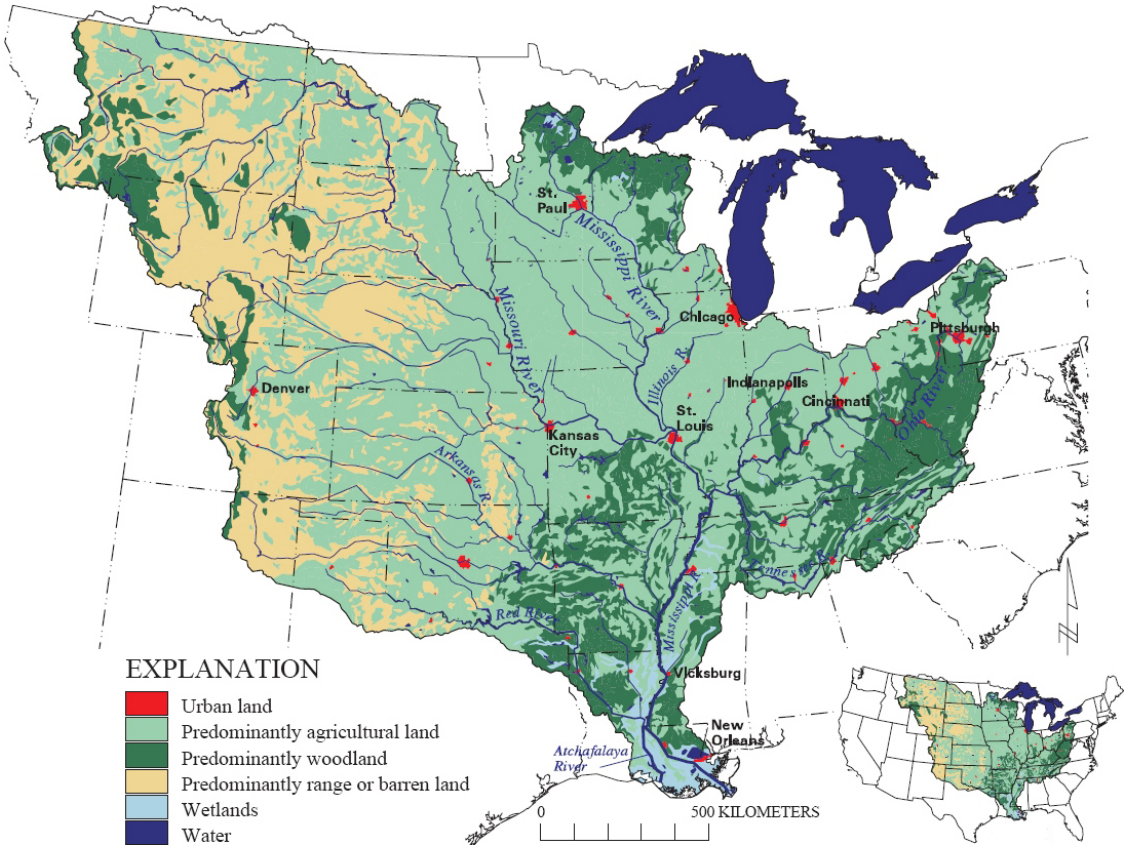

Figure 2.1 Drainage and land use in the Mississippi-Atchafalaya River basin (from Goolsby, et al., 1999)

Over the last 7000 to 8000 years, the modern Mississippi River Deltaic Plain has experienced six major delta-building or delta-switching events, occurred every 1000-2000 years (Roberts,

1997) (Figure 2.2). The deltaic cycles are separated by fluvially dominated regressive phases and marine-dominated transgressive phases, forming two types of shelf-stage deltas, thick inner shelf delta, such as the Balize delta, or thin inner shelf deltas, such as the St. Bernard and Lafourche (Roberts, 1997). Since the last century, human activities have extensive impacts on the deltaic system, superimposed on the natural processes (Coleman, et al., 1998). The latest delta building event is now taking place in the Atchafalaya River diversion, represented by two bayhead deltas at Atchafalaya River mouth and Wax Lake Outlet (Roberts, 1998).

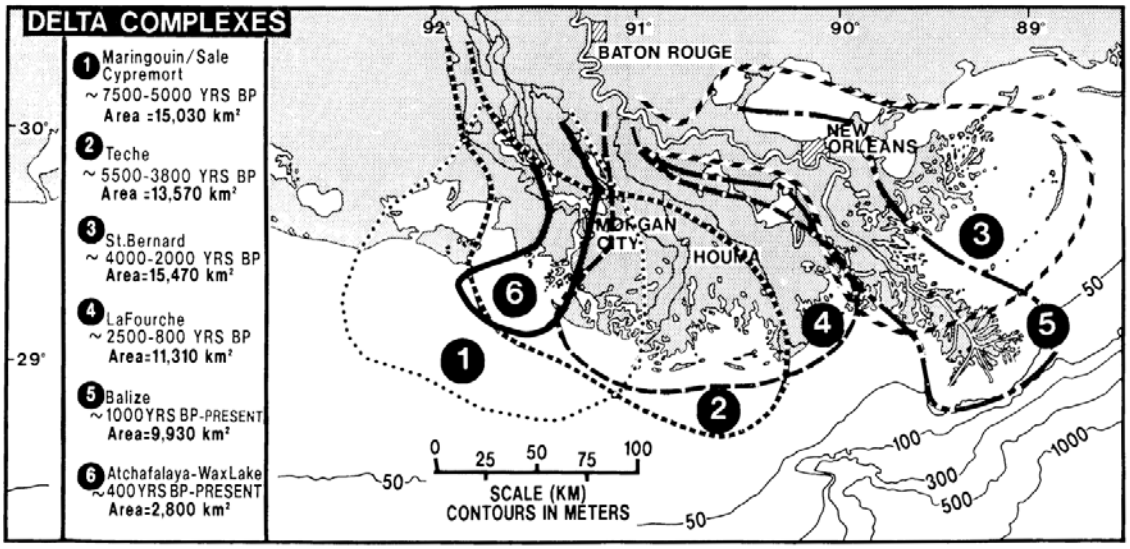

Figure 2.2 The Mississippi River deltaic plain, showing the locations of six major delta complexes (from Roberts, 1997)

2.2 Circulation over the Louisiana-Texas Shelf

Long-term hydrographic measurements and numerical simulations have been widely used to study the circulation over the Louisiana-Texas (LATEX) shelf. The Transport Processes Study and Louisiana-Texas Shelf Physical Oceanography Program and the Texas-Louisiana Shelf Circulation Program, all sponsored by the Minerals Management Service, largely improved the understanding of dynamical processes and mechanisms governing circulation, transport, and cross-shelf mixing on the LATEX shelf. The synthesis reports were written by Murray (1994;

1998), Murray and Donley (1995), Nowlin et al. (1998a; 1998b), Walker (2001b) and Walker et al. (2001), Walker (2005).

Cochrane and Kelly (1986) suggested a cyclonic gyre to demonstrate the low-frequency circulation over the Louisiana-Texas (LATEX) self throughout the year except July and August, when the prevailing cyclonic gyre disappeared, being replaced by an anticyclone centered off Louisiana due to the shoreward prevailing wind in the summer time (Figure 2.3).

Oey (1995) used a three-dimensional, primitive equation ocean model to verify the observed cyclonic gyre and explained the detailed processes and mechanisms of wind, river buoyancy and Loop Current eddies (LCEs) on the generation of the circulation. The inshore limb of the gyre is primarily driven by wind, but the total transport depends on all three types of forcing. Currents on the other three limbs of the gyre are driven by the combined effects of wind and LCEs. The westward transport varies with seasons and becomes very small during summer months with predominant southerly wind. The model also showed that the shelf break current is driven by Loop Current Eddies and seasonally modulated by the wind stress curl, with maximum intensity in late summer and fall and minimum in winter.

Cho et al. (1998) analyzed 31 current meter moorings of 32-month length in the LATEX shelf. The mean velocity stream function patterns also agree with Cochrane and Kelly (1986). The first empirical orthogonal function (EOF) pattern explains 89% of the monthly variance and is also strongly correlated with along-shelf wind, evidencing that the low-frequency circulation is wind-driven. The second and residual EOFs reveal the influence of LCEs on the shelf break.

Zavala-Hidalgo et al. (2003) applied the Navy Coastal Ocean Model (NCOM) to study the seasonal circulation on the western shelf of the GoM, and confirmed that the cyclonic circulation existed over the LATEX shelf except during summer months. Besides, the model gave new results on the connection between LATEX shelf and Tamaulipas- Veracruz (TAVE) shelf to the

south. Cool low-salinity water from the Mississippi and Atchafalaya rivers advect westward across the LATEX shelf to the TAVE shelf, developing fronts along the outer shelf or the shelf break during autumn and winter. While during summer, water from TAVE shelf advect onto the LATEX shelf. The along shelf currents plus the low-frequency barometric pressure can account for about 80% of the seasonal sea level variability.

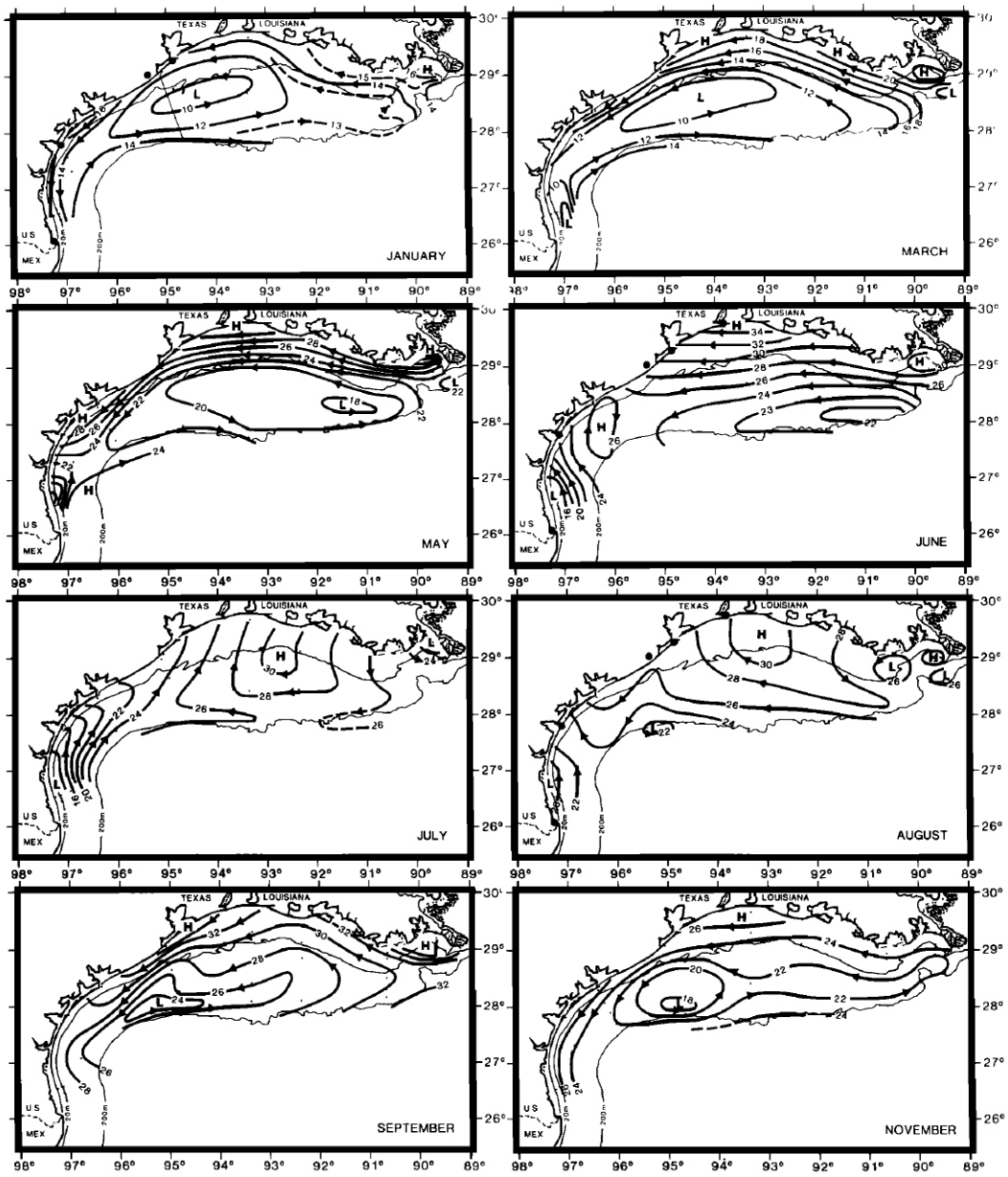

Figure2.3 Monthly mean geopotential anomaly (dyn·cm or 10^{-1} J/kg) of the sea surface relative to 70 dB or 0.7 MPa (from Cochrane and Kelly, 1986)

Ohlmann and Niiler (2005) studied the circulation over the northern continental shelf of GoM consisting of LATEX shelf and Florida-Alabama shelf, based on more than 750 surface drifters deployed from 1993 to 1998. The circulation observed from monthly mean surface currents generally supports Cochrane and Kelly (1986), but gives more detailed information. The connection between two shelves east and west of Mississippi River Delta only occurred under strong wind conditions associated with the passages of tropical storms, indicating the effect of the Mississippi Delta as a barrier to the flow. Mean flow along the shelf break are to the east and relatively weak, suggesting large variations in both magnitude and direction. LCEs play an important role in moving drifter off the shelf to the deep Gulf or backward onto the shelf, and also in driving the shelf break current.

Smith and Jacobs (2005) assimilated velocity measurements from current meter moorings, shipboard acoustic Doppler current profilers (ADCPs), and satellite-tracked drifters to calculate the seasonally averaged barotropic circulation field over the entire northern GoM. The deviations between the assimilated observational results and dynamical equations revealed that the southwest corner of the LATEX shelf cannot be explained by the simplified barotropic dynamics, which is believed due to the convergence caused by LCEs.

Walker (2005) investigated wind- and eddy-driven circulation on the LATEX shelf by analyzing satellite imagery and in situ measurements. In non-summer months, there are four distinct circulation regimes: (1) wind-induced down-coast jet on the western Louisiana and Texas inner shelf regions; (2) cross-shelf entrainment, referred to as the Texas jet; (3) seaward entrainment by slope eddies along the Mexico coast; (4) weak cyclonic gyre on the outer Louisiana shelf. A 4- to 6-week up-coast flow and coastal upwelling were also detected in the summer months.

In summary, the LATEX shelf has a cyclonic low-frequency circulation throughout the year

except during summer months when the flow may reverse its direction. The circulation is mainly driven by local wind, but also strongly influenced by Mississippi and Atchafalaya River discharge, Loop Current and Loop Current eddies.

2.3 Barrier Islands in Louisiana

Barrier island chains play an important role in protecting the back-barrier bays, lagoons, and wetlands by mitigating wave energy (Stone and McBride, 1998; Stone et al., 2005). In today's Louisiana, millions of people rely directly or indirectly on the barrier islands and adjacent marshes from economical, social, cultural, and environmental aspects (van Heerden and DeRouen, 1997; Pope, 1997). Isle Dernieres, Bayou Lafourche, Plaquemines shoreline, and the Chandeleur Islands are four main barrier/strandplain systems located from west to east along the Mississippi Deltaic Plain coast (Davis, 1997; McBride, and Byrnes, 1997). The formation and evolution of the barrier islands in the abandoned delta complexes can be well explained by the transgressive Mississippi Delta barrier model (Penland et al., 1988), comprising three stages (Figure 2.4):

Stage 1: erosional headland and flanking barrier islands (e.g., Bayou Lafourche and Plaquemine);

Stage 2: barrier island arc (e.g., Isle Dernieres and Chandeleur Islands);

Stage 3: the inner-shelf shoal (e.g., Ship Shoal).

Louisiana's Barrier islands erosion problems have been intensively studied by examining the relationships between meteorological and hydrodynamic processes, sediment transport trends, and geomorphologic changes. Due to the combined effects of eustatic sea level rise, subsidence, reduction of sediment supply, physical processes (e.g., waves and storms), and intense human activities (e.g., levees, jetties, and dredging), Louisiana's low-lying barrier islands systems are diminishing, disappearing and migrating landward rapidly (Penland and Ramsey, 1990; Davis,

1997; McBride and Byrnes, 1997; Georgiou et al., 2005). The landward retreat of the barrier islands exceeds 20 m/yr, and 40 to 75 percents of the subaerial mass of the islands has been reduced over the last century (Stone et al., 1997a).

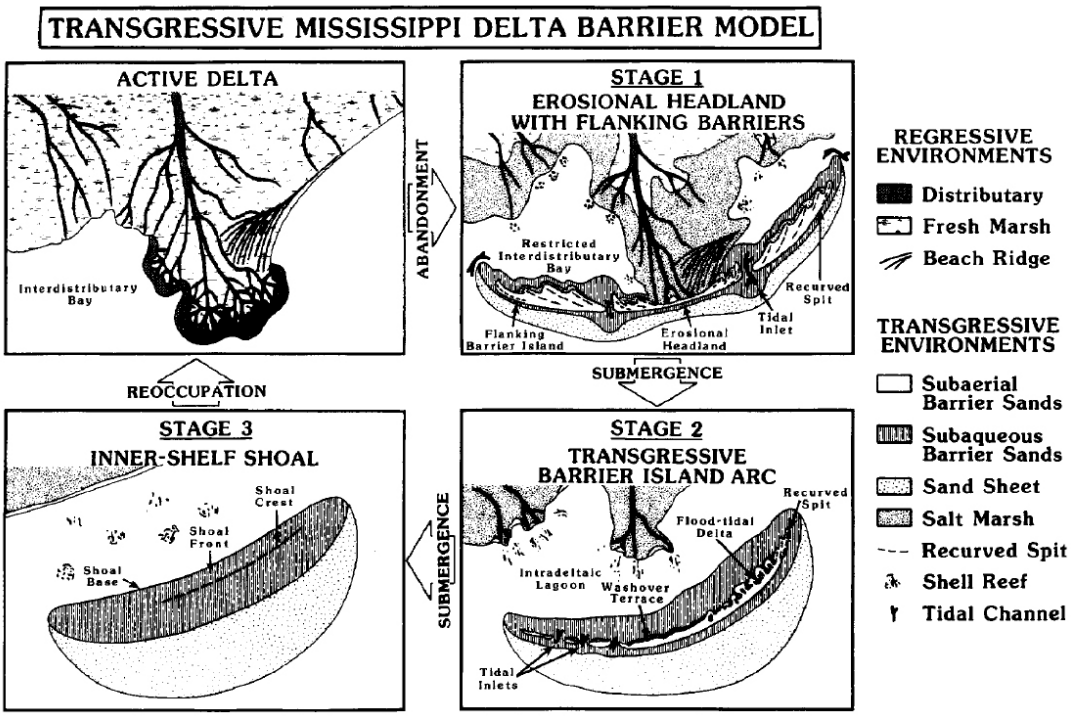

Figure 2.4 The transgressive Mississippi Delta barrier model (from Penland et al., 1988)

Many studies depicted the synoptic historical changes of barrier system along the entire Louisiana coast to determine the trend and extent of barrier island deterioration. Particularly, the importance of storms on the short-term transgressive evolution of barrier island systems in the northern GoM have been emphasized in recent years (e.g. Stone, et al., 1997b; Stone and Orford, 2004; Stone et al., 2004; Stone et al., 2005).

McBride and Byrnes (1997) applied National Ocean Service (NOS) topographic sheets and near-vertical aerial photography to quantify historical shoreline change of the Mississippi delta plain from 1855 to 1989. The results indicated that most of Louisiana's barrier shorelines have been experiencing high rates of retreat, of which the Bayou Lafourche at East Timbalier Island

has the highest rate of landward migration.

List et al. (1997) synthesized bathymetric and shoreline-position data of 1880s, 1930s, and 1980s to compare the bathymetric changes of the Louisiana's barrier islands. The comparisons demonstrated that large-scale sea-floor erosion and accretion are related to the rapid erosion and fragmentation of barrier islands. They believed that massive longshore transport in the littoral zone and at shoreface depths, and increased sediment storage in ebb-tidal deltas are the primary factors inducing the rapid shoreline retreat, while high relative sea-level rise is only an indirect factor.

Stone et al. (1997b) pointed out that 55 tropical storms or hurricanes have made landfall along the Louisiana coast since 1901, and also estimated that these storms may account for 90% of barrier islands' shoreline retreat by the overwash processes and inlet breaching. They, however, suggested that sediments can also be deposited in the coastal marshes during hurricanes, which offsets ongoing wetland loss.

Recent work also included applications of numerical models for processes and mechanisms of hydrodynamics, sediment rework and transport, and morphological changes of barrier islands under different weather conditions (fair weather vs. extreme weather). Such work will further benefit future prediction of barrier island evolution and better regional restoration strategies.

Suhayda (1997) quantitatively modeled the influences of Louisiana's barrier islands on wetland hydrology using the overland flooding model developed by Federal Emergency Management Agency (FEMA). The model results indicated that although the depth and duration of wetland flooding only slightly increased if barriers were removed from the model, inlet size and island height significantly affected the depth and duration of flooding under extreme conditions (e.g., hurricanes).

Stone and McBride (1998) combined historical shoreline change data and STWAVE model to

predict the disintegration of Isle Dernieres and the resultant wave climate in the adjacent bays. The model results showed that wave height in the bays could increase 7 times if barriers were reduced to shoals. They also suggested additional constructions around portions of the fringing marshes to mitigate wave energy, along with the large-scale barrier island restoration.

Stone et al., (2005) coupled a Hurricane Planetary Boundary model, a storm surge model ADCIRC and wave model SWAN, and demonstrated that the surge and wave height in Atchafalaya Bay and east Chenier Plain largely increased from 1950s to 1990s after landfall of a category-3 hurricane in 1915 and actual physical breakdown of the coast. They also predicted that the increasing trends will still continue over the following 30 years. Another interesting result from the model was that the muddy shelf adjacent to the coast of western Louisiana, supplied by the sediment from the Atchafalaya River, could significantly dissipate wave energy, especially during storm events.

Ellis and Stone (2006) used a wave refraction model, WAVENRG, to investigate the net longshore sediment transport along Chandeleur Island. The model results showed a bidirectional longshore transport system, and also indicated that southern portion of the island was suffering from the most severe deterioration. Besides, the predicted volume transport revealed that the degree of wave refraction, or breaker angle, was more important than the breaker wave heights in controlling the rate of longshore sediment transport.

One of the most important aspects in barrier island restoration is the demand of large amount of high quality sand, which is usually limited to isolated shoals or infilled fluvial channels on the inner shelf (Stone et al., 2004). One example of such study in Louisiana is Ship Shoal, a transgressive sand body off south-central Louisiana considered as a potential sand source for barrier island restoration (Stone et al., 2004; Kobashi et al., 2007a). Hydrodynamic and sediment transport measurements, as well as numerical simulations, have been widely carried out in that

area (e.g. Pepper and Stone, 2002; Kobashi et al., 2007a; Kobashi et al., 2007b; Jose et al., 2007). Results from STWAVE model indicated that the removal of Ship Shoal will increase significant wave height by as high as 90-100% during extreme weather, while only 10-20% during fair weather or weak storm conditions (Stone, et al., 2004). The shoals are effective in protecting the vulnerable coast against the tropical and extratropical storms (Jose et al., 2007).

2.4 Louisiana Bays and Wetlands West of Mississippi Delta

The coastal land loss problems in Louisiana have become catastrophic, with rates exceeding 100 km^2 per year over the last century (Penland, et al., 1990). Without restoration, Louisiana could potentially lose an additional 1800 km^2 in the next 50 years (Barras, et al., 2003) (Figure 2.5). In addition, hurricanes and tropical storms significantly affect wetlands of the Mississippi Deltaic Plain. On one hand, hurricanes can introduce freshwater, nutrients, and large amount of resuspended sediments onto the wetlands; on the other hand, storm surges induced by hurricanes easily convert wetland to open water (Day et al., 2007). For example, the landfall of Hurricane Katrina and Rita in the 2005 hurricane season caused land loss of 562 km^2, in term of direct removal of wetlands and transitory changes in water area due to remnant flooding (Barras, 2007).

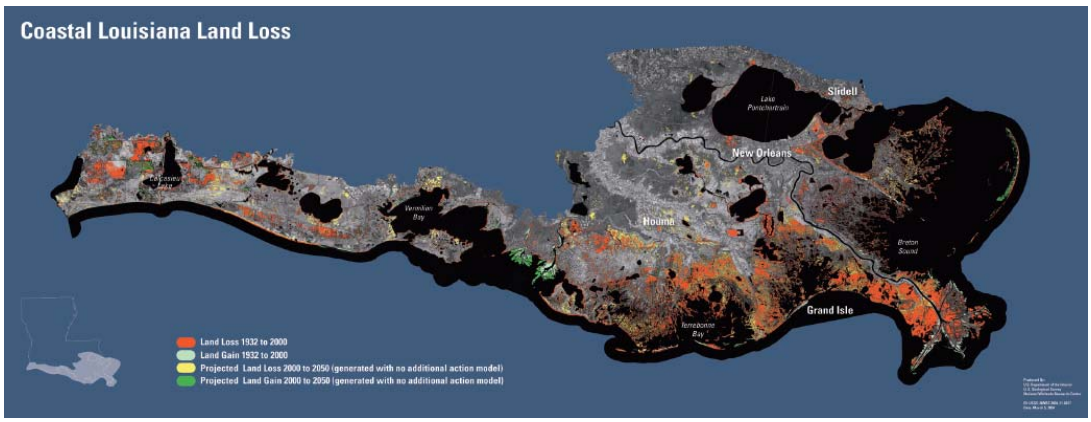

Figure 2.5 Coastal Louisiana historical land change between 1932 and 2000, and projected land change between 2000 and 2050. Red and yellow areas represent vast historical and projected land loss, while light green and green represent small areas of land gain mainly inside Atchafalaya-Vermilion Bays due to the Atchafalaya River diversion of Mississippi River water and sediment (from Barras, et al., 2003).

From west to east, Atchafalaya-Vermilion Bays, Timbalier-Terrebonne Bays, and Barataria Bay are three large bay and estuary systems along Louisiana coast west of the Mississippi Delta. Characteristics of these bays are summarized in Table 2.1.

Table 2.1 Characteristics of bays along Louisiana coast west of Mississippi Delta (modified from USEPA, 1999)

Name	Surface Area (km^2)	Drainage Area (km^2)	Average Daily Freshwater Inflow (m^3/s)	Average Depth (m)	Average Salinity (psu)	Coastal Wetlands (km^2)
Atchafalaya-Vermilion Bays	1821	260600	6337	2	1	1870
Barataria Bay	1673	5700	156	2	13	-
Timbalier-Terrebonne Bays	1761	4100	130	2	18	1020

The Atchafalaya-Vermilion Bays consist of five interconnected bays, including Fourleague Bay, Atchafalaya Bay, East Cote Blanche Bay, West Cote Blanche Bay and Vermilion Bay. The Atchafalaya River discharges 30% of the Mississippi River water and 40-50% of the sediment load, entering the coastal ocean mainly through the Atchafalaya River and Wax Lake Outlet (Mossa and Roberts, 1990). Due to the Atchafalaya River diversion of Mississippi River waters and sediments since 1950s, two bayhead deltas have being built in such previously abandoned delta system (Roberts et al., 1980). High water level events associated with floods or water level setup caused by winter frontal passages transport turbid water to adjacent marshes (Mossa and Roberts, 1990). Abundant suspended sediment supplies altered the marshes from deterioration to accretion after 1950s (Roberts, 1997). Detailed work on geomorphic and sedimentologic features and descriptions of the growth of new bayhead deltas can be found in Roberts et al. (1980); van Heerden and Roberts (1980); Roberts (1997); and Roberts (1998). Details on circulation and sediment dynamics in the Atchafalaya-Vermilion Bays and adjacent shelf responding to frequent

cold front passages and occasional tropical storms or hurricane impacts can be found in Walker and Hammack (2000); Walker (2001a); Li et al. (2009).

The Timbalier-Terrebonne Bays are broad shallow estuaries, receiving freshwater from ambient bayous and canals. Although these two bays are interconnected, they belong to two different barrier systems: Terrebonne Bay is part of the Isle Dernieres system while Timbalier Bay pertains to the Bayou Lafourche barrier system (Penland et al., 1988). In the bay basins, tidal forcing often dominates the circulation but local wind forcing is also important in controlling general flow directions (Inoue and Wiseman, 2000). Canal dredging significantly and directly influences loss of adjacent wetlands because canals and spoil banks disturb the natural hydrology and sedimentation patterns, especially during intentional or unintentional impoundments (Bass and Turner, 1997).

The Barataria Bay is a restricted interdistributary bay within the Bayou Lafourche barrier system, separated by a chain of barrier islands from the Gulf of Mexico (Penland et al., 1988). Due to submergence and land loss, Barataria Bay is continuously increasing in size and depth, leading to an increase of volume of stored water, inlet cross-sectional area, tidal current velocity, and sediment storage capacity (Penland et al., 1988). The man-made Davis Pond Freshwater Diversion, located on the west bank of the Mississippi River, has been designed to introduce river water into the upper Barataria Basin, to protect and rebuild deteriorating marshes, to enhance emergent marsh vegetation, and to increase commercial and recreational fisheries and wildlife productivity (Walker, et. al, 2003; The State Wetlands Conservation and Restoration Authority, 2004). However, Harmful Algal Blooms (HABs), associated with the low oxygen problem, caused by excess nutrient being brought into the Barataria Basin, may have negative effects to the fish, shellfish, birds and even humans (Walker, et. al, 2003).

2.5 The Responses of Coastal Environments to Cold Front Passages

2.5.1 Meteorological Characteristics of Cold Fronts

About 30 to 40 cold fronts pass through the Louisiana coast from October to April every year (Moeller et al., 1993). A cold front event has three basic phases: the prefrontal, frontal passage, and postfrontal or cold air outbreak phases (Huh, et al., 1978; Roberts, et al., 1987). Figure 2.6 illustrates a schematic cold front system. The prefrontal phase usually has a falling barometric pressure and strengthening wind from southerly quadrant, with very small diurnal air temperature fluctuations (Huh, et al., 1984). Then, with the cold polar continental air mass overrunning warm tropical maritime air mass, a synoptic-scale convergence of two air masses, characterized by a squall line at its leading edge, abruptly reverses the conditions induced by the prefrontal phase with winds rapidly clockwise rotating to northerly (Huh, et al., 1984). Finally, during the postfrontal or cold air outbreak phase, winds blow strongly from northerly quadrant; air temperature and humidity significantly decrease while barometric pressure rises (Moeller et al., 1993). The orientation of frontal system to the roughly east-west Louisiana coast can be oblique or parallel, depending on the origin of air mass and evolution of the system (Henry, 1979; Georgiou et al., 2005). The typical duration of a cold front event is 12 to 24 hours, depending on the advancing speed (Georgiou et al., 2005). When cold fronts enter the GoM, they may have different fates: either returning as a warm front or extent of push into the tropics, or frontolyzing (Henry, 1979). Roberts et al. (1987) classified cold fronts as two end-member types: arctic surges and migrating cyclones (Figure 2.7). Pepper and Stone (2004) summarized that arctic surges have a very weak prefrontal phase and a fairly strong postfrontal phase with dominant northeasterly winds, while migrating cyclones are characterized by a strong low pressure cell with fairly strong prefrontal southerly winds and strong northwesterly winds.

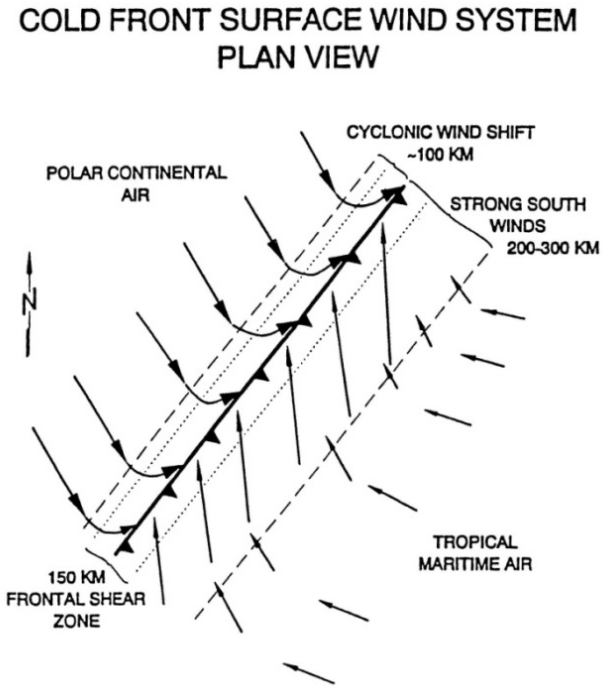

Figure 2.6 Schematic figure of the cold front system (from Roberts, 1987 and shown in Moeller et al., 1993)

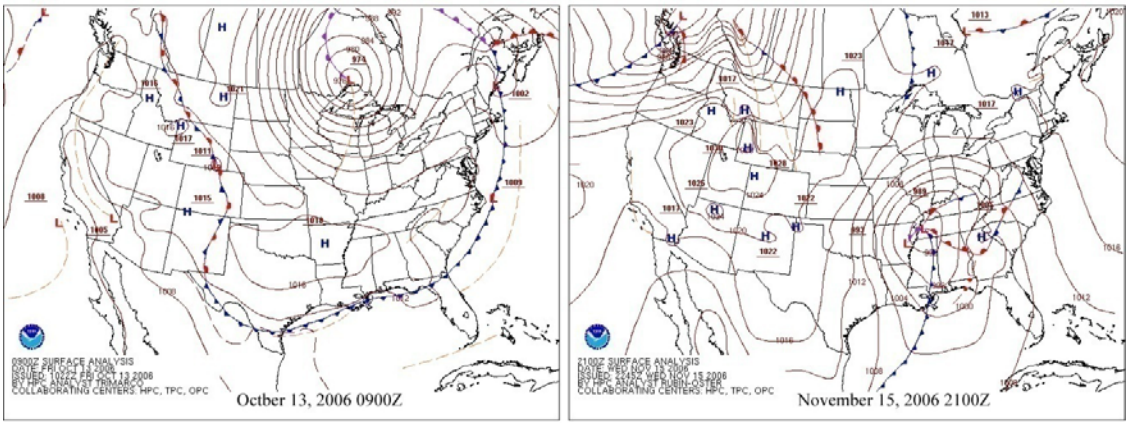

Figure 2.7 Surface weather maps illustrates two end-member types of cold fronts: arctic surge (left) and migrating cyclone (right) (from Hydrometeorological Prediction Center's surface analysis archive)

Early studies mainly emphasized the cold front events in the GoM regions from the meteorological points of view. Fernandez-Partagas and Mooers (1975) examined the kinematic features of 15 selected cold fronts in Florida based on the time series of surface wind observations and six-hourly synoptic charts. They inferred that in the steady wind regimes, the

major wind change across the fronts only occurs in the N-S directions. DiMego et al. (1976) studied the mean monthly frequency and duration of frontal incursion into the GoM and the results suggested that the frequency and duration are directly related to topographic features and the position, strength and amplitude of the mid-latitude circulation. Davidson et al. (1992) studied the atmospheric boundary-layer properties in the GoM, and found that the neutral drag coefficient, specified for surface roughness of wind stress, is about 25% higher in the coastal region than in the open ocean, and can be increased by a factor of 2 for 3-4 h after a cold front passage.

2.5.2 Air-sea Interaction during Cold Front Passages

Nowlin and Parker (1974) conducted two surveys in the northwestern GoM before and after a major cold air outbreak event. The results indicated that shallow shelf water are well mixed, and the temperature and salinity decrease 5°C and 1 psu through the evaporation and sensible heat exchange from sea surface to the atmosphere. Huh et al., (1978) studied the synoptic SST patterns: the outbreak of cold air made the coastal lakes and bays 3.5-4°C cooler than offshore surface water; west of Mississippi River, the river discharge caused strong stratification and cooler water extended tens of kilometers offshore. Huh and Rouse (1984) conducted thermal experiments in the northeastern GoM and showed that rate of heat loss during severe cold air outbreaks was more than three times that of mild outbreaks, and also pointed out that evaporation was the dominant heat loss mechanism on the upwind continental shelf. Walker et al., (1987) examined the shelf waters of southern Florida and northern Bahamas, chilled by cold air outbreaks, using satellite-infrared and in situ measurements. Shallow waters were more rapidly chilled, and the northerly winds induced a net off-shelf circulation, moving the cooler shallow waters to deep regions.

An interesting phenomenon of air-sea interaction in the northwestern GoM is winter- time

cyclogenesis, defined as the development or strengthening of cyclonic circulation in the atmosphere (Hsu, 1993; Lewis and Hsu, 1992). During 1972-1982, an average of 10.4 winter cyclones developed each year over the GoM (Johnson et al., 1984). Walker (1993) and Schumann et al. (1995) analyzed an extreme cyclogenesis, named as "Storm of the Century" or "Blizzard of March 1993", the intensity of which is comparable in strength to a Category 1 hurricane. The strong cyclogenesis was initiated by the presence and vicinity of a strong, low-level baroclinic zone (stationary front) coinciding with a strong SST gradient (Walker, 1993; Schumann et al., 1995).

Van de Voorde and Dinnel (1998) discussed the observed directional wave spectra during a cold front passage and testified that the time lag between a change in the magnitude of the wind field and a corresponding change in wave-energy field for higher frequency waves was shorter than that for lower frequency waves. They also found some apparent exchange of energy between high and low wave fields via a mid-range frequency energy bridge.

2.5.3 Sea Level Response to Cold Front Events

Coastal sea level responses to cold front passages in the GoM were examined to study the relationship between low-frequency continental shelf dynamics and atmospheric forcing. Marmorino (1982) determined that the dominant 6-day period signals in sea level, alongshore wind stress, and atmospheric pressure, were consistent with southward movement of cold fronts across the west Florida shelf, and the response of sea level variations lagged the local wind by 18 h in the north and 9 h in the south. Marmorino (1983) also found two important periods from sea level variations in the West Florida Bight: 3.5 days, which responded to cross-shore wind with 6-10 h lag, and 5-10 days, which was coherent with dominant alongshore wind with one day lag. Similar findings can also be found in Cragg et al.'s work (1983).

Chuang and Wiseman (1983), however, believed that due to the unique east-west coastline

associated with frontal passages in the northern GoM, prevailing cross-shore winds strongly affect the sea level fluctuations, which seemed different from most of other U.S coast where sea level variations appeared to be driven by alongshore winds. They examined 5-month hourly sea level data observed at Eugene Island, Louisiana and Galveston, Texas and concluded that sea level fluctuations were relatively large and responded to alongshore wind stress in Galveston, but responded to cross-shore wind in Eugene Island. They argued that the difference was mainly due to the different water depth over the inner shelf. Denes and Caffrey (1988) studied seasonal water transport in Fourleague Bay, a very shallow estuary within the Atchafalaya-Vermilion Bays. One survey in February 12-14, 1982 with a cold front passage and high river discharge indicated that northerly winds caused a significant net export of water out of bay. After winds shifted to easterly, an unfavorable pressure gradient due to Ekman process reduced the outflow and increased the averaged water level by 0.06m. Lee et al. (1990) compared the current measurements and water level variations in Calcasieu Lake, Louisiana, and found the predominant wind-induced barotropic volume exchange mode. Noble et al. (1996) studied the subtidal circulation in Mobile Bay, Alabama, and observed the highly sheared currents due to combined effects of wind stress and river discharge. Walker and Hammack (2000) investigated the impacts of winter storms on circulation and sediment transport in the Atchafalaya-Vermilion Bays and demonstrated that strong northwest winds could flush 30-50% of water out of the shallow bays and reduced water level by more than 1 m. Snedden et al. (2007) concluded that the subtidal sea level variation was mainly driven by remote wind forcing in Breton Sound, a very shallow (0.7 m) Louisiana deltaic estuary, while effect of local wind forcing is minimal due to limited fetch. Li et al. (2009) conducted a 1-month survey near the mouth of Wax Lake Outlet within the Atchafalaya Bay and determined two saltwater intrusion events occurred after a high water slack caused by combined effects of tides and southerly wind surge prior to a cold front

passage. They also estimated that half of the water level setup was due to local wind stress, the other half due to wave and low barometric pressure, while Coriolis Effect was negligible.

2.5.4 Geomorphic Response to Cold Front Events

Recent studies have focused more on the importance of cold fronts on short- and long-term geomorphic evolution of coastal systems, relating the geophysical processes with sediment rework and transport. Different coastal environments have different response to cold front events, depending on hydrodynamics, geomorphic characteristics, and sediment dynamics.

Roberts et al. (1987) first analyzed the effects of cold fronts on coastal morphology along the Louisiana coast, composed of three major categories: sediment-rich coast (Atchafalaya Delta), transitional coast (Chenier Plain), and sediment-poor coast (barrier islands). They suggested some preliminary results on the short-term sedimentary processes influenced by the physical processes associated with winter frontal passages. In the Atchafalaya Delta and Chenier coast, active wave and water setup sustained by the prefrontal winds eroded subaerial lobes, resuspended and transport bottom sediment into marshes, while regions of Chenier coast without offshore fluid mud were severely eroded by wave actions. Postfrontal winds caused a rapid drop of water level and advected turbid bay water to the shelf. Barrier islands were strongly eroded by waves generated by long-fetch prefrontal winds, and constant onshore winds could also cause eolian transport and dune migration. Postfrontal winds reworked landward ends of washover lobes and also deflated lobe surface by eolian processes.

Some studies indicated that winter cold fronts played important roles in barrier island erosion, through eolian processes, wave-sediment interactions, and wind-generated or tidally-driven transport.

Dingler and Reiss (1990) conducted repeated surveys between August 1986 and September 1987 along the central Isle Dernieres and showed that the beach face retreated about 20 m during

the cold-front season but with no recovery during the rest of the year. Their results also suggested that cold fronts first removed the sand from the beach face and then eroded underlying marsh deposits. Later study by Dingler et al., (1992) showed that sand could be eroded and transported by the strong northerly wind from backshore to the upper beach face, while only part of the sand was moved backshore after wind shifted southerly.

Keen (2002) coupled POM and SWAN models to determine barrier island erosion in the Mississippi Sound and Chandeleur Sound during a winter cold front. The wave model, SWAN, presented steep waves with significant wave height of 0.9 m and wave periods of less than 4 s, which played important roles in sound-side erosion. The hydrodynamics model, POM, indicated that tidal currents were predominant within Mississippi Sound during the cold front, and shoreface sediment transport was sensitive to the tidal stage as well as wind strength and direction.

Pepper and Stone (2002) deployed instrumentation at two sites on the Louisiana inner shelf during a 2-month winter period. The increases of wave height, mean oscillatory flow and shear velocities, mean near-bottom currents, as well as decreases of wave period and apparent bottom roughness, due to extratropical storms, induced resuspension and net offshore transport of fine bed sand. Such in situ measurements were further reanalyzed by contrasting the hydrodynamic and sedimentary responses to two winter storm types: arctic surges and migrating cyclones (Pepper and Stone, 2004). The arctic surges generate northeasterly winds, southerly storm waves, and southwestward currents and sediment transport, whereas the migrating cyclones induce energetic, rotational winds and currents, and northerly swell to southerly sea, and overall southeastward sediment transport.

Stone and Wang (1999), Stone et al. (2004) and Stone et al. (2007) addressed the importance and relationship of tropical and extratropical cyclones on the short-term evolution of Gulf coast

barrier islands. They showed that along the Florida panhandle, cold fronts played a crucial role in the post-storm adjustment of the barriers by deflating the subaerial portion of the overwash terrace and eroding its marginal lobe along the bayside beach through locally generated, high frequency, steep waves. The cold-front-related high wave energy conditions seemed more effective in reworking sediment after the occurrence of extreme weathers, especially during the clustering of tropical storms. However, along western Louisiana, fluid mud environments of cohesive sediments (fine silts and clays) damped and attenuated wave energy, resulting in minor beach erosion. The hypothesized sequence of events responded to post-frontal northerly winds is illustrated in Figure 2.8.

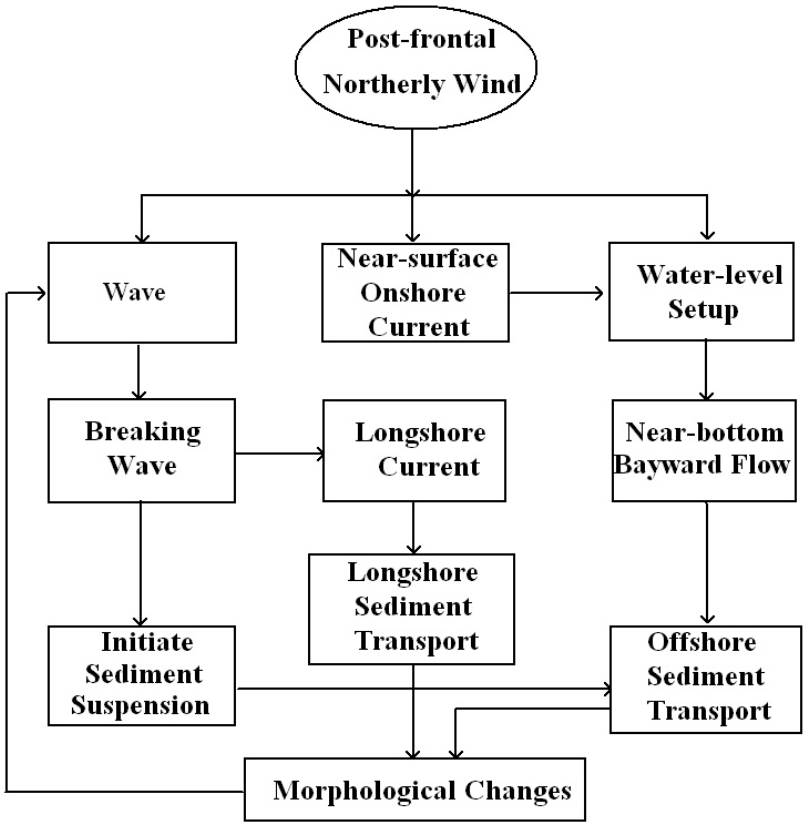

Figure 2.8 A hypothesized sequence of events along beaches exposed to postfrontal northerly winds in the northern Gulf of Mexico (from Stone and Wang, 1999)

Inside the shallow bays and fringing marshes, wave actions are minimal, but tidal pumping

effects may be important, although the dominant diurnal tidal range is usually less than 0.5 m in Louisiana. Local wind forcing also affects the circulation in the bays. Reed (1989) examined surface sedimentation in salt marshes adjacent to Terrebonne Bay during cold front passages. The results showed that marsh surface sedimentation was a discontinuous process, requiring both the availability of suspended sediment and flood waters that transport sediment to the marshes. Strong pre-frontal southerly winds could mobilize sediments from bays and increase water level in the marshes, while post-frontal northerly winds decreased water level and allowed the newly deposited sediments to drain and consolidate. Wang et al. (1993) studied transport processes of suspended sediment from tidal creek/bayou onto its adjacent salt marshes near Terrebonne Bay by examining both tidal and prevailing wind forcing. The results showed that during strong southerly winds, suspended sediment concentrations (SSC) in the bayou were much higher than those in the marshes; while during partial inundation and strong northerly winds, the phenomena were just opposite. The results also indicated that sediment concentration varied in bayou and marsh during flood and ebb tides; however, the computed friction velocity and bottom shear stress induced by tidal current were not sufficient to resuspend the deposited sediment.

Mossa and Roberts (1990) also found that the winter cold front passages can supply suspended sediments from Atchafalaya River to coastal marshlands through a sequence of processes of entrainment, transportation, deposition, desiccation and accretion, which counterbalanced the ongoing coastal land loss. Walker and Hammack (2000) point out that during winter storms, sediment flux in the East Cote Blanche Bay was mainly southeastward onto Atchafalaya Bay while net sediment flux through Southwest Pass was into Vermilion Bay, due to the asymmetry of inflow and outflow. Perez et al. (2000) sampled SSC and fluxes between Fourleague Bay and the northern GoM and found that the highest SSC occurred during cold front passage and lowest during calm periods. The high concentrations were originated from Atchafalaya River and

resuspension of benthic sediment, due to strong northerly wind associated with cold front.

West of Atchafalaya Bay, the Chenier plain has been prograding over the last few decades due to the sediment supply from Atchafalaya River. Draut et al., (2005) concluded that abundant supply of fine-grain fluvial sediment, dominant onshore winds during energetic conditions, and low tidal range contributed to the mudflat accretion. Kineke et al., (2006) suggested that pre-frontal conditions resuspended and transported sediment onshore, while post-frontal conditions also induced onshore transport through upwelling of turbid bottom water.

2.5.5 Mississippi and Atchafalaya River Plume

The Mississippi River plume areas have the highest biomass density and primary production in the GoM (Lohrenz et al., 1999). River discharge and wind forcing are identified as main factors affecting the Mississippi River plume variability (Walker, 1996).

From satellite-retrieved sea surface temperature, Walker et al. (1996) detected a 200-km-long and 10- to 30-km-wide southwestward squirt of cool and low-salinity water from the Mississippi delta region, which was found to be primarily driven by strong and sustained northeasterly winds. Walker and Hammack (2000) analyzed the Atchafalaya River plume in different wind regimes: the most frequent easterly winds induced a westward turbid flow along the coast; westerly winds reversed the direction of plume movement and increased the plume size; the strong northerly winds could produce a large plume by wind-wave bottom resuspension and wind-induced seaward transport of bay and inner shelf waters. Walker et al. (2005a) also systematically examined the Mississippi River plume in different winds and river discharge conditions. The westward flow associated with nutrients, driven by prevailing easterly winds, favored the development of hypoxia. Frequent cold front passages with short-term wind veering reversed plume direction and initiated offshore transport. With simulations from numerical model H3D, Rego et al. (2009) proposed a best conceptual Mississippi River diversion scenario in terms of

retention of sediments within the continental shelf, which delivered 70% and 30% of the Mississippi sediment to the west and the east of the Mississippi delta, respectively.

2.5.6 Cold Fronts and Larval Transport and Recruitment

Norcross and Shaw (1984) reviewed the oceanic and estuarine transport of fish eggs and larvae, trying to identify the important mechanisms controlling the distribution, transport, and survival of eggs and larvae. They proposed that the successful recruitment of larvae depended on various physical processes (e.g., atmospheric fronts, ocean currents, winds, tides, and river plumes) and biological conditions which were favorable for survival, as well as interactions of these physical and biological factors.

Shaw et al. (1985) studied the transport of larval gulf menhaden in the western Louisiana coastal waters. They hypothesized that longshore advection within the horizontally stratified coastal boundary layer was the major mechanism which controls the transport of larvae to the nursery ground, rather than cross-shelf transport from immediately offshore of the estuary. Cold fronts may effectively influence the recruitment of larvae by inducing significant water exchange between shelf and estuary, which may control the concentration of postlarvae and, therefore, juveniles within the estuary.

Shaw et al. (1988) integrated ichthyoplankton in the shelf and late-stage larvae and juveniles in Louisiana estuaries to document recruitment processes and identified the shelf-to-estuary transit time of 40-73 d for gulf menhaden and an upper range of 30-94 d for sand seatrout, during which larvae are displaced hundreds of kilometers westward or northwestward from their offshore spawning areas.

Rogers et al. (1993) investigated recruitment of postlarval brown shrimp to the Calcasieu River estuary in western Louisiana, based on continental shelf distribution and abundance data for postlarval brown shrimp as well as marsh postlarval and juvenile data. Catches of postlarvae

peaked in February for offshore sampling, while peaked in March for marsh. They hypothesized a behaviorally-mediated transport mechanism for the enhancement of postlarval brown shrimp recruitment, relating the postlarval data with meteorological data on cold front passages. In this model, postlarvae utilized water temperature and salinity variation associated with cold front passages as environmental cues in combination with a diel activity cycle that put them in contact with the bottom.

Horton (1998) sampled postlarval brown shrimp at Oyster Bayou, a tidal channel of Fourleague Bay and found that cold fronts appeared to have a highly negative effect on the recruitment and retention of postlarval brown shrimp at Oyster Bayou. The results also showed that net postlarval fluxes were always negative during these intense weather events, while peak recruitment and density distributions were recorded in periods without cold front events.

2.6 Numerical Modeling of Louisiana Coastal Environments

Numerical models have become effective tools to provide better understandings of hydrodynamics, sediment transport processes and mechanisms, forecasts over large coastal regions, and efficient coastal management.

Jose et al. (2007) implemented a spectra wave model, MIKE 21, to estimate wave attenuation and to study the directional wave spectrum with winter-storm-generated waves cross Ship Shoal. The shoal could reduce wave height by 22% when southerly storm waves propagated over the shoal. The dominant direction in the energy evolution spectra abruptly shifted from southwest to north across the shoal, which was attributed to wave refraction due to the shoal and veering of the winds associated with cold front passages.

Cobb et al. (2008a) used NCOM to simulate tide, river, wind-driven circulation and sediment transport in the Atchafalaya Bay system during a period of three cold front passages. The modeled water levels, salinity, and currents agreed reasonably well with in situ measurements,

whereas discrepancies were mainly due to low spatial and temporal resolution of the model's wind fields and freshwater source, as well as old bathymetry data used for inner bays and inner shelf. Cobb et al. (2008b) further examined river plume dynamics and found that wind-driven plume waters moved parallel to the alongshore bathymetric contour, unless forced by strong postfrontal winds to mix with higher salinity waters.

2.7 Remote Sensing of Louisiana Coastal Environments

The ocean color and infrared satellites have been developed for affording rapid, repeated, synoptic, and concurrent assessment of environmental parameters in oceanic areas since late 1970s (Muller-Karger et al., 2005). Scientists and researchers have successfully utilized one or more sensors, or multiple channels in the study of coastal environments in Louisiana, e.g., very high resolution radiometer (VHRR) (Huh et al., 1978), Multispectral Atmospheric Mapping Sensor (MAMS) (Moeller, et al., 1993; Huh, et al., 1996), NOAA-14 Advanced Very High Resolution Radiometer (AVHRR) (Walker and Hammack, 2000; Walker, 2001a), Moderate Resolution Imaging Spectroradiometer (MODIS) (Miller and Mckee, 2004; Miller et al., 2005; Walker et al., 2005a), Ocean Color Monitor (OCM) (Walker et al., 2005a), Sea-viewing wide field-of-view (SeaWiFS) (Myint and Walker, 2002; Walker et al., 2005b; Walker and Rabalais, 2006; Del Castillo and Miller, 2008), and GOES-12 (Walker et al., 2005b).

MAMS imagery revealed that a cold front system could force or modulate coastal circulation patterns and river plume structures by chilling waters, water level setup and setdown, and wind veering (Moeller, et al., 1993). MAMS imagery was also used to quantitatively distinguish coastal water types in the Louisiana coast and it was found that the differences between water types were enhanced by the cold front passages (Huh, et al., 1996).

AVHRR imagery with one-kilometer resolution was applied in studying the changes in circulation, sediment resuspension, sediment flux and salinity and their response for cold front

passages in Atchafalaya Bay regions and demonstrated that wind direction and speed were the major controlling factors for circulation, SSC, and sediment transport (Walker and Hammack, 2000). The wind-induced resuspension of bottom sediment in Barataria Bay was examined by combining visible and near-infrared AVHRR data with model predications, revealing the importance of resuspension as a process that affected sediment and biogeochemical fluxes (Booth, et. al, 2000).

Myint and Walker (2002) obtained an AVHRR Channel 1 (580-680 nm) cubic model, Channel 2 (725-1100 nm) linear model and SeaWiFS Channel 6 (660-680 nm) power model to derive surface SSC. However, the SSC retrieved from SeaWiFS may not be as good as those from AVHRR, mainly resulted from the atmospheric correction technique, the shallow water depth and absorption from non-sediment constituents (Myint and Walker, 2002). Miller and McKee (2004) established a linear relationship between atmospherically-corrected band 1 MODIS Terra 250 m reflectance and in situ measured concentration of Total Suspended Matter (TSM). The linear algorithm was further applied in examining bottom sediment resuspension and sediment transport associated with cold front passages in Lake Pontchartrain, Louisiana. The satellite-retrieved TSM agreed with numerical-modeled Resuspension Potential (RP) and Resuspension Intensity (RI) (Miller, et al., 2005). However, such linear algorithm was not applicable to regions of very turbid waters. Bellotte (2007) established exponential relationship in the Atchafalaya Bay regions, where TSM can reach to nearly 200 mg/l.

SeaWiFS has been extensively used to study chlorophyll-a concentration in both open and coastal oceans. Estimating the total chlorophyll-a is also the most common method to identify harmful algal blooms (HABs), based on the standard bio-optical algorithms based on green/blue ratio of reflectance developed by Gordon, et al. (1988). However, such techniques developed for chlorophyll-a in open ocean waters (Case 1 waters) may not be applicable for coastal waters

(Case 2 waters) with chlorophyll, non-algal particles (NAP), and chromophoric dissolved organic matter (CDOM), due to the overlap of these substances in the blue spectrum (Stumpf and Tomlinson, 2005; D'Sa and Miller, 2005). Walker and Rabalais (2006) established a quadratic polynomial algorithm to fine-tune the satellite-derived estimates of chlorophyll-a for the Louisiana coastal waters, based on field-satellite matches. The satellite-measured chlorophyll-a concentration was further used to assess the relationships with river discharge, nitrate load, and hypoxia.

A combination study of three different sensors, AVHRR, MODIS and OCM in estimating SST, SSC and chlorophyll-a concentration associated with Mississippi River plume indicated that short-term wind reversals due to cold front passages also reversed plume direction, generated offshore transport, and decreased the residence time for freshwater, sediments, nutrients and phytoplankton (Walker, et al., 2005b).

2.8 Subtidal Water Level Variation and Barotropic Volume Transport

The wind-induced subtidal water level variation and barotropic volume transport have been extensively studied in the estuaries of the Atlantic coast as well as the Gulf coast of the United States. The general mechanisms of the subtidal sea level variation are: (1) direct setup and setdown by local winds, and (2) indirect or remote action upon the estuary through Ekman transport over the adjacent shelf (Garvine, 1985).

Wang (1979) examined the wind-induced barotropic circulation in Chesapeake Bay and found that coastal remote forcing was mainly responsible for the oscillations of longer periods (>10 days) while shorter oscillations of time scales less than 4-days were induced by local and longitudinal winds. East-west winds mainly drove ocean-bay coupling in the time scales of 4-10 days. Valle-Levinson et al. (2001) identified three major scenarios on the water exchange through the entrance of Chesapeake Bay. Northeast winds were the most effective in flushing water out

of the bay and northwest winds also caused a net outflow, while southwest winds drove near-surface outflow through the entrance and near-bottom inflow restricted to the deep channels. Wong and Valle-Levinson (2002) pointed out that the volume exchange patterns and relative importance of local and remote winds were different with seasons, depending on the frequency of wind events and the degree of stratification in the estuary. Salas-Monreal and Valle-Levinson (2008) addressed that barometric pressure effect, which was not included in most studies, may account for 1/3 of total subtidal sea level variations in Chesapeake Bay. On the Delaware estuary, Wang and Garvine (1984) found that remote wind effect was more important than local wind effect in forcing the subtidal water level fluctuation. Garvine (1985) further constructed a barotropic model, which indicated that remote forcing was the most important factor for both sea level and barotropic current fluctuations while local winds determined the estuarine surface slope.

CHAPTER 3 DATA DESCRIPTION AND METHODOLOGY

This chapter describes the data sets available for the study and methodology used in the analysis. This study utilizes multiple data sources along the Louisiana coast west of bird-foot delta: tidal gauges, buoys, oil platforms, USGS surveys. In general, the data can be mainly categorized as meteorological and oceanographic data. The methods consist of low-pass filter, spectra analysis, and rotary spectra analysis.

3.1 Data Description

3.1.1 Meteorological Data

The meteorological data are available from four major sources along the Louisiana coast: wave-current information system (WAVCIS) stations maintained by Coastal Studies Institute (CSI) at Louisiana State University (LSU), National Data Buoy Center (NDBC) stations maintained by NOAA's National Ocean Service (NOS), stations maintained by NOAA's Center for Operational Oceanographic Products and Services (CO-OPS), and LUMCON stations maintained by Louisiana University Marine Consortium (LUMCON) (Figure 3.1). The parameters include: wind speed and direction, barometric sea-level pressure, air temperature and humidity. In this study, the winds are plotted in vector format, and also converted into east-west and north-south components, or alongshore and cross-shore components if the coastline in specific area is not exactly east-west orientation. In addition, the United State surface weather analysis maps have been downloaded from the archive of NOAA's Hydrometeorological Prediction Center (HPC) (http://www.hpc.ncep.noaa.gov/) (see Appendices). These maps are generated every 3 hours, illustrating the location of isobars, high and low-pressure centers, and the fronts, which can be used to identify the exact location and advancing speed of cold fronts, and the orientation of fronts relative to the coastline.

3.1.2 Oceanographic Data

The oceanographic data are also available from the stations mentioned above including sea surface temperature (SST), water level, current and wave measurements. Time-series water level data are transformed to frequency domain to identify the relative importance of low-frequency (i.e., winds) and high-frequency forcings (i.e., tides) for different locations. Water level data collected inside the bays are also used to quantify the estuary-shelf water exchange. A 40-hour Butterworth low-pass filter is applied to remove the tidal and inertial effects. The analysis of water level also includes the interpretation of winds and river discharge. Bottom-mounted ADCPs from two WAVCIS stations provide current data which can be analyzed to determine the effects of different forcings, such as winds, tides, river discharge, and the Coriolis force on current variability.

3.1.3 Other Data

The USGS website (http://waterdata.usgs.gov/la/nwis/rt) provides real-time water data for Louisiana. In this study, the daily mean river discharge data from two stations, Mississippi River at Baton Rouge, LA (USGS No.07374000) and Atchafalaya River at Morgan City, LA (USGS No.07381600), are used to represent the discharge conditions of Mississippi River and Atchafalaya River, respectively (Figure 3.1). The river discharge data are integrated with other data to assist the interpretation.

3.1.4 Data Summary

All stations used in this study are shown in Figure 3.1. Hourly water level data can be obtained across the entire coast and from different geographic locations: (1) inner shelf (CSI-3, CSI5 and CSI-6); (2) bays (CP, LAP, LUML1, TAML1 and GISL1); (3) river estuaries (FCL, TMT, PF and PSTL1); (4) bayous (WBBG and FD). ADCP data are available from two WAVCIS stations (CSI-3 and CSI-6).

The data sets are summarized in Table 3.1. In general, WAVCIS and LUMCON stations have more instruments which can provides more parameters, while some NOAA stations can only provide water level data. The time-series are almost complete for some stations (e.g., FCL, CP, TMT and PF), but somewhat gappy for stations like LAP, GISL1 TAML1 (Figure 3.2). Moreover, the ADCP data from CSI-3 have a two-month gap from late September to middle November.

3.2 Methodology

3.2.1 Low-pass Filtering

In this study, a 6th-order Butterworth low-pass filter with a cutoff frequency at 0.6 cycles per day (CPD), or 40-hour long, is used to remove tidal oscillations in the time-series measurements. Figure 3.3 demonstrates the frequency response of the Butterworth filter in frequency domain. Note that oscillations with frequencies higher than 1 CPD are almost totally cut off, while the low-frequency signals less than 0.5 CPD (equivalent to period of 48 hours) are well retained. The Louisiana coast has dominant diurnal tides and the period of local inertial oscillation is around 24.7 hours, while cold fronts have recurrent periods of 3 to 7 days (Chuang and Wiseman, 1983; Li et al., 2009), which are longer than 48 hours. Therefore, this filter is very effective in the study of low-frequency, or subtidal oscillations.

3.2.2 Fast Fourier Transform (FFT)

The fast Fourier transform (FFT) is a method to convert dataset from the time domain to frequency domain. Different from traditional Fourier series method, FFT is an algorithm for the discrete Fourier transform using exponential forms instead of sine and cosine forms, which significantly increases the computational speed while still retaining the accuracy (Emery and Thompson, 2004). All gaps in the time-series are removed using a linear interpolation method before FFT. All calculations are implemented using MATLAB functions.

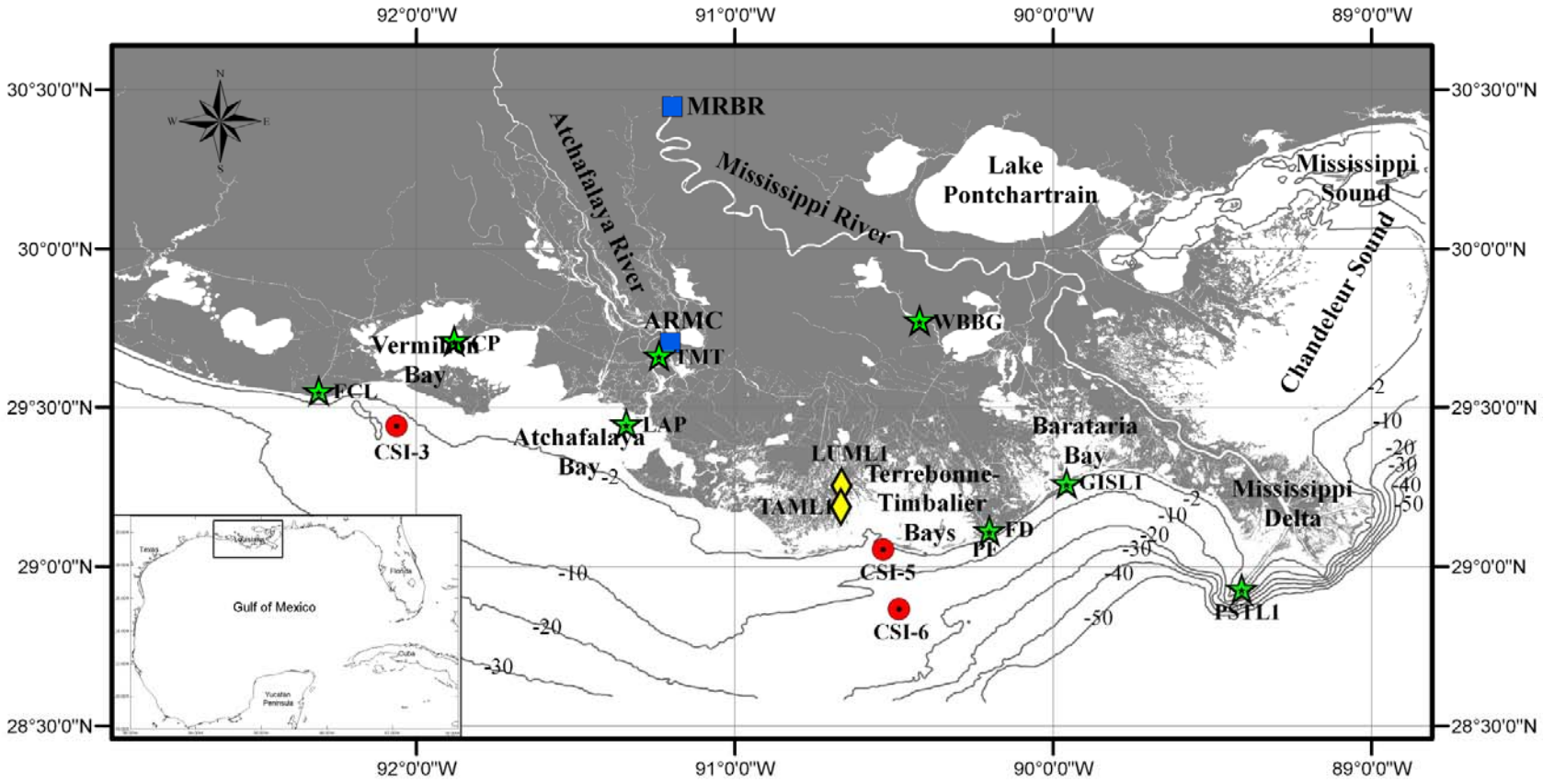

Figure 3.1 The Louisiana coast and observational stations in the northern GoM. NOAA, LUMCON, WAVCIS, and USGS stations are shown with stars, diamonds, circles, and squares, respectively. CP: Cypremort Point; LAP: LAWMA, Amerada Pass; FCL: Freshwater Canal Locks; TMT: Tesoro Marine Terminal; LUML1: LUMCON Marine Center; TAMIL1: Tambour Bay; PF: Port Fourchon; FD: Fourchon deployment; GISL1: Grand Isle; WBBG: West Bank Bayou Gauche; PSTL1: Pilot's Station East, SW Pass; MRBR: Mississippi River at Baton Rouge; and ARMC: Atchafalaya River at Morgan City, LA.

Table 3.1 Summary of data sources: WACIS, CO-OPS, NDBC, and LUMCON stations (stars mean data are available)

Station	Location		Observational Parameters							
	Longitude	Latitude	Wind	Barometric Pressure	Air Temperature	Humidity	Water Level	SST	Current	Wave
CSI-3	92°03.68'	29°26.47'	*	*	*	*	*	*	*	*
CSI-5	90°32.00'	29°03.20'	*	*	*		*	*		*
CSI-6	90°29.00'	28°52.00'	*	*	*		*	*	*	*
Cypremort Point	91°52.80'	29°42.80'					*			
Freshwater Canal Locks	92°18.30'	29°33.30'					*			
GISL1	89°57.40'	29°15.80'	*	*	*		*	*		
LAWMA Amerada Pass	91°20.40'	29°27.00'					*			
LUML1	90°39.80'	29°15.20'	*	*	*	*	*	*		
Port Fourchon	90°12.00'	29°06.90'					*			
Fourchon Deployment	90°11.04'	29°06.83'					*		*	
PSTL1	89°24.40'	28°55.90'	*	*	*	*	*	*		
TAML1	90°39.92'	29°11.25'	*	*	*	*		*		
Tesoro Marine Terminal	91°14.20'	29°40.00'					*			
West Bank Bayou Gauche	90°25.10'	29°46.60'	*	*	*		*	*		

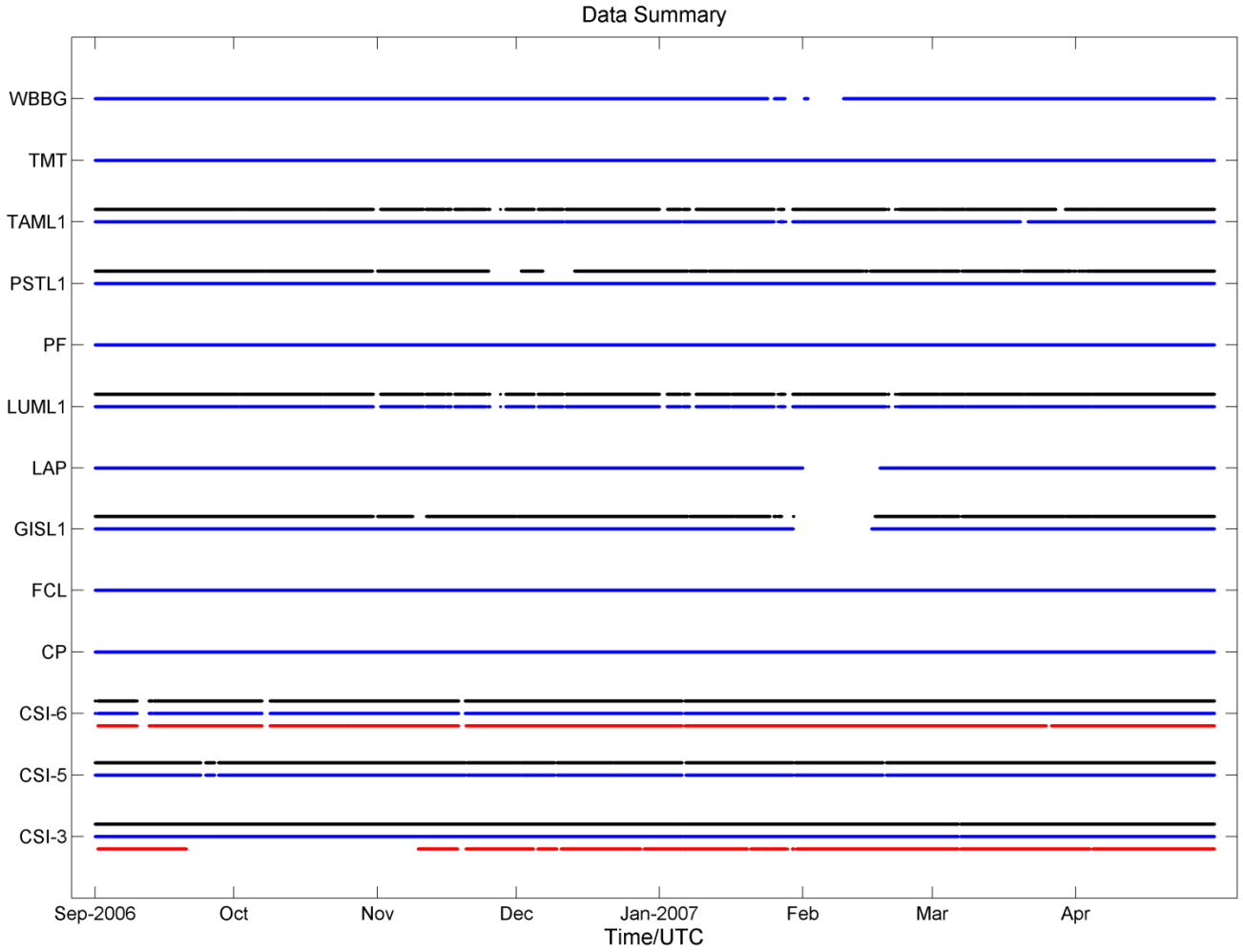

Figure 3.2 Data Summary (Time-series measurements are from September, 2006 to April, 2007. Blue, black and red lines represent water level, meteorological, and current data, respectively. Gaps indicate no data within the time periods)

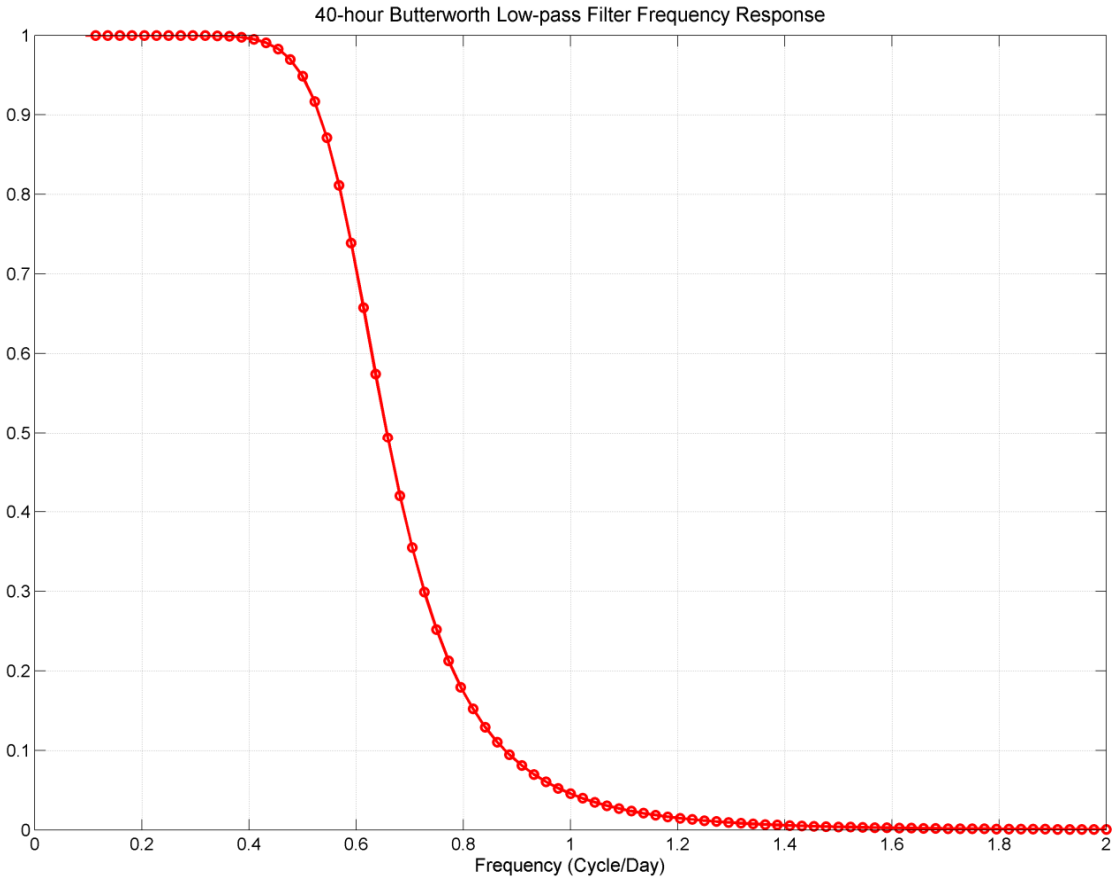

Figure 3.3 Frequency response of the 6th-order, 40-hour Butterworth low-pass filter

3.2.3 Rotary Spectra Analysis

The rotary spectra analysis is used to calculate the spectra of vectors (e.g., currents and winds) in a time series. In this study, the objective is to investigate the relative importance of wind-induced, tidal, and inertial oscillations. Raw wind and current data are first converted to east (u) and north velocity (v) components or a rotated coastal coordinate of cross-shore (u') and longshore (v') components (Emery and Thompson, 2004). The relationship is illustrated in Figure 3.4 and can be expressed in the following equations.

$$\begin{cases} u' = u\cos\theta + v\sin\theta \\ v' = -u\sin\theta + v\cos\theta \end{cases} \tag{3-1}$$

where the angle θ is the orientation of coastline rotated counterclockwise from the east direction.

For a single frequency (f) oscillation, the vector (w) and two components u and v can be expressed by:

$$w = u + iv \qquad i = \sqrt{-1} \tag{3-2}$$

$$u = a_1 \cos(2\pi ft) + b_1 \sin(2\pi ft) \tag{3-3}$$

$$v = a_2 \cos(2\pi ft) + b_2 \sin(2\pi ft) \tag{3-4}$$

The actual expression can be easily obtained by summing expressions of all frequencies.

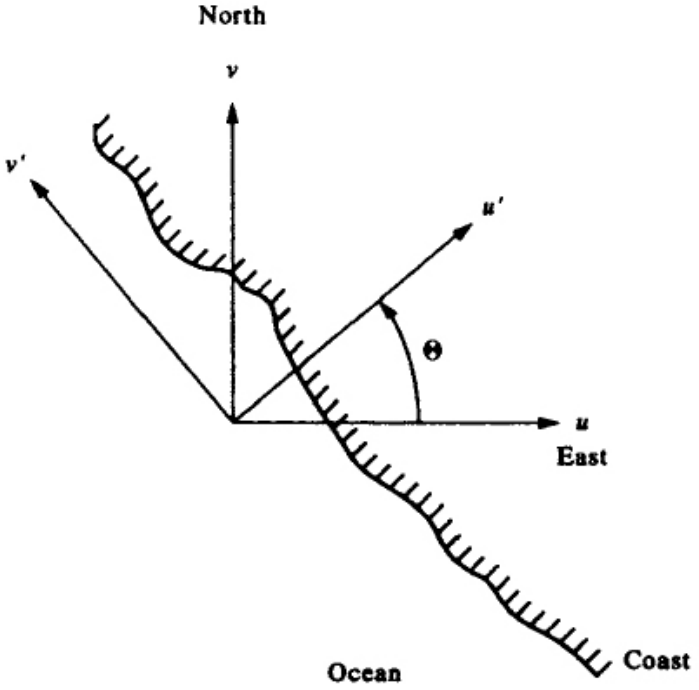

Figure 3.4 Rotation of an earth-referenced coordinate to a local coastal coordinate with cross-shore and longshore components (from Emery and Thompson, 2004)

(3-3) and (3-4) are transformed to exponential forms, and w becomes:

$$\begin{aligned} w &= (a_1 + a_2)\cos(2\pi ft) + (b_1 + b_2)\sin(2\pi ft) \\ &= (a_1 + a_2 i)\frac{e^{i2\pi ft} + e^{-i2\pi ft}}{2} + (b_1 + b_2 i)\frac{e^{i2\pi ft} + e^{-i2\pi ft}}{2} \\ &= \left(\frac{a_1 + b_2}{2} + i\frac{a_2 - b_1}{2}\right)e^{i2\pi ft} + \left(\frac{a_1 - b_2}{2} + i\frac{a_2 + b_1}{2}\right)e^{-i2\pi ft} \end{aligned} \tag{3-5}$$

Here, $\frac{a_1+b_2}{2}+i\frac{a_2-b_1}{2}$ and $\frac{a_1-b_2}{2}+i\frac{a_2+b_1}{2}$ are the complex amplitude of counterclockwise and clockwise component at f, respectively.

The counterclockwise (A) and clockwise (B) spectrum are:

$$A=\frac{1}{2}\sqrt{(a_1+b_2)^2+(a_2-b_1)^2} \quad (3\text{-}6)$$

$$B=\frac{1}{2}\sqrt{(a_1-b_2)^2+(a_2+b_1)^2} \quad (3\text{-}7)$$

All variables in (3-2) to (3-7) can be calculated in MATLAB through FFT algorithms.

3.2.3 Volume Exchange Flux Calculation

Assuming a quasi-steady state of water level in the entire bay and no other major source and sink of water, the volume exchange rates between a bay and the inner shelf were calculated by:

$$F=\frac{d\eta}{dt}\times A$$

where F is flux (m^3/s), η is water level (m) measured in the bay, or mean water level (m) if two or more stations can be obtained, t is time (s) in UTC, and A is the water body area of the bay (m^2).

The areas of the bays are measured by ArcGIS under the projection of WGS UTM1984 Zone 15N. The areas of the Atchafalaya-Vermilion Bays (AVB), Terrebonne-Timbalier Bays (TTB), and Barataria Bay (BB) are 2025.98, 892.48, and 570.11 km^2, respectively. Here, the total area of BB also includes Little Lake, which is directly connected to BB through a couple of bayous, but other lakes in the upper Barataria Basin are not taken into account. The volumes of the bays are also calculated, based on the DEM bathymetry data (1 arc second resolution) obtained from NOAA's NOS Estuarine Bathymetry database. The estimated total volumes of the AVB, TTB, and BB are 3.87×10^9, 1.30×10^9, and 6.33×10^8 m^3, respectively.

The subtidal volume exchange fluxes are finally achieved by applying a 40-hour 6th-order Butterworth low-pass filter with a cutoff frequency of 0.6 cycles per day.

3.2.4 Wind Stress Calculation

The wind stress is calculated from the quadratic law:

$$W = \rho_a C_d |u| u$$

where ρ_a is the density of air (1.3 kg/m^3), u is the wind velocity, and C_d is the drag coefficient for the ocean surface, which usually increases with wind speed (Gill, 1982). Here, C_d is determined by the following relationship (Gill, 1982):

$$C_d = \begin{cases} 1.1 \times 10^{-3} & for\ |u| \leq 6\ m/s \\ (0.61 + 0.063|u|) \times 10^{-3} & for\ 6\ m/s < |u| < 22\ m/s \end{cases}$$

CHAPTER 4 RESULTS

4.1 Cold Front Passages between September 2006 and April 2007

With climatological data, Roberts et al. (1987) categorized cold fronts as two end-member types: (1) arctic surge, which is less frequent, powerful, and moving southward; (2) migrating cyclone, which is accompanied by a strong low pressure cell. The essential differences are the orientation of the front related to the east-west Louisiana coastline, and the resultant behavior of the wind-driven surface waters (Roberts, 1987; Pepper and Stone, 2004).

In the present study, by examining the United States surface weather maps, twenty-nine cold front events are identified between September 2006 and April 2007 (Table 4.1). Note that only 4 events are arctic surges, while the remaining 25 are all migrating cyclones. For migrating cyclones, they usually move southeastward across the Louisiana coast, so the Atchafalaya/Vermilion Bays (AVB) are the first to be impacted by the cold fronts, followed by Terrebonne/Timbalier Bays (TTB) 3-4 hours later and Barataria Bay (BB) after about one more hour. Arctic surges affect the entire Louisiana coast almost simultaneously because the orientation of those fronts is typically parallel to the coastline (refer to Figure 2.7).

4.2 Water Level Variation

4.2.1 Amplitude Spectra of Water Level

A four-month time series of water level data from 12 stations for September to December 2006 is chosen to compute amplitude-frequency spectra. Before applying FFT, the original time series are linearly interpolated to remove some small gaps. Figure 4.1 shows the amplitude spectrum, covering the frequency range of 0-2.5 cycles per day (CPD). All stations except West Bank Bayou Gauche (WBBG) show dominant diurnal tidal signals. Two highest peaks have frequencies of 0.9265 and 1.0003 CPD, equivalent to periods of 25.90 and 23.99 hours, respectively. The third peak near 1 CPD has a frequency of 0.8937 CPD or an equivalent period

of 26.85 hours. Note that O1, K1, and Q1 tides have periods of 25.82, 23.93, and 26.87 hours, which are very close to the peaks identified from the spectra.

Table 4.1 Summary of cold front events passing through CSI-5 and CSI-6 between September 2006 and April 2007 identified from weather maps (MC: migrating cyclone; AS: arctic surge).

Month	Times of Events	Number	Time of cold front passage	Orientation of cold front related to coastline	End-member Type
September 2006	3	060901	09/19 1200Z	oblique	MC
		060902	09/25 0100Z	oblique	MC
		060903	09/29 0400Z	parallel	AS
October	4	061001	10/06 1800Z	parallel	AS
		061002	10/13 1200Z	parallel	AS
		061003	10/22 1200Z	oblique	MC
		061004	10/27 1600Z	oblique	MC
November	4	061101	11/02 0200Z	oblique	MC
		061102	11/07 1000Z	oblique	MC
		061103	11/11 1400Z	oblique	MC
		061104	11/15 2000Z	oblique	MC
December	4	061201	12/01 0200Z	oblique	MC
		061202	12/22 1400Z	oblique	MC
		061203	12/26 0700Z	oblique	MC
		061204	12/31 0300Z	oblique	MC
January 2007	4	070101	01/07 2000Z	oblique	MC
		070102	01/15 2300Z	oblique	MC
		070103	01/21 1900Z	oblique	MC
		070104	01/28 1500Z	oblique	MC
February	4	070201	02/09 1200Z	parallel	AS
		070202	02/13 2300Z	oblique	MC
		070203	02/17 2100Z	oblique	MC
		070204	02/25 1300Z	oblique	MC
March	3	070301	03/02 0100Z	oblique	MC
		070302	03/03 1000Z	oblique	MC
		070303	03/16 1700Z	parallel	MC
April	3	070401	04/04 1900Z	parallel	MC
		070402	04/14 2200Z	oblique	MC
		070403	04/26 1300Z	oblique	MC

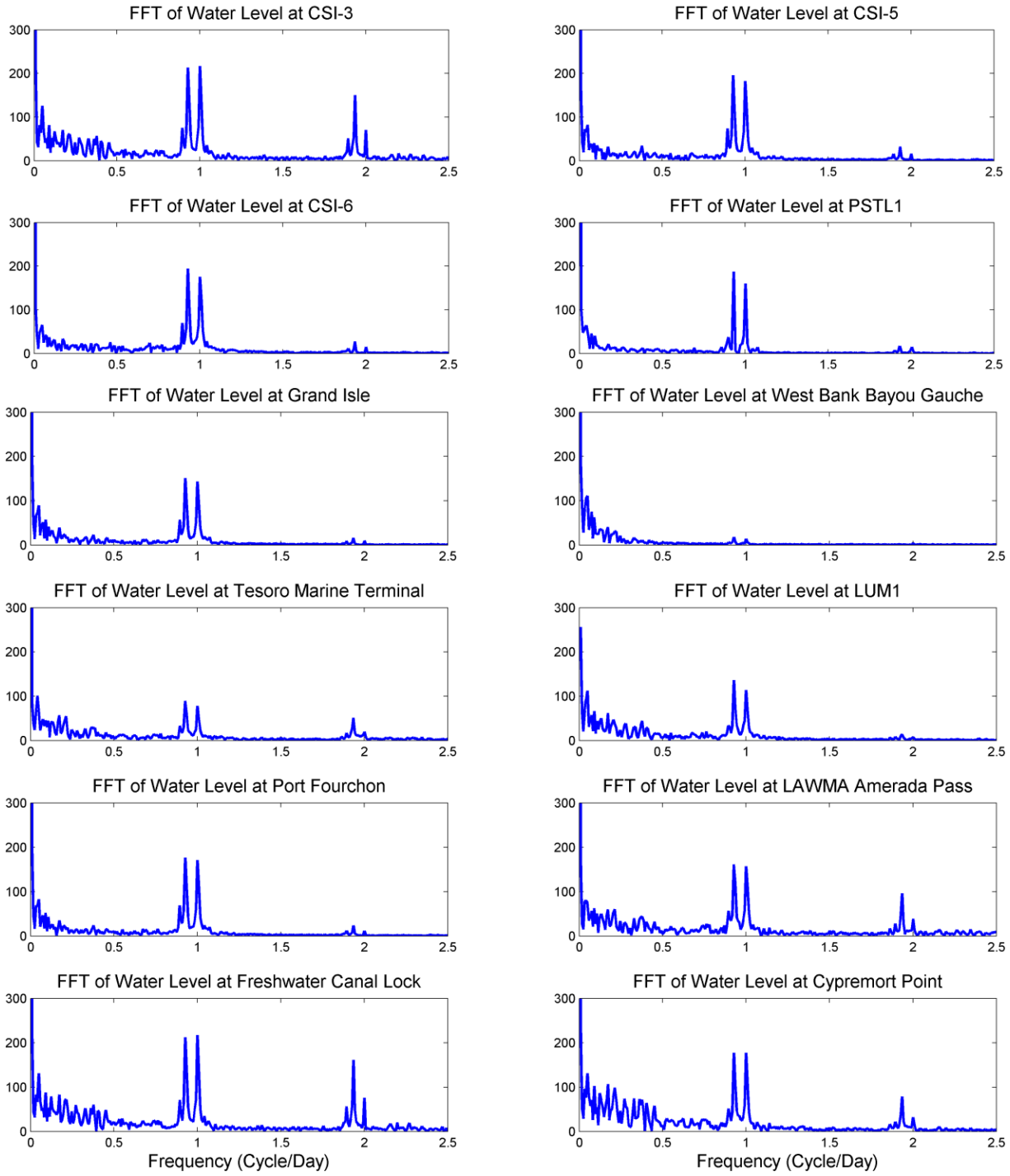

Figure 4.1 Amplitude spectra (0-2.5 CPD) of water levels at 12 stations.

Although semidiurnal tidal signals can be seen from the spectra of most stations, their energies are lower than diurnal tides. Three major peaks are identified with frequencies of 1.8941, 1.9351, and 2.0007 CPD, or periods of 12.67, 12.40 and 12.00 hours, which are very close to N2 (12.66

hours), M2 (12.42 hours), and S2 (12.00 hours) or K2 (11.97 hours) tides. Because S2 and K2 tides have very close frequencies, it is estimated that time-series measurements of 800 consecutive days are required to distinguish these two peaks. 4-month data sets cannot separate these frequencies, which is not important for the current study.

Station WBBG is located in the upper Barataria Basin, and more than 50 km upstream of Barataria Bay, with two barely identifiable small peaks of diurnal tides. Low-frequency fluctuations less than 0.5 CPD are dominant. Tesoro Marine Terminal (TMT) is about 30 km upstream of Atchafalaya River mouth, where the diurnal and semidiurnal tidal signals are both relatively lower.

Within the semidiurnal frequency band, five stations, including CSI-3, TMT, LAWMA Amerada Pass (LAP), Freshwater Canal Lock (FCL) and Cypremort Point (CP), have relatively higher semidiurnal signals than the others. The amplitudes of highest semidiurnal peaks account for 44% to 70% of those of diurnal peaks. Also note that all these stations are west of 91°W, inside, offshore or west of Atchafalaya-Vermilion Bays. CSI-3 is located near the 5 m isobath on the inner shelf south of Vermilion Bay, and FCL is near the mouth of Freshwater Bayou Canal, just west of Vermilion Bay. These two stations have the largest semidiurnal tidal signals. CP and LAP, which are inside Vermilion Bay and Atchafalaya Bay, have relatively lower semidiurnal tidal signals. These results are consistent with current meter records that areas southwest of the Atchafalaya Bay have the largest M2 tidal current of the entire Louisiana-Texas shelf (DiMarco and Reid, 1998).

Figure 4.2 illustrates the amplitude spectra of water level, which are zoomed into the lower frequency range of 0-0.5 CPD, since the frequencies of cold-front-induced oscillations are usually less than 0.5 CPD (Li et al., 2009). Unlike tidal oscillations, cold-front-induced oscillations do not have stable or fixed frequencies. In general, the energy of most stations

distributes throughout the low frequency range, covering the recurrent frequencies of cold front events (i.e., equivalent periods of 3 to 7 days).

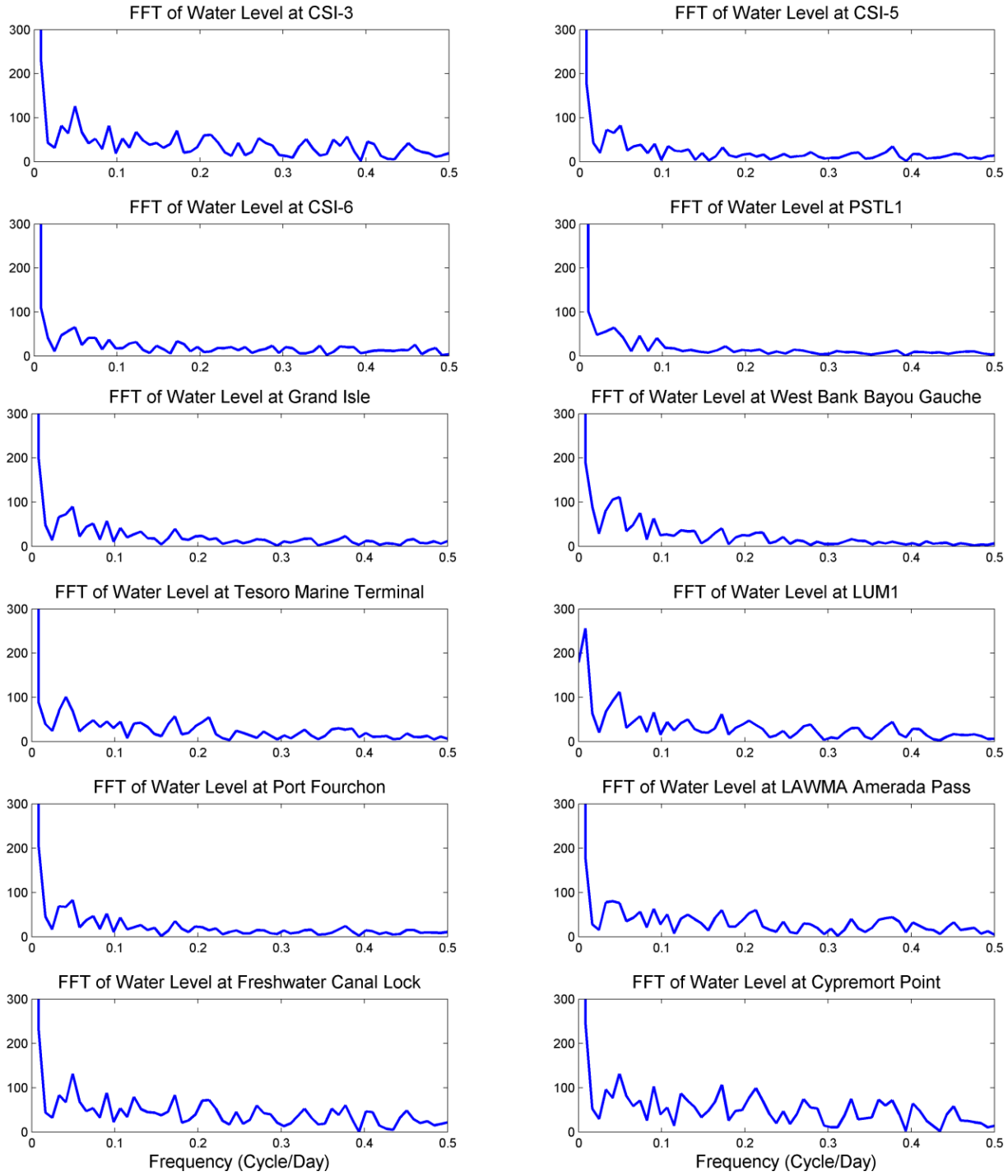

Figure 4.2 Amplitude spectra (0-0.5 CPD) of water levels at 12 stations.

The spectra of FCL and CP seem similar in the low frequency range although they are located differently, which may suggest that subtidal water levels of the two stations respond to wind forcing closely. The spectrum of LAP is slightly different and its amplitude is lower than that of CP, although both stations are in the AVB. It may be explained by the geographic differences: CP is surrounded by the bay systems with shallow depth, while LAP is more open to the inner shelf and deeper.

4.2.2 Subtidal Water Level Variation

The general subtidal (low-frequency) wind-induced oscillations can be clearly illustrated by low-pass filtered water level curves. Figure 4.3 demonstrates the measured (blue lines) and subtidal (red lines) water levels at CSI-3, CSI-5, and CSI-6. Although all three stations show similar low-frequency oscillation patterns, the variability of CSI-3 is highest while that of CSI-6 is lowest. This is mainly due to differences of water depth: the mean depths of CSI-3, CSI-5, and CSI-6 are roughly 5, 6, and 20 m. Shallow water seems more sensitive to wind forcing. Also note that cold front events (dashed vertical lines) coincide with major set-up and set-down of water level. The pre-frontal winds from southern quadrant pile up the water masses. After cold fronts pass through the stations, northerly winds dominate and water level is abruptly set down by the reversed wind stress. The variability between different events is large. The magnitudes range between less than 0.1 m and close to 1 m, depending on the strength of the cold front events and wind stress, direction and duration.

Figure 4.4 shows the measured and subtidal water levels at Port Fourchon (PF), Grand Isle (GISL1), and WBBG. It can be clearly seen that the tidal oscillations at WBBG are minimal while wind-induced subtidal oscillations dominate. Moreover, the low-pass filtered water level curves of all three stations show very similar patterns, which also support the idea that the low-frequency oscillations are mainly wind-induced because synoptic winds have larger spatial scales.

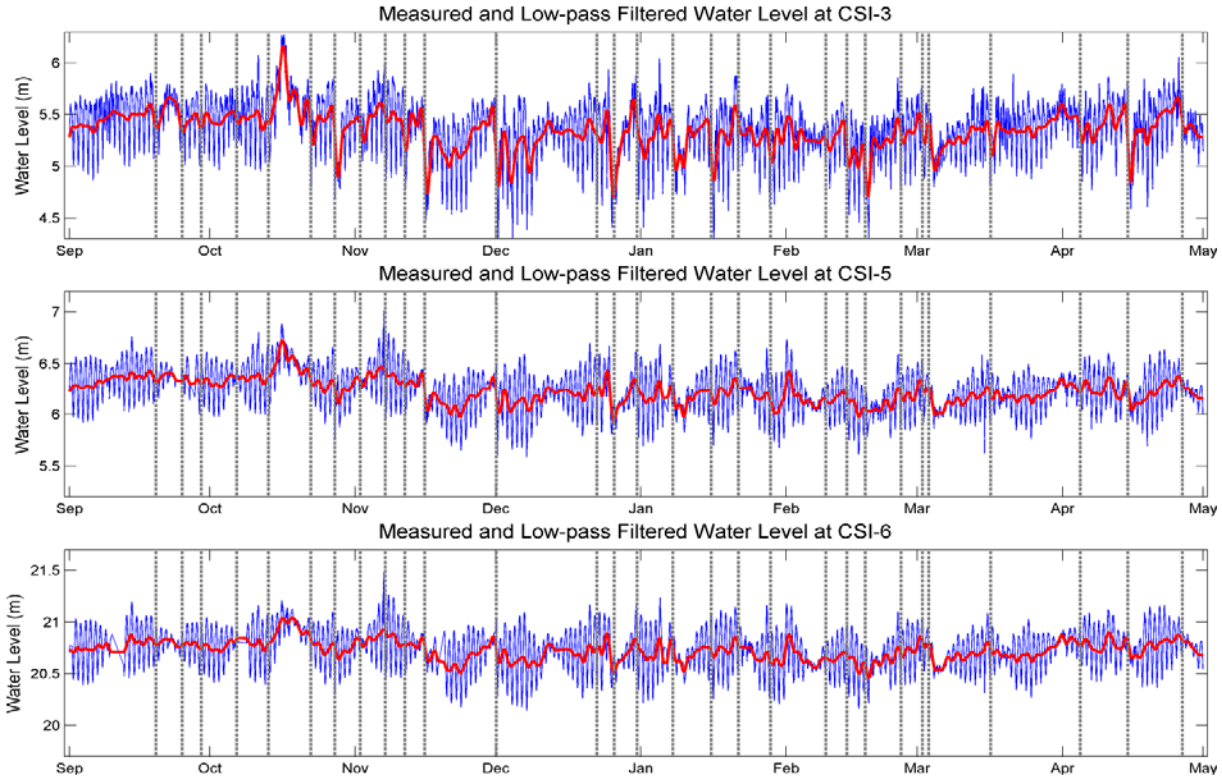

Figure 4.3 Measured and subtidal water levels at Station CSI-3, CSI-5 and CSI-6 from September 1, 2006 to April 30, 2007. Vertical lines indicate time of cold front passages.

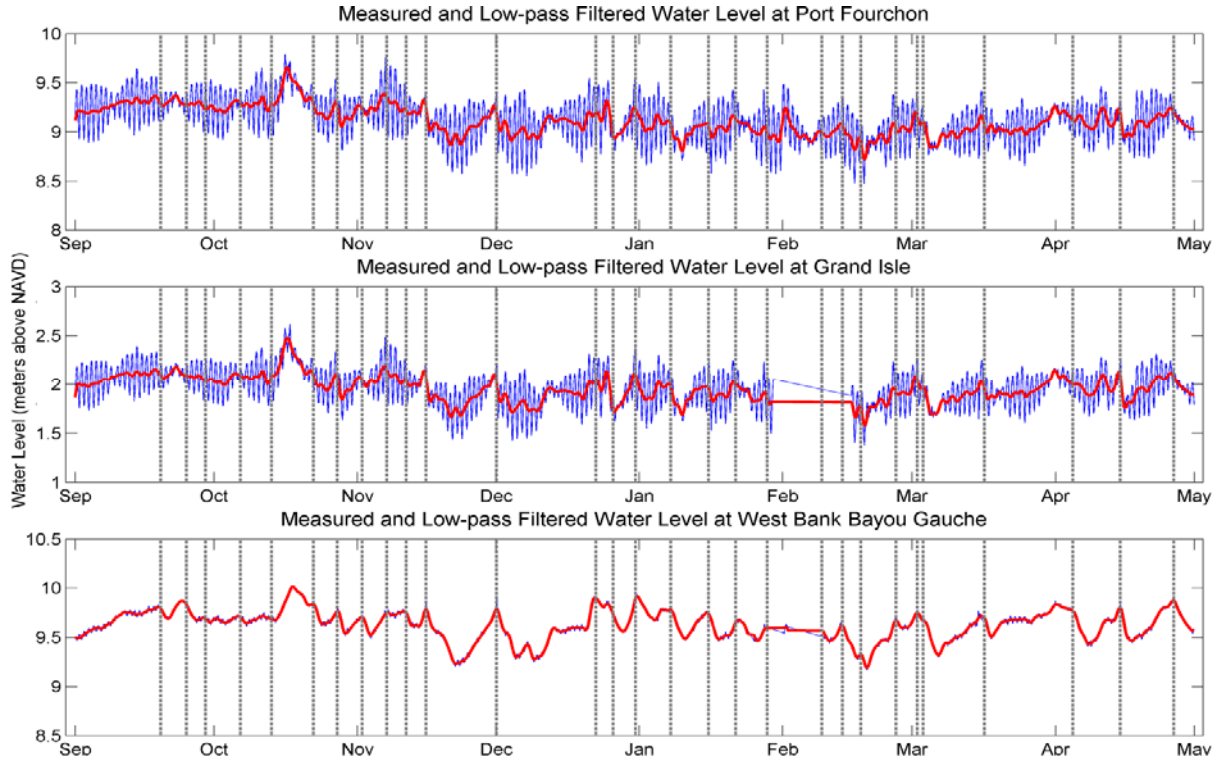

Figure 4.4 Measured and subtidal water levels at Station Port Fourchon (PF), Grand Isle (GISL1), and West Bank Bayou Gauche (WBBG) from September 1, 2006 to April 30, 2007. Vertical lines indicate time of cold front passages.

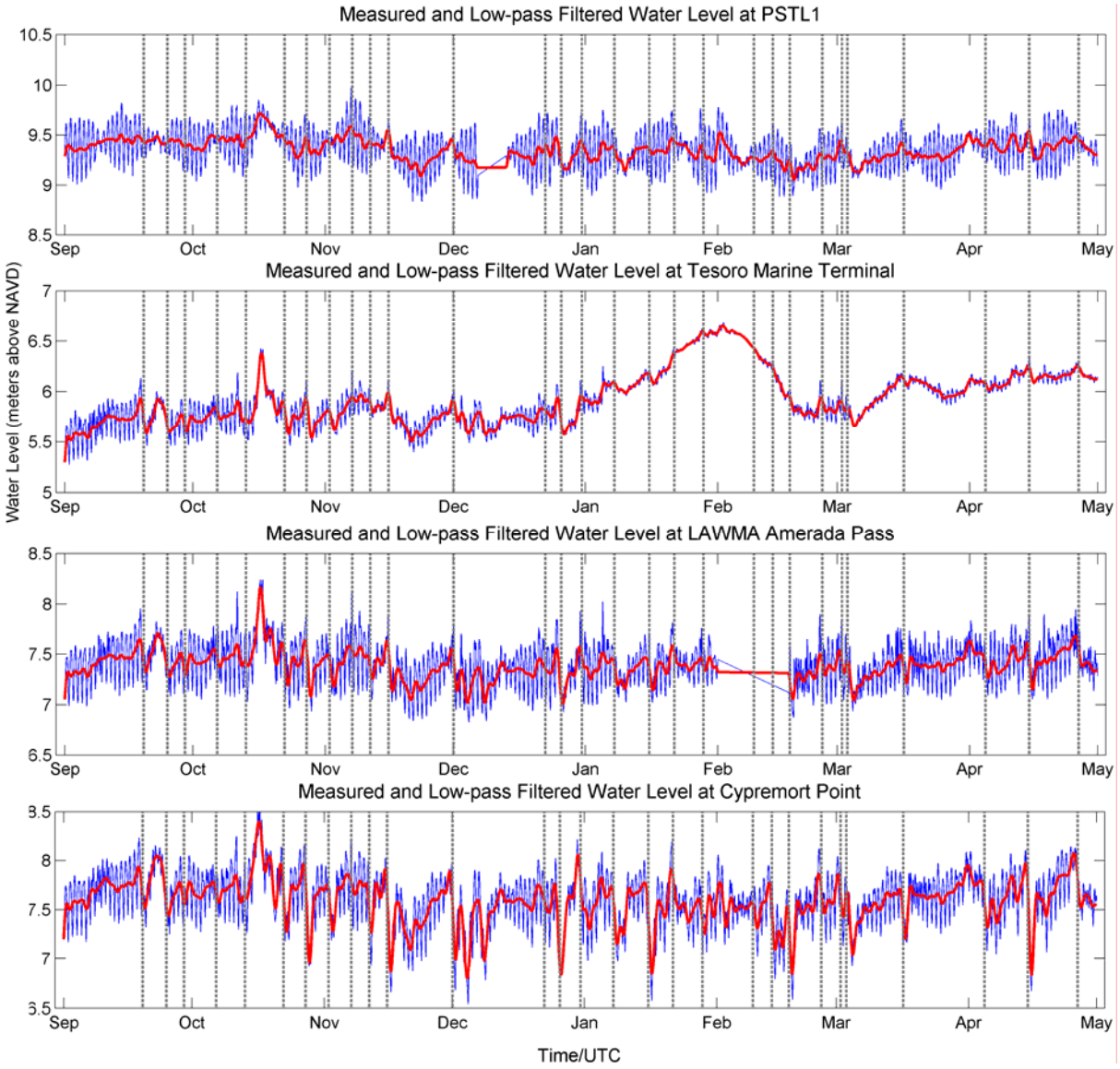

Figure 4.5 Measured and subtidal water levels at PSTL1, Tesoro Marine Terminal (TMT), LAWMA Amerada Pass (LAP) and Cypremort Point (CP) from September 1, 2006 to April 30, 2007. Vertical lines indicate time of cold front passages.

Figure 4.5 illustrates the measured and subtidal water levels at PSTL1, TMT, LAP and CP. There is a period between middle January and middle February, when the water stage is abnormally high at TMT, a station inside the channel of the Atchafalaya River. Such high water stage coincides with the highest river discharge in Mississippi and Atchafalaya Rivers during the same period (Figure 4.6). Other components at higher frequencies are almost overwhelmed by the river flood. Furthermore, the second highest water stage in the middle March also agrees with

the second highest river discharge record. Nevertheless, river discharge seems to have less influence at the other two stations, LAP and PSTL1, which are located at the mouth of Atchafalaya River and Southwest Pass of Mississippi River, respectively.

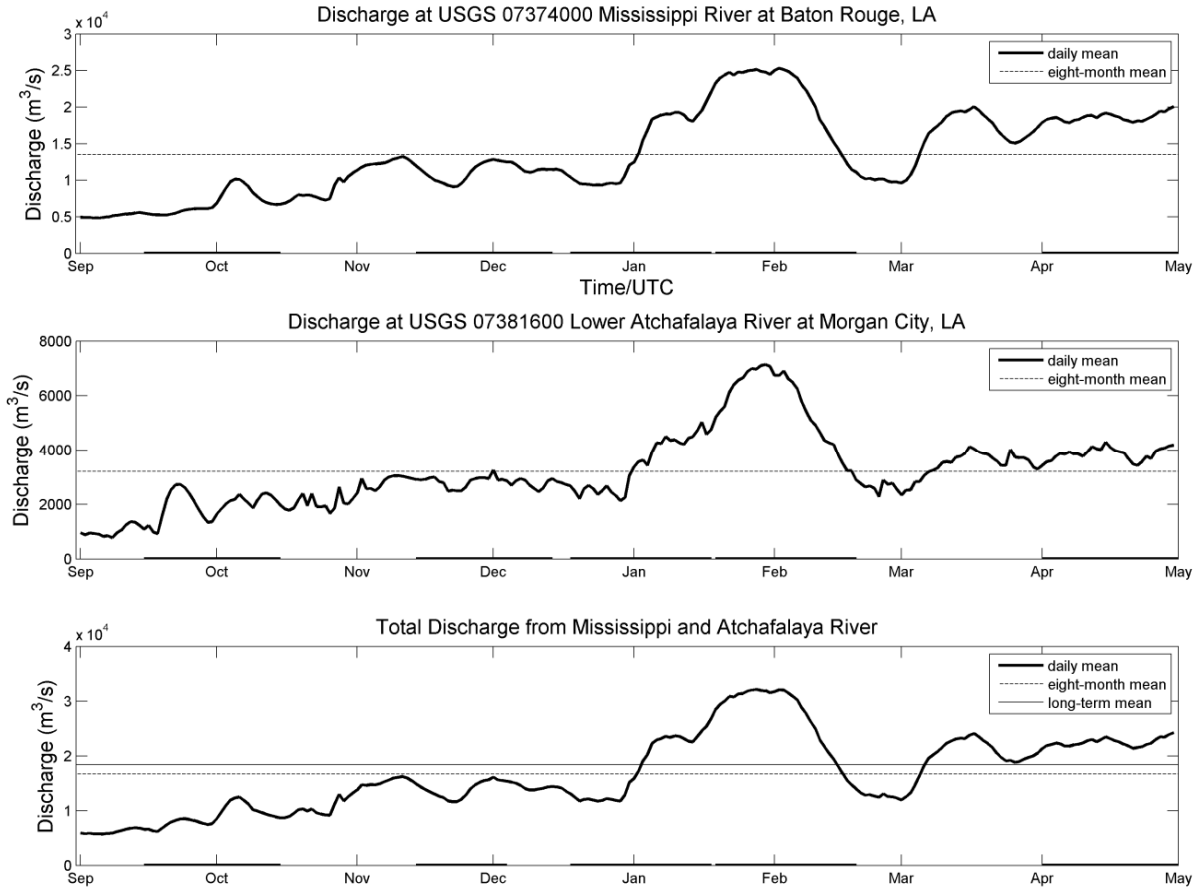

Figure 4.6 Daily mean discharge of Mississippi River (upper panel, measured at Mississippi River at Baton Rouge, LA or USGS 07374000, which is downstream of the Old River control structure), Atchafalaya River (middle panel, measured at Lower Atchafalaya River at Morgan City, LA or USGS 07381600), and total discharge (lower panel) from September 1, 2006 to April 30, 2007. The parallel dashed lines are eight-month mean discharge, and parallel solid line in the third panel indicates long-term mean Mississippi and Atchafalaya river discharge (i.e., 18400 m3/s; Milliman and Meade, 1983).

There is an obvious and distinct wind surge event shown in the water level curves of all stations. The highest water level is recorded in October 16th, 2006. The wind surge event occurs between two successive cold front passages, caused by strong, persistent and long-fetch winds (magnitude near or large than 10 m/s) from south or southeast quadrants for 2-3 days (Figure 4.7).

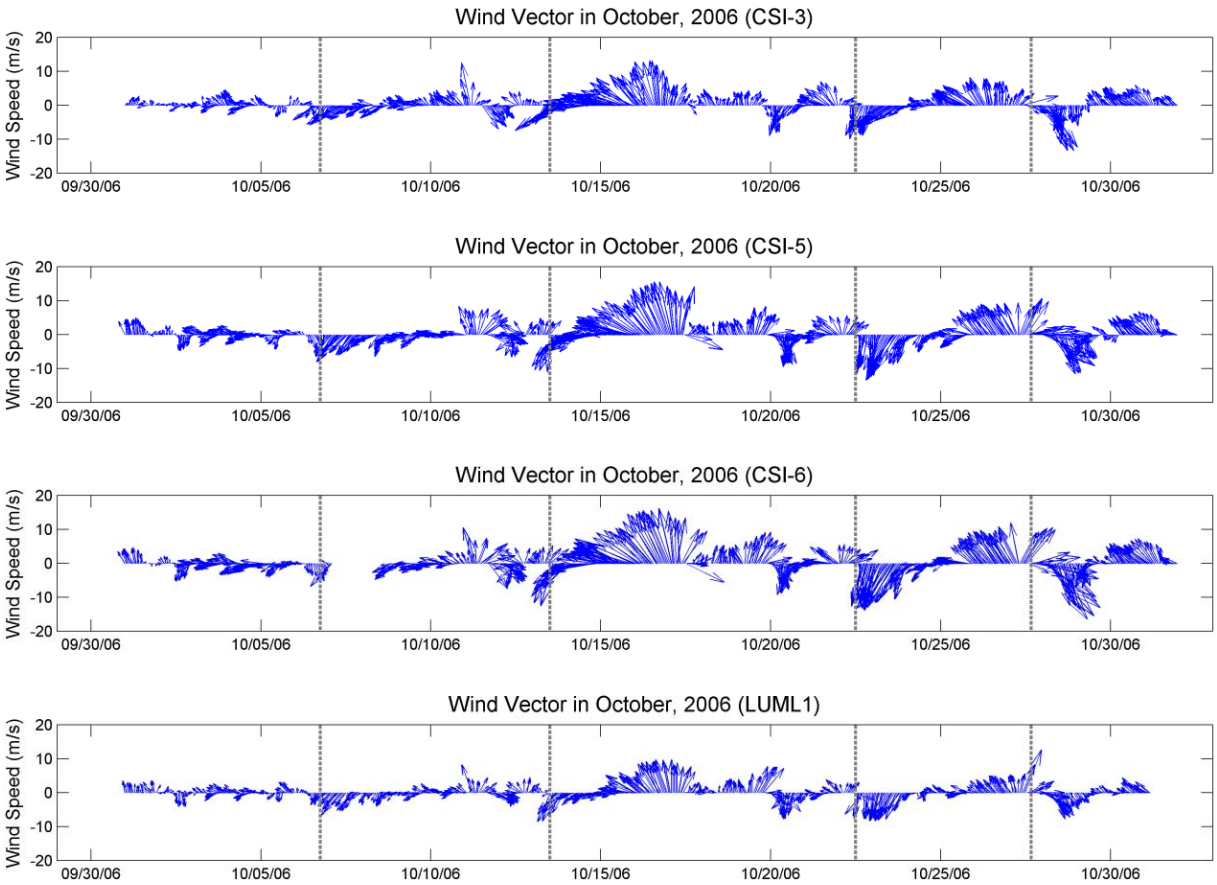

Figure 4.7 Wind vector at CSI-3, CSI-5, CSI-6, and LUML1 during October 2006. The winds are plotted in vector format that points to direction of motion. Vertical lines indicate time of cold front passages.

4.3 Cold-front-induced Bay-shelf Water Exchange

Cold-front-induced bay-shelf water exchange is quantitatively studied for the three major bay systems along the Louisiana coast west of the Mississippi Delta: AVB, TTB and BB (Figure 3.1). Subtidal volume exchange rates are calculated from time-series measurements of water level (Figure 4.8). In general, the subtidal water fluxes show a similar pattern in all the three bays, but with different orders of magnitude. The AVB have the largest flux amplitude, which is approximately 4 times of that of TTB, and an order of magnitude higher than that of BB. Such differences can be explained by two factors: water body area and basin geometry. The AVB has the largest area, which is roughly 2.3 and 3.6 times of those of TTB and BB. Basin geometry also

influences the magnitude of water exchange. The AVB has a much wider open boundary with Atchafalaya Bay directly open to the Gulf of Mexico; while the TT and BB are protected by barrier island chains, preventing large amount of water exchange between the bays and the inner shelf.

Cold front passages (vertical lines in Figure 4.8) coincide with the timing of the outward flushing of the bays, but the rates of flushing vary with different cold fronts. In addition, most major flush-out events are associated with cold fronts, except two events in the middle of October and two events in the beginning of December. Prior to the two events in October, a wind surge event is induced by strong, persistent and long-fetch onshore winds (speed near or large than 10 m/s) that blow for 2-3 days from southern or southeastern quadrants (Figure 4.7). The water level is piled up by about 0.8 m at both LAP and CP. The subsequent rapid decrease in water level may be a result of the weakening winds and the barotropic pressure gradient between bays and shelf waters. The two events in December follow a major cold-front-induced flushing event, and are mainly induced by strong offshore winds. Between two water level drops, the subtidal water levels rebound for two days when the winds are weakened and reversed to southeasterly.

To better understand cold front process, the five largest flushing events are isolated for more in-depth analysis (vertical solid lines in Figure 4.8). One interesting finding is that all these events are associated with migrating cyclones, and the cold fronts pass through three bays from west to east at right angles to the coastline. This finding suggests that wind direction plays an important role in determining the water flushing rate. There are two mechanisms which may explain such large exchange rates: (1) transport due to offshore-wind-induced set-down; (2) Ekman pumping due to alongshore northwest winds. Figure 4.9 shows cross-shore and alongshore components of low-pass filtered winds, measured at CSI-3 (16 km south of Vermilion

Bay). Note that during these events, cross-shore wind component abruptly changes from positive to negative, illustrating the abrupt reverse of wind direction from south to north. This phenomenon indicates that the conditions suddenly switch from inflow favorable onshore winds to outflow favorable offshore winds. Also note that strong and persistent northwest wind components are correlated with these events, which suggested that the Ekman effect appears to be important.

The AVB is selected as an example to examine the relationship between winds, subtidal water level and subtidal volume flux, associated with the five extreme events (Figure 4.10). The responses of low-frequency water level to all the major cold fronts show similar patterns, except the fourth event. Due to the Ekman pumping effect, the water level starts to drop 6-9 hours prior to the frontal passage when wind direction gradually rotates clockwise. The outflux reaches the maximum 8-11 hours after the frontal passage caused by the persistent and strong northwest winds (>10 m/s), and then decreases with the weakening of wind stress and further clockwise rotation of wind direction. The northwest/north winds appear to be the most effective forcing in flushing water out of the bays, which agree with previous satellite imagery and numerical model studies that the northwest winds maximized bay flushing and the Atchafalaya River plumes (Walker and Hammack, 2000; Cobb et al., 2008b).

The wind regime and subtidal water level variation during event 4 are different from the others. As the low pressure system located in the northern Kentucky intensifies, the distinct cold front forms at around 0300Z December 26, extending from Kentucky to the eastern Louisiana. Only three hours after the formation, the front moves eastward and leaves Louisiana. Although the front influences the study area, it does not actually pass through the middle and western Louisiana, including the AVB. As a result, the wind variation is different from a typical cold front passage.

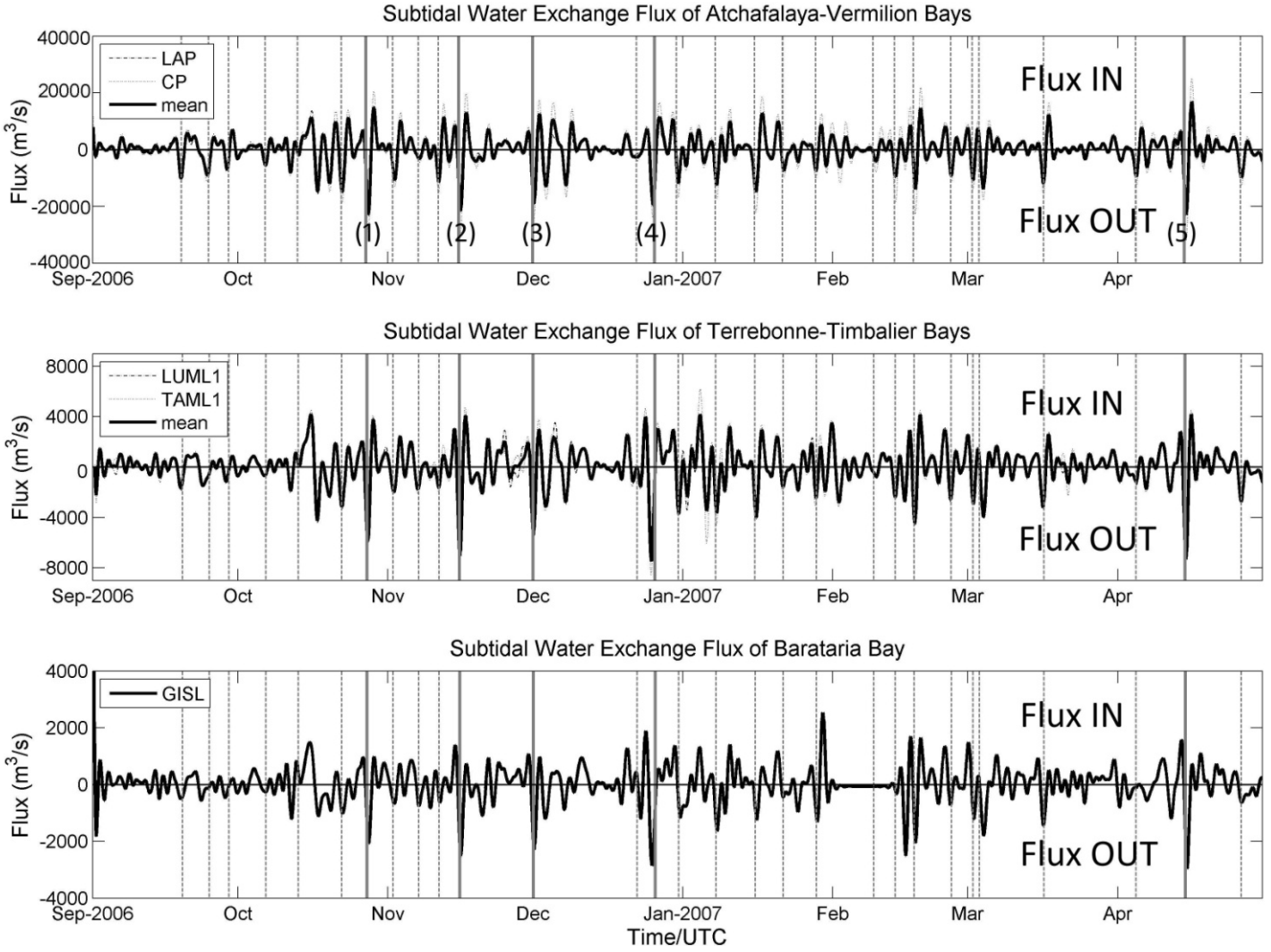

Figure 4.8 The subtidal water exchange flux of the Atchafalaya/Vermilion Bays (upper panel), the Terrebonne/Timbalier Bays (middle panel), and the Barataria Bay (lower panel) from September 2006 to April 2007. The positive and negative values correspond to flux in and out, respectively. Vertical lines indicate time of cold fronts passing through the bays, and the solid thick lines are cold fronts associated with five largest flush-out events (numbered from 1 to 5 in the time sequence).

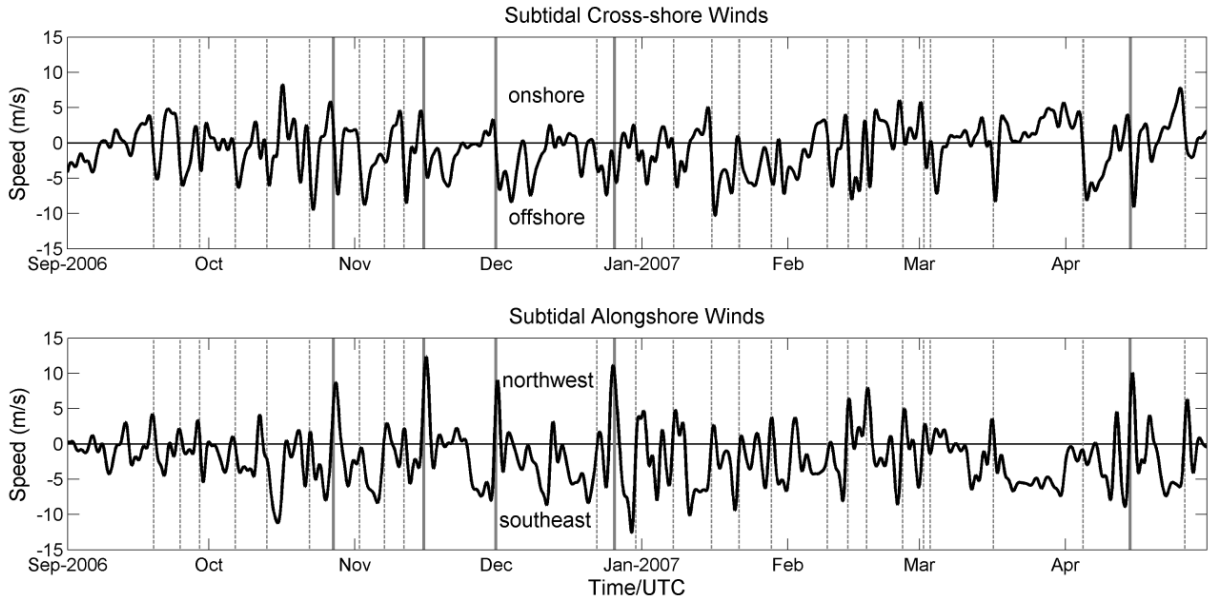

Figure 4.9 Subtidal cross-shore wind (upper panel), and alongshore (lower panel) of winds that measured at CSI-3. The axis of onshore wind is 24° clockwise rotated from the north direction.

In addition, high air pressure and considerably strong winds from northern quadrants dominates since the passage of the previous front. Subtidal water level decreases with the switch of wind direction from northeast to northwest, mainly due to the Ekman transport. With the strengthening of wind stress, the outflux gradually increases to the peak value of 19530 m^3/s about 7 hours before the frontal formation. The wind direction reverses to southeasterly one day after the frontal formation, but the water level starts to rebound 15 hours prior to the wind reversal, which may be related to the weakening of wind stress and barotropic pressure gradient between shelf and bay, as well as the east wind components. Previous study suggested that the shallow water of Atchafalaya Bay and adjacent shelf was more sensitive to cross-shore wind stress than alongshore wind stress (Chuang and Wiseman, 1983), but our study indicates that within the AVB strong alongshore wind may also drive considerably large water level variation through Ekman process.

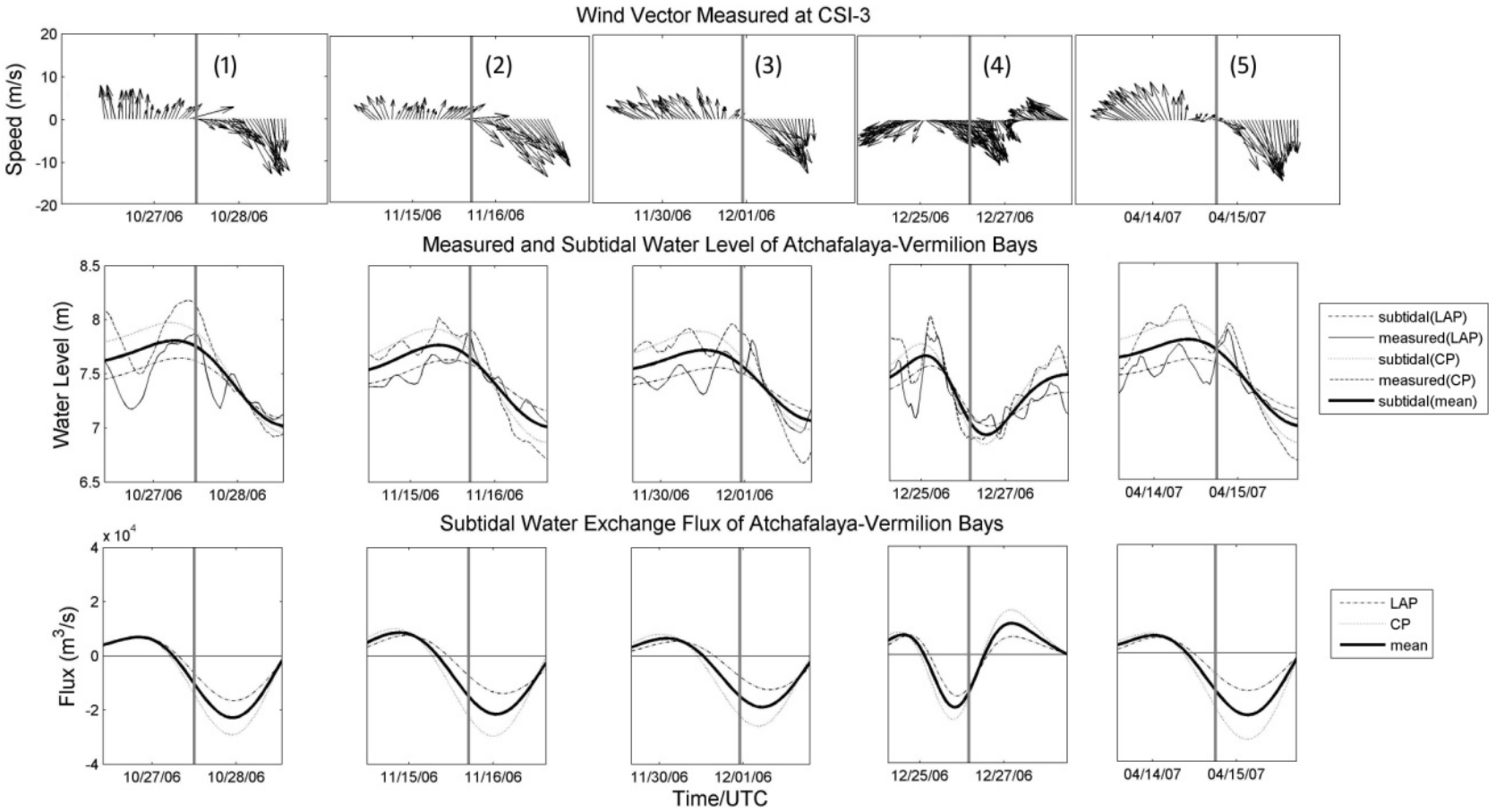

Figure 4.10 Wind vectors (upper panels), measured and subtidal water level (middle panels), and subtidal water exchange flux (lower panels) of the Atchafalaya-Vermilion Bays, associated with the five largest flush-out events. The winds are plotted in the standard oceanographic vector orientation that points to the blowing direction

The amounts of total water volume flushed out by cold fronts are compared with the total volume of the bays (Table 4.2). The flushing lasts for 31-33 hours, except event 4, which is several hours longer. The flushed volume during event 4 is also larger than other events. For the AVB, 34.4% to 41.9% of the total bay waters are flushed out by these five events. For the TTB, the range is slightly wider, from 28.5% to 44.9%. The upper (37.8%) and lower limits (23.7%) for the BB are both the smallest, which suggests that this system is the least favorable to water exchange. In short, strong cold front events may flush more than 40% of the bay waters onto the shelf within a less than 40-hour period. The bay waters are usually rich in nutrients and organic matter, which may impact ecological activities on the adjacent shelf. Previous satellite imagery study revealed that westward Atchafalaya flow during cold front passages stimulated high chlorophyll-a concentrations and primary productivity on the shelf area southwest of Atchafalaya Bay (Walker and Rabalais, 2006).

Table 4.2 The length of time and total volume and percentage of volume flushed out during five selected events (the numbers in the brackets also include the effect from Atchafalaya River discharge).

Event	Parameters	AVB	TTB	BB
1	Time (h)	32	32	33
	Volume (km^3)	-1.60 (-1.85)	-0.415	-0.15
	Percentage (%)	41.3 (47.8)	31.9	23.7
2	Time (h)	32	32	34
	Volume (km^3)	-1.54 (-1.88)	-0.491	-0.18
	Percentage (%)	39.8 (48.1)	37.8	28.9
3	Time (h)	32	32	33
	Volume (km^3)	-1.33 (-1.69)	-0.371	-0.16
	Percentage (%)	34.4 (43.7)	28.5	25.9
4	Time (h)	35	36	39
	Volume (km^3)	-1.48 (-1.81)	-0.584	-0.24
	Percentage (%)	38.2 (46.8)	44.9	37.8
5	Time (h)	32	31	33
	Volume (km^3)	-1.62 (-2.10)	-0.510	-0.21
	Percentage (%)	41.9 (54.3)	39.2	33.3

The river discharge, which is not included in the previous estimation, may serve as a major water source for the AVB because approximately 30% of the total Mississippi River water is discharged through the Atchafalaya River (Walker and Hammack, 2000). For the study periods, the daily mean discharge measured at Lower Atchafalaya River at Morgan City, LA (USGS 07381600) is 3,300 m^3/s, equivalent to a flushing time of 13.6 days. The maximum discharge (~7,000 m^3/s) occurs in the late January and early February (Figure 4.6). River discharge contributes additional amount of freshwater of 0.25, 0.34, 0.36, 0.33, and 0.48 km^3 during the same periods as the five events. The total flushed volume from the combined effects of winds and river discharge can account for about half of the bay volume (Table 4.2).

The impacts of other factors (e.g., rainfall, evaporation, and runoff) are usually minor. However, the opening of the man-made Davis Pond Freshwater Diversion, which is located in the upper Barataria Basin and intended to rebuild marshes and relieve Mississippi River flood, may introduce a substantial amount of freshwater from the Mississippi River to the Barataria Basin during the major floods. On November 30 and December 1, 2006, the daily mean discharge measured at Davis Pond Freshwater Diversion near Boutte, LA (USGS 295501090190400) was 133 and 113 m^3/s. The total freshwater volume flowing into the Barataria Basin during event 3 was 0.014 km^3, or 2% of the volume of BB. Particularly, the maximum daily mean discharge through the diversion could reach 323 m^3/s during spring 2008 of the great Mississippi River flood. Therefore, occasionally diverted Mississippi water may influence the Barataria Basin.

4.4 The Relationship between Winds, River Discharge and Currents

4.4.1 Synoptic Features

Wind data from CSI-6 are compiled to plot wind rose (Figure 4.11). In the eight-month period, four most frequent winds are from east, northeast, southeast, and north directions, occuring about

21%, 20%, 18%, and 15% of the time, respectively. Winds from all other directions occur less than 10% of the time. Strong winds of speed more than 10.0 m/s are very rare, only being observed from two directions: northwest (~0.1%) and west (~0.05%). Those winds are mostly associated with cold front passages (Walker and Hammack, 2000). Wind roses also show large monthly variabilites, suggesting that Louisiana coastal winds vary significantly throughout the year. In September, south wind is the most frequent (~20%), followed by northeast (~19%) and north (~17%) winds. Winds in this month are also weak, when they are less than 6.0 m/s in more than 96% of the time. In October, east winds are the most prevalent, occuring about 28% of the time and followed by southeast (~21%) and northeast (~13%) winds. The strong winds (>10 m/s) are only northwesterly, usually observed immediately after cold front passages. East (~22%), northeast (~18%), north (~17%), southeast (~17%), and northeast (~13%) winds are the five most prevalent winds in November. The wind roses of December and January are similar, when northeast winds are the most prevailing, occurring about 29% and 35% of the time. However, east winds in January are less frequent than those in December. The frequencies of occurrence in Febuary follow such sequence: northeast (~20%) > north (~18%) > southeast (~15%) > east (~14%) > west (~9%) > northwest (~6%) > southeast (<6%). Winds in this month are relatively weak with nearly 96% of time less than 6.0 m/s. The predominant winds in March is from east and southeast, occurring about 39% and 28% of the time, respectively. In April, five most frequent winds are: southeast (~21%), east (~18%), northeast (~16%), south (~12%), and north (~11%). The frequencies of occurrence of other winds are less than 10%.

In this study, two bottom-mounted ADCPs are used to examine the relationship between winds, river discharge and current field. These ADCPs are in different geographic locations. CSI-6 is located near the 20-m isobath south of Terrebonne Bay, which may be influenced by the freshwater advected westward from Southwest Pass of the Mississippi River. CSI-3 is near the 5-

m isobath south of Vermilion Bay, generally within the influencing area of the Atchafalaya River plume (Walker and Hammack, 2000).

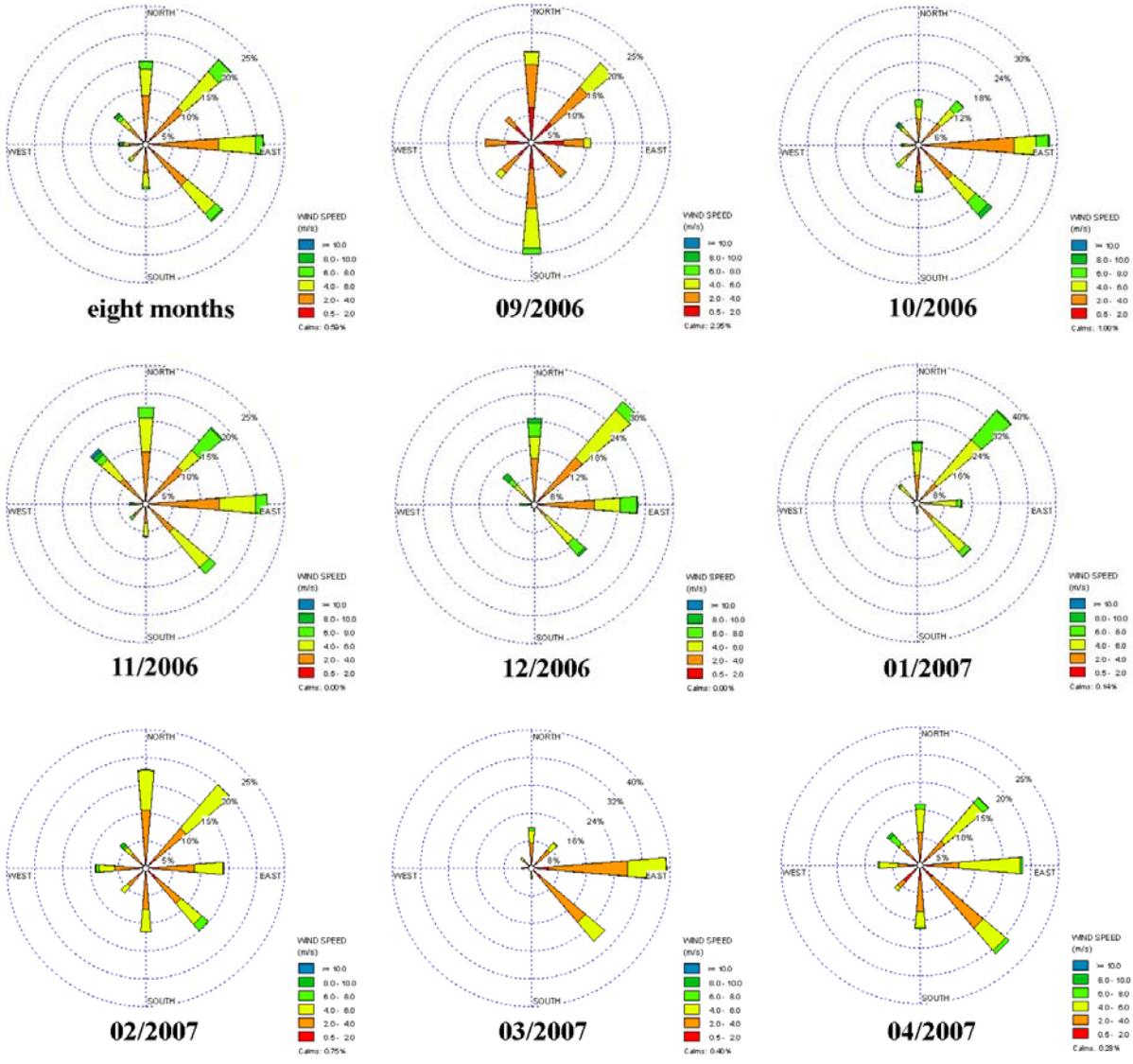

Figure 4.11 Monthly wind roses compiled from CSI-6 wind data from September, 2006 to April, 2007 (Courtesy of Lakes Environmental Software for providing WRPLOT software). Percentage frequencies are shown for each 45° wind delineation.

The contour of subtidal current clearly demonstrates that the westward component dominates the entire eight months (Figure 4.12 and 4.13). During the eight-month period, the down-coast flow occurs 81% and 70% of the time at CSI-6 and CSI-3, repectively. This alonghore down-coast flow is know as the Louisiana Coastal Current (LCC) (Wiseman and Kelly, 1994; Rouse et

al., 2004; Rouse et al., 2005; Walker, 2005), which forms the inshore limb of a cyclonic gyre, the prevailing low-frequency circulation on the LATEX shelf (Cochrane and Kelly, 1986). At CSI-6, the near-surface current is much stronger than the mid-layer and near-bottom current during most of the time (Figure 4.12). The strongest current is found within 0.5-1 m below the surface. The magnitude of north/south component is slightly smaller than that of east/west component. Strong cold front events may disturb the westward flow system, which is illustrated in the contour as color changes from light or dark blue to yellow or red during some short periods. Surface current direction adruptly switches to eastward, lasting for 1-3 days. The westward flow then reestablishes untile the coming of next storms. Note that during the winter storm around December 26, the current reverses direction throughout almost the entire water column, which suggestes strong vertical mixing by wind-induced shear. Previous observations also indicated that shelf waters could be well mixed to about 100 m depth, or the bottom in shallower area by a major outbreak of cold air (Nowlin and Paker, 1974). The north/south components also show response to cold front events. The north current is weak in the pre-frontal phase, but abruptly reverses to southward and also intensifies after the outbreak of cold air masses. Between mid January and mid Febuary, a very strong westward current dominates at CSI-6 for one month and cold fronts have little influence during this period (Figure 4.12). Such strong flow coincides with the high water stage of the Mississippi River (Figure 4.6), suggesting a significant impact of Mississippi discharge on the coastal current system during flood seasons. Our finding is consistent with Wiseman et al.'s (1997) results based on the CTD and hypoxia surveys on the Louisiana inner shelf.

Due to the shallow water depth (< 5m) at CSI-3, the subtidal current is generally uniform throughout the vertical column and only slightly decreases with depth. (Figure 4.13). The strongest current is observed within the depth 0.5-1.5 m below the surface. The flow strcture is

somewhat similar to the near-surface current of CSI-6, but also demonstrates some distinct characteristics. Firstly, the prevailing down-coast flow is not as strong as that observed at CSI-6. Secondly, the current field at CSI-3 seems more sensitive to the cold front events than at CSI-6, which can be seen from the fact that the post-frontal eastward current is usually stronger than that at CSI-6. Thirdly, the north/south component does not show large variability, with magnitudes always less than 0.4 m/s. A possible explaination is that CSI-3 is very closed to the coastline so the cross-shore wind fecth is limited.

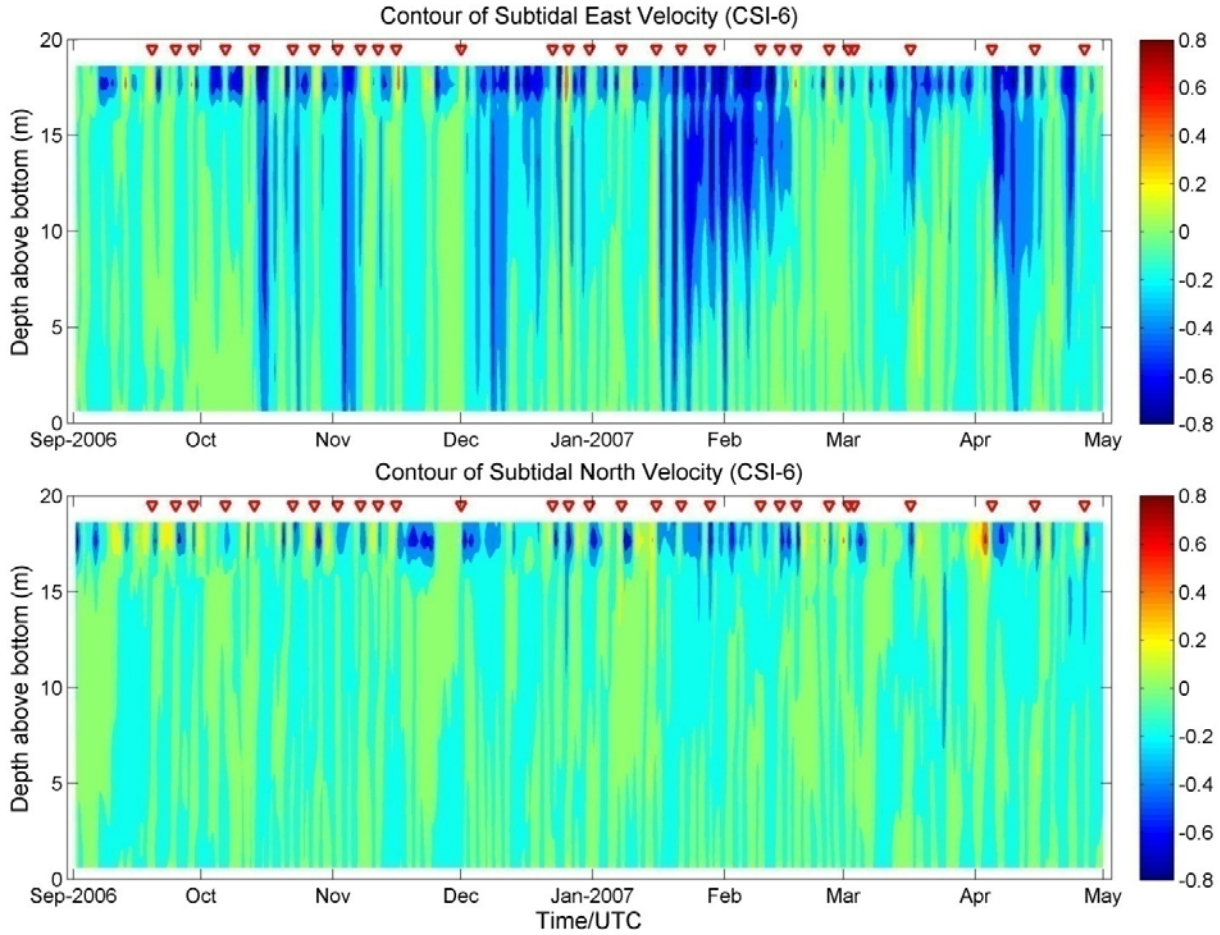

Figure 4.12 Contours of subtidal east/west (east positive) and north/south (north positive) components of current measured by bottom-mounted ADCP at CSI-6. The red triangles indicate cold fronts passed through CSI-6.

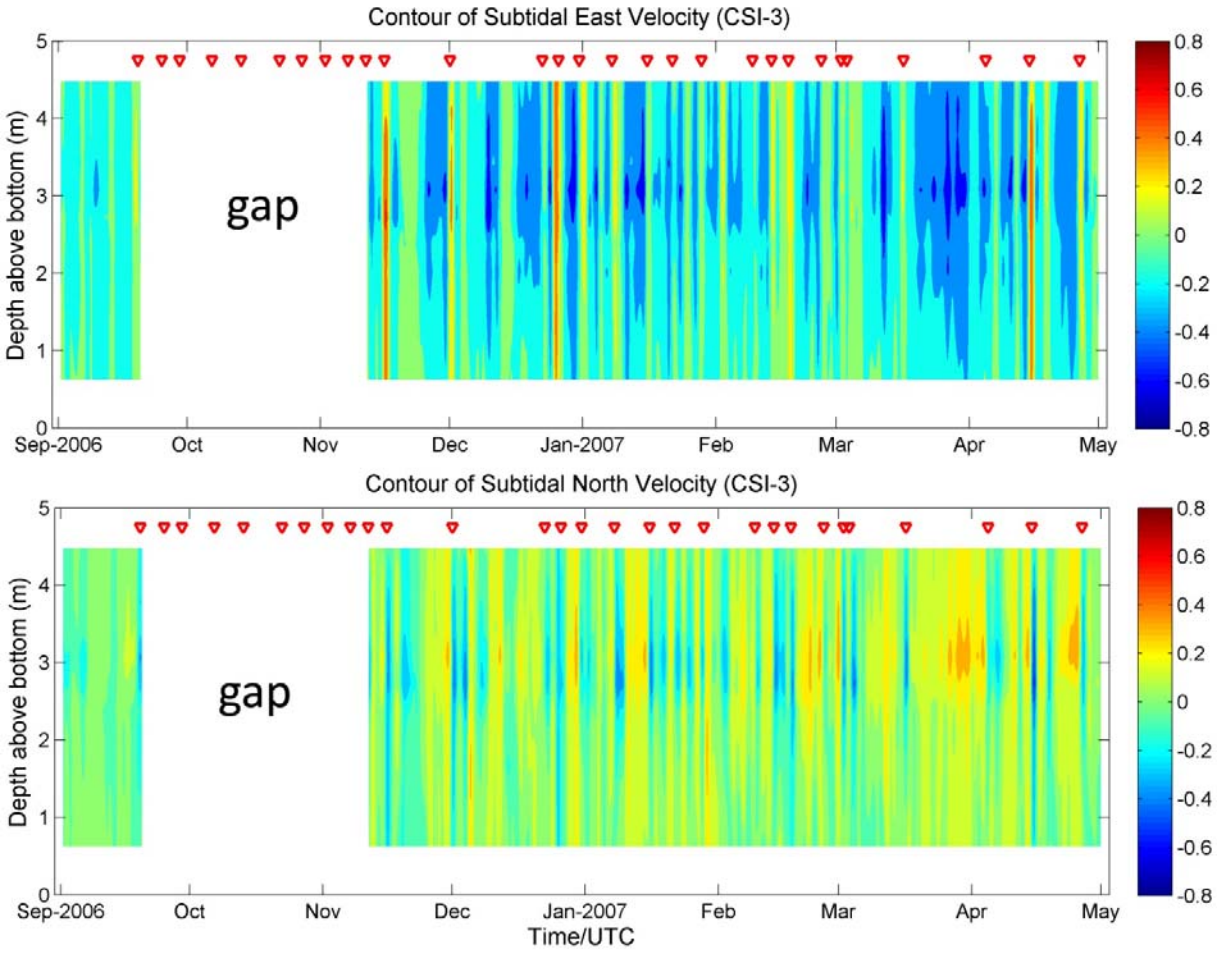

Figure 4.13 Contours of subtidal east/west (east positive) and north/south (north positive) components of current measured by bottom-mounted ADCP at CSI-3. The red triangles indicate cold fronts passed through CSI-3.

4.4.2 Rotary Spectra of Winds and Currents

The eight-month wind data measured at 4 stations are used to calculate the rotary spectra (Figure 4.14). Energy distributions are similar for all stations, although the magnitudes are variable. As a whole, LUML1 has the smallest magnitude while CSI-6 has the largest. The difference of the energy magnitudes is mainly due to the geographic differences because land has more frictional effect on winds than ocean. The LUML1 is a station located at LUMCON marine center, an onshore station, while CSI-6 is on the inner shelf near the 20-m isobath, the most offshore station in this study. Note that most of the energy is within the frequency band of 0-0.5

CPD, which covers the synoptic weather band (3-10 days). The magnitudes of clockwise components are also larger than those of counterclockwise components, agreeing with the property that wind vectors rotate clockwise for the prevailing local weather pattern. In addition, the largest two spectral peaks for clockwise component center at frequencies of 0.1736 and 0.1364 CPD, equivalent to periods of 5.76 and 7.32 days. The clockwise-rotating spectra also have some smaller peaks around 0.75, 1, and 2 CPD. The fluctuation of 1 CPD is believed to represent the energy of sea breeze, which is expected to be much stronger during summer seasons. In addition, the onshore station, LUML1, seems to have the relatively strongest sea breeze signal, while the most offshore station, CSI-6, has the weakest.

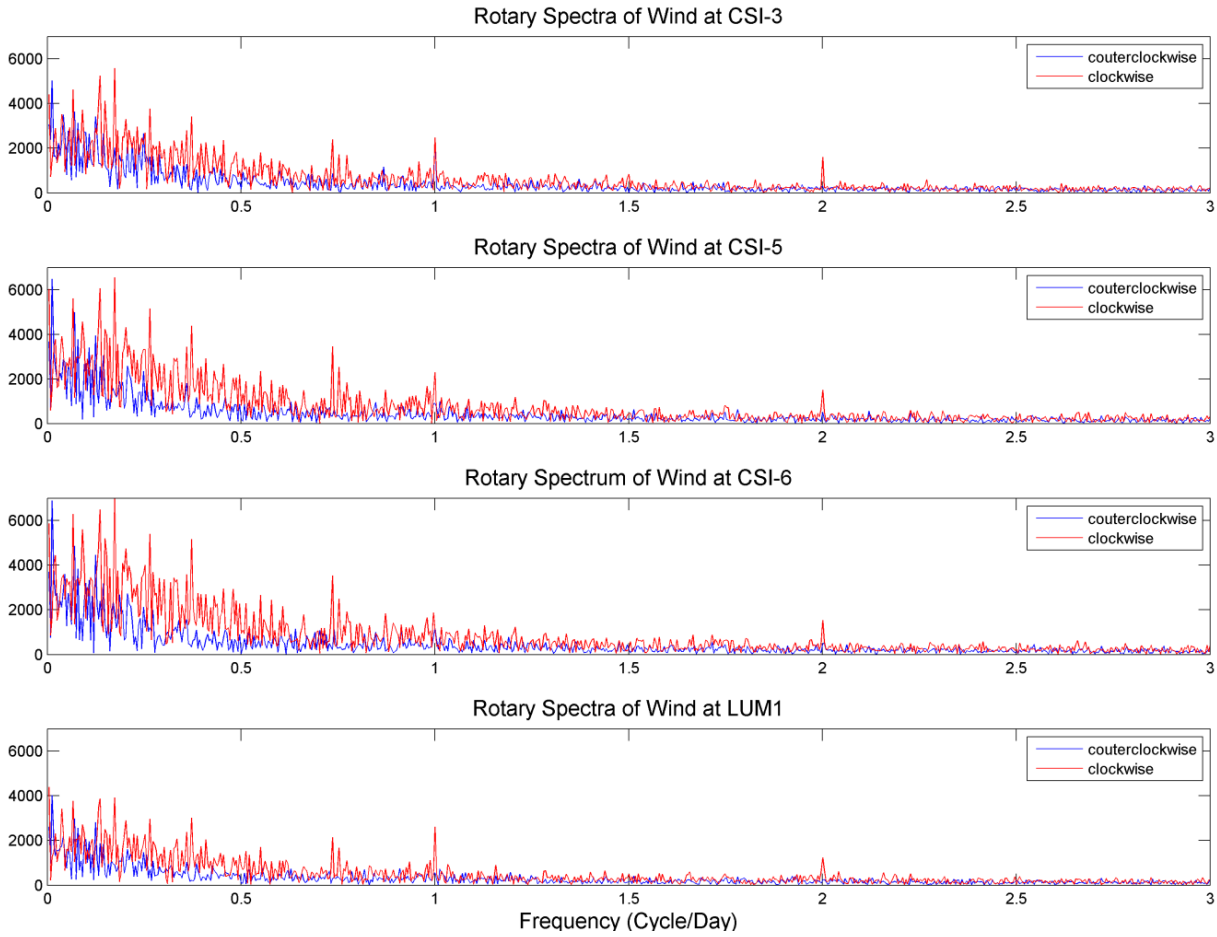

Figure 4.14 Rotary spectra of winds, measured at CSI-3, CSI-5, CSI-6 and LUM-1.

Rotary spectra are also calculated for the near-surface, mid-layer, and near-bottom currents measured at CSI-6 (Figure 4.15). For near-surface current, major spectral peaks are within the frequency band of 0-0.5 CPD, which are consistent with the dominant frequencies of wind oscillations (Figure 4.14), evidencing that the near-surface current is mainly wind-driven. There are also some relatively lower energy distributions within the band of 0.7-1.2 CPD, which is believed to be driven by the combined effects of winds, inertial oscillation (i.e., 0.968 CPD) and diurnal tides. Tidal forcing is the most important in the mid layer as the rotary spectra show two largest peaks near diurnal frequency: 1.002 and 0.930 CPD, which approximate K1 and O1 tides. Two other peaks near diurnal frequency are at 0.895 and 0.849 CPD, which is close to Q1 tide. The subtidal oscillations are of secondary importance in the mid layer. Although subtidal frequency has slightly more spectral energy distribution than near-diurnal frequency for the near-bottom current, the peaks have similar heights. This suggests that both subtidal and diurnal tidal forcings are important near the bottom. Furthermore, currents in all three layers have small semidiurnal peaks at 1.934 (M2) and 2.007 CPD (K2).

Figure 4.16 is rotary spectra of near-surface and near-bottom current at CSI-3. The energy distribution patterns of the two layers are very similar, although the amplitude of near-bottom current is slightly smaller than that of near-surface counterpart. Even in the near-surface layer, the peaks of diurnal oscillations are higher than those of low-frequency oscillations and the peaks of semi-diurnal oscillations are as high as those of subtidal oscillations. This suggests that tidal forcing at CSI-3 seem more important than wind forcing on inducing current variations. The current rotary spectra of CSI-3 also agree with the spectra of water levels that semidiurnal forcing is more obvious in the shelf areas adjacent to the Atchafalaya Bay.

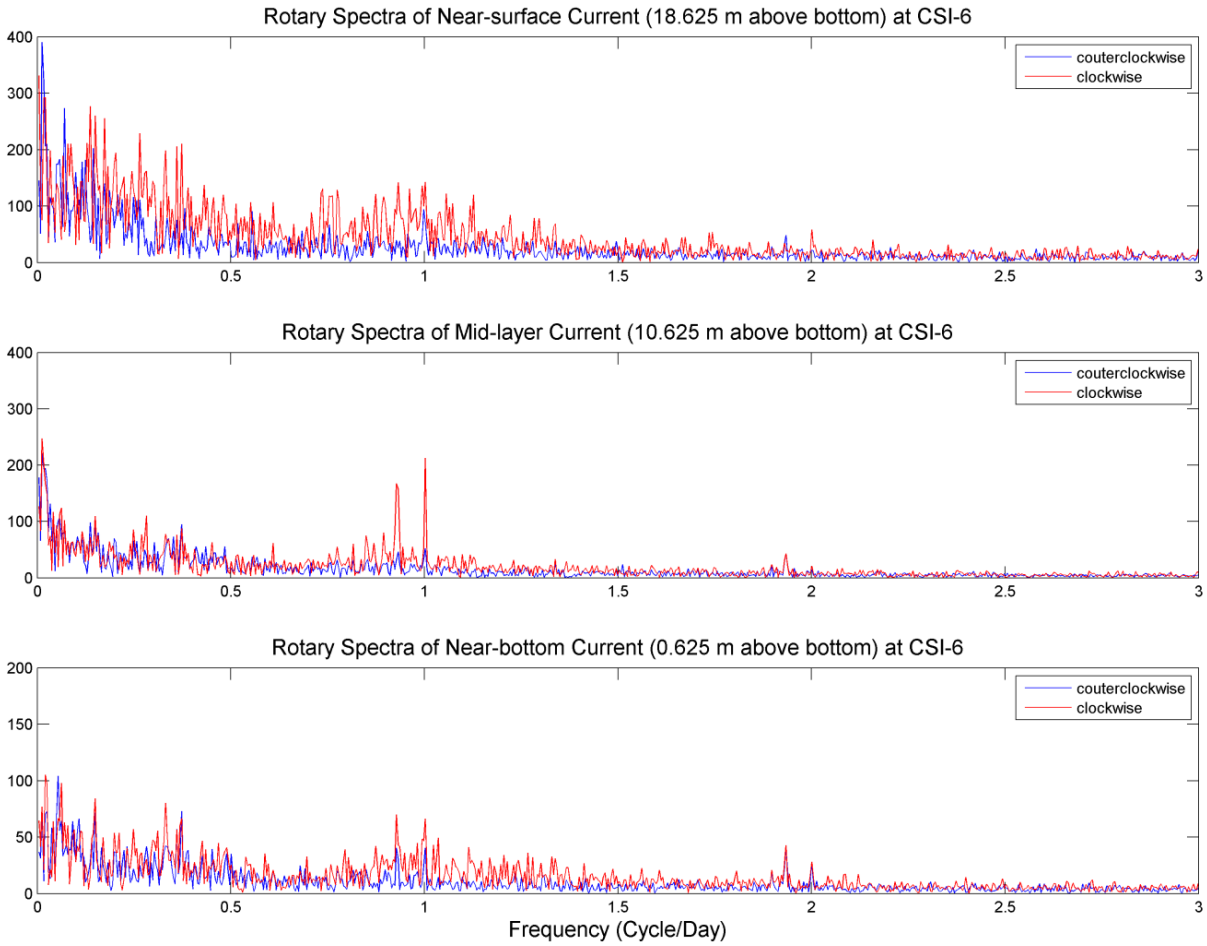

Figure 4.15 Rotary spectra of near surface, mid-layer and near-bottom current measured at CSI-6.

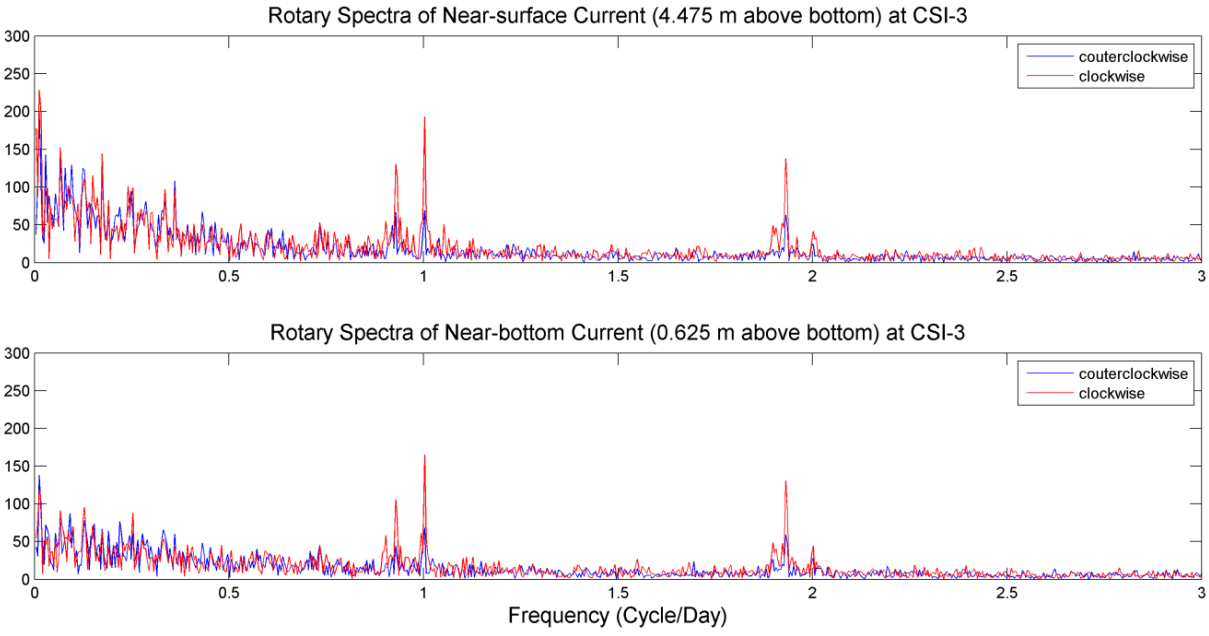

Figure 4.16 Rotary spectra of near surface and near-bottom current, measured at CSI-3.

4.5 Case Studies: the Relationship between Wind, River Discharge and Current

4.5.1 Introduction to Case Studies

Five one-month periods are selected as case studies to investigate and compare the response of flow field to cold front passages during different river discharge scenarios. A criterion, defined by Walker (1996), is applied to divide the river discharge conditions into three scenarios: low discharge (0-10,000 m^3/s), moderate discharge (10,001-20,000 m^3/s), and high discharge (>20,000 m^3/s). The eight-month total discharge from Mississippi and Atchafalaya Rivers is typical of ordinary years (Figure 4.6). The Atchafalaya River is a distributary of the Mississippi River, delivering 30% of the Mississippi discharge through the Old River diversion structure (Roberts, 1998). During the study period, however, the percentage of river discharge down to the Atchafalaya River course is generally lower than 30%, varying from 13% to 33%. The mean total discharge for the eight months is 16,732 m^3/s, and 9% less than long-term mean discharge estimated by Milliman and Mead (1983) (Figure 4.6). Low discharge occurs in September. During the subsequent three months, the river discharge has an increasing trend, oscillating within the range of 10,000-20,000 m^3/s. The discharge significantly increases from the beginning of January, and reaches the maximum (32,100 m^3/s) at the end of January. The high water stage (>30,000 m^3/s) lasts for nearly half a month. The discharge largely decreases in February. After March, the discharge rebounds again, becoming slightly higher than the mean discharge. Satellite imagery indicated that the mean plume area in high discharge condition doubled that in moderate discharge condition (Walker, 1996). The river discharge conditions for the five selected periods are summarized in Table 4.3.

Table 4.3 The river discharge conditions during five selected one-month periods

Case	Time Period	Scenario	Discharge Range (m^3/s)
1	09/15/06-10/15/06	low	6,190~12,474
2	11/14/06-12/14/06	moderate	11,633~16,112
3	12/18/06-01/18/07	moderate to high	11,729~26,816
4	01/19/07-02/19/07	extremely high to moderate	13,989~32,111
5	04/01/07-04/30/07	high	21,323~24,239

4.5.2 September 15 - October 15, 2006

From September 15 to October 15, 2006, four cold fronts affect the Louisiana coast, but their strengths are generally weak. Only the first cold front is a migrating cyclone, while the other three fronts are arctic surges. River discharge during this period is the lowest of the eight-month record (Figure 4.6; Table 4.3), suggesting that the buoyancy effects are minimal. Southerly winds dominate the first week with relatively strong prefrontal winds (~10 m/s) (Figure 4.17). In the middle of the week, however, a sudden wind reversal occurs for 30 hours, which also reverses the near-surface current. The approach of the first cold front weakens the southerly winds. After the frontal passage, winds reverse to northeasterly lasting for about three days. The other three cold fronts are relatively weak, and the post-frontal northeasterly and northwesterly winds blow for only one day. From October 3, easterly winds dominate for one week, being perturbed by the third frontal passage for less than a day. The down-coast westward flow is intensified by the easterly winds, but weakened for one day by the third frontal passage (Figure 4.18). The near-surface currents agree well with winds, consistent with past research that wind is the prevailing cause of near-surface current over the inner Louisiana-Texas shelf (Cochrane and Kelly, 1986; Cho et al., 1998; Walker, 2005). Current measurements at CSI-3 are unavailable for this period due to instrumental problems.

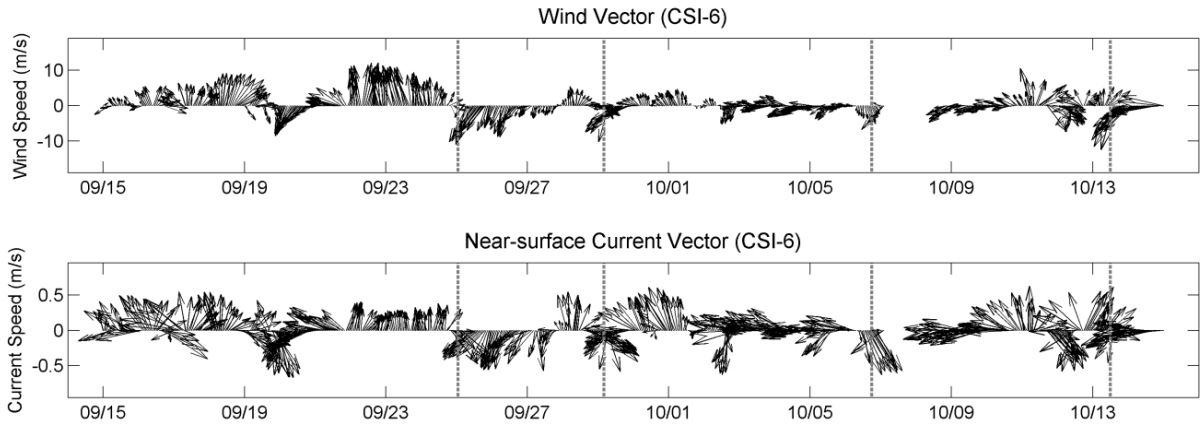

Figure 4.17 Winds and near-surface currents measured at CSI-6 between September 15 and October 15, 2006.

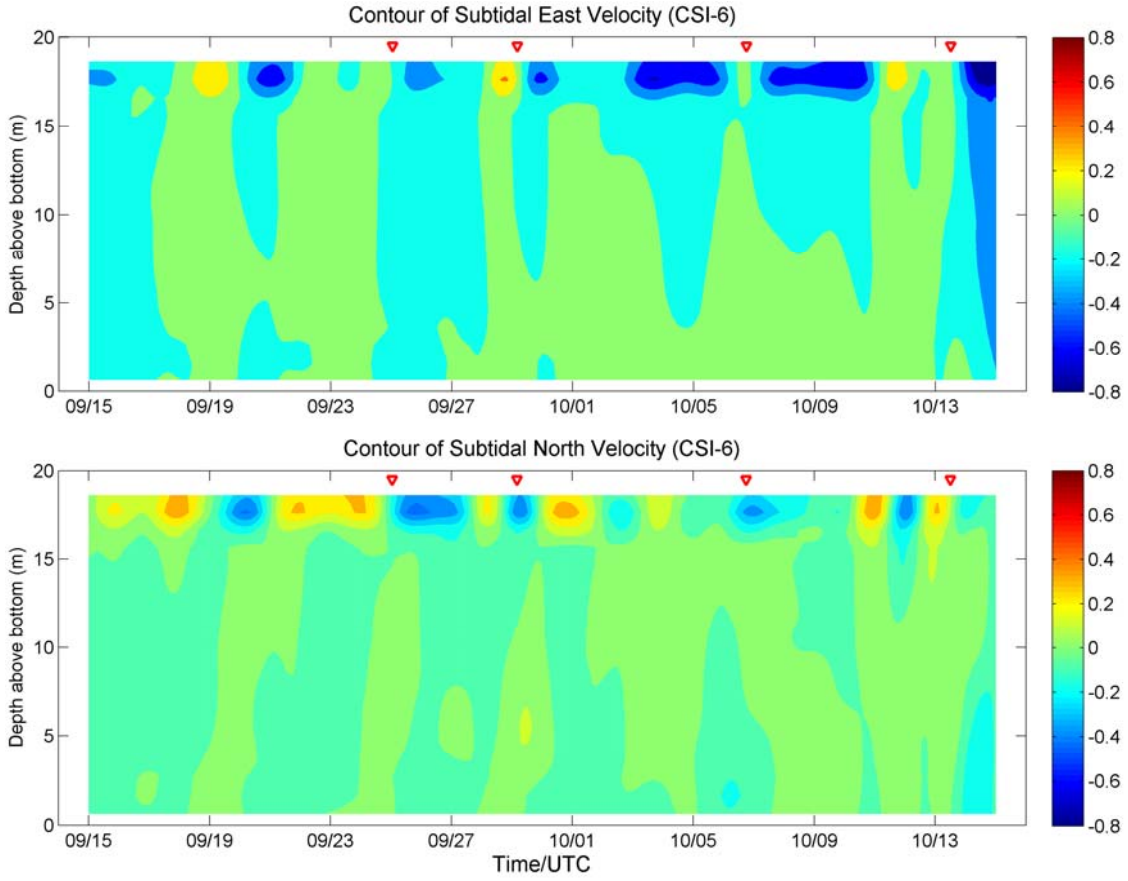

Figure 4.18 Contours of subtidal east/west (east positive) and north/south (north positive) components of current measured by bottom-mounted ADCP at CSI-6 from September 15 to Octber 15, 2006. The red triangles indicate cold front passages.

4.5.3 November 14 - December 14, 2006

Between November 14 and December 14, 2006, the synoptic weather patterns are simple with

only two similar cold fronts translating from west to east at right angles to the Louisiana coastline. Both cold fronts are migrating cyclones, associated with strong low-pressure center systems. The wind patterns are also similar and the typical clockwise rotation of winds can be identified for both events (Figure 4.19 and 4.21). After the outbreak of cold air, northerly, northwesterly or northeasterly winds are maintained for nearly 10 days. The northwesterly winds are relatively strong immediately after the frontal passage (wind speed exceeds 10 m/s), when eastward wind momentum can be transferred from sea surface down to the bottom (Figure 4.20). River discharge during this period is moderate, oscillating between 11,633~16,112 m^3/s. The synoptic wind reversals associated with both cold front passages cause current reversals on the inner shelf, and almost the entire vertical water column at CSI-6 and CSI-3 are affected. The subtidal currents shift from the prevailing down-coast direction to up-coast direction for nearly two days and the maximum speed exceeds 0.5 m/s (Figure 4.20 and 4.22). The responses of the cross-shelf current component show that the predominant north wind component induces strong offshore current in the near-surface layer at CSI-6, but the cross-shelf current at CSI-3 seems less sensible to wind forcing.

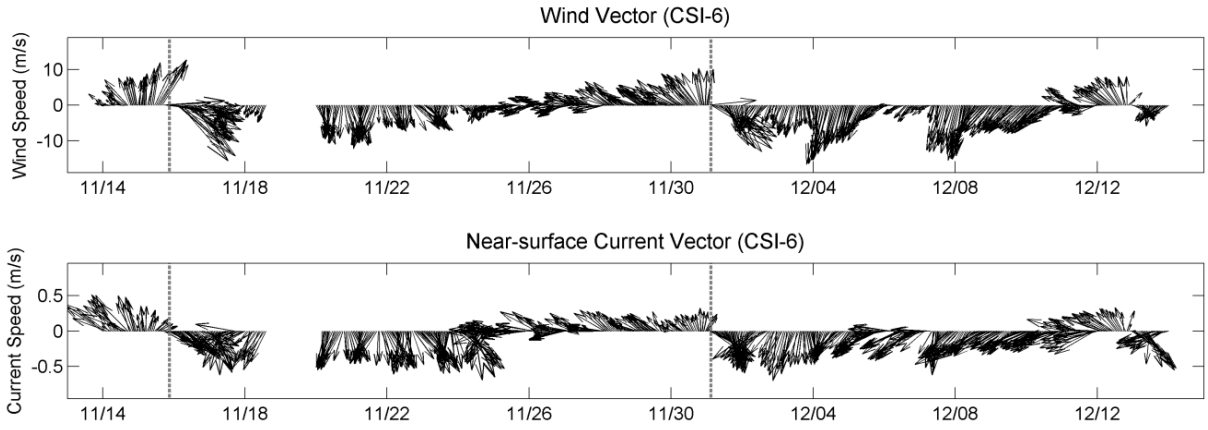

Figure 4.19 Winds and near-surface currents measured at CSI-6 between November 14 and December 14, 2006.

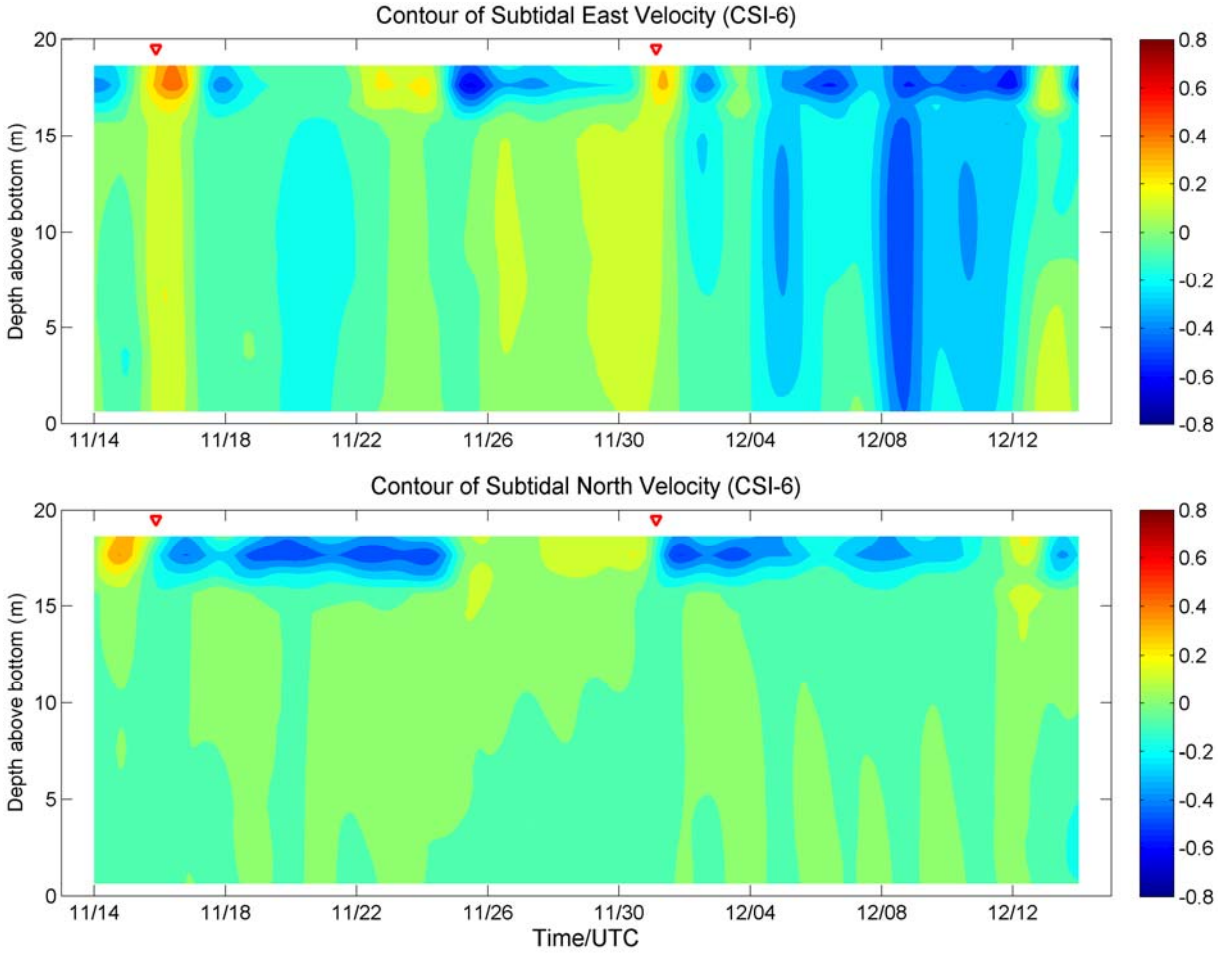

Figure 4.20 Contours of subtidal east/west (east positive) and north/south (north positive) components of current measured by bottom-mounted ADCP at CSI-6 from November 14 to December 14, 2006. The red triangles indicate cold front passages.

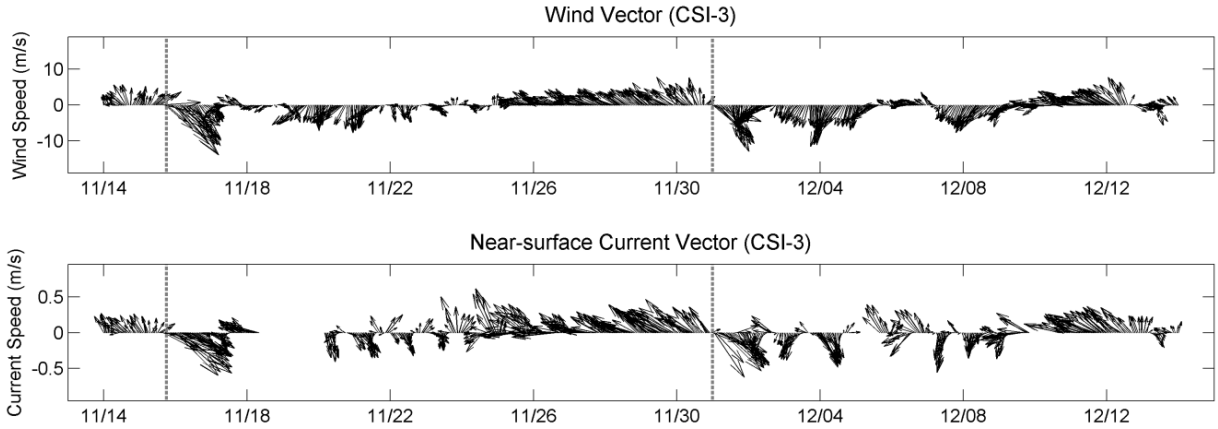

Figure 4.21 Winds and near-surface currents measured at CSI-3 between November 14 and December 14, 2006.

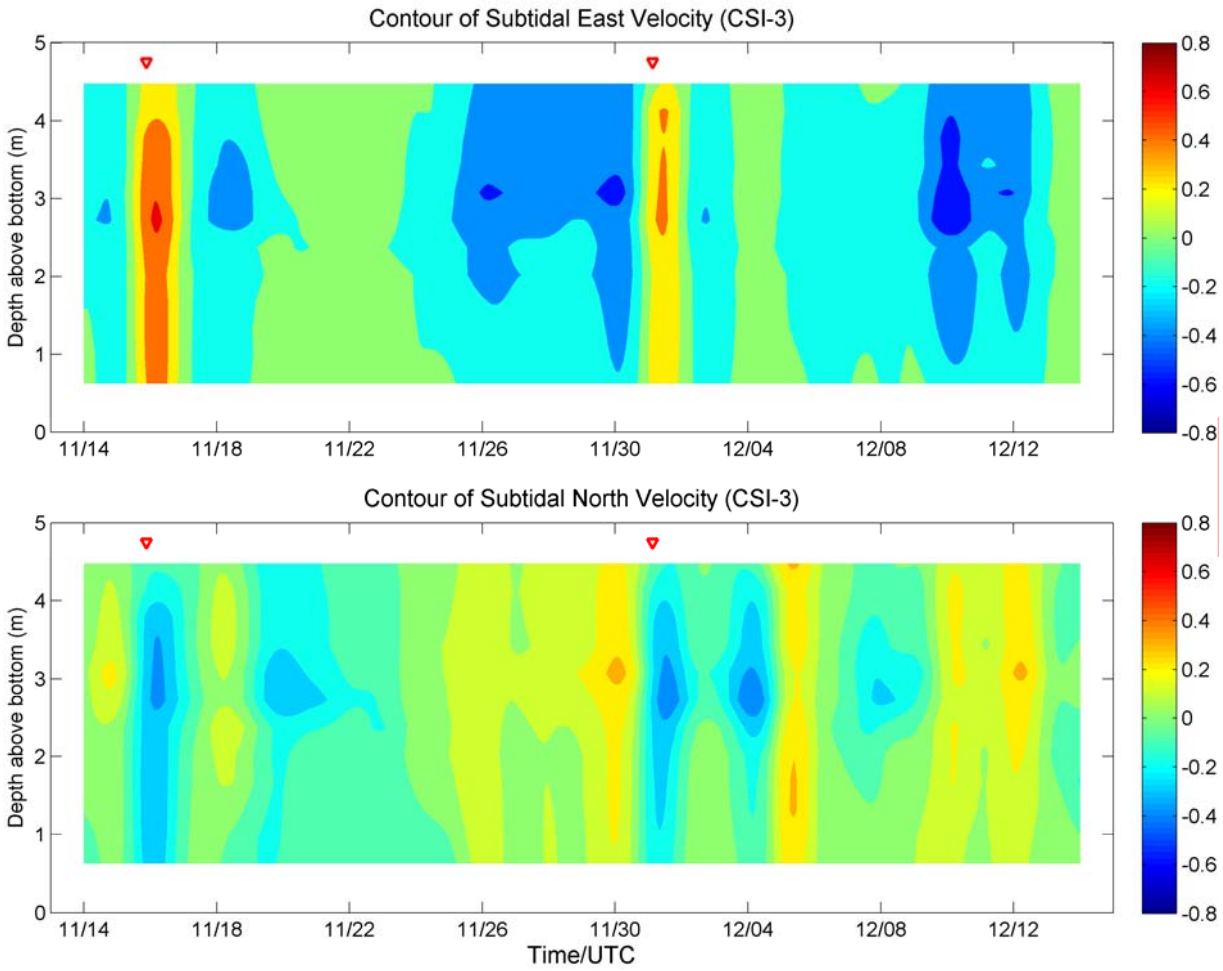

Figure 4.22 Contours of subtidal east/west (east positive) and north/south (north positive) components of current measured by bottom-mounted ADCP at CSI-3 from November 14 to December 14, 2006. The red triangles indicate cold front passages.

4.5.4 December 18, 2006 – January 18, 2007

The synoptic weather patterns during this period are complex. Within the first two weeks, three cold fronts affect the study area. Before moving into the study area (December 22), the first front is a stationary front associated with two low pressure centers: one in middle Arkansas and the other offshore Texas coast. Being pushed eastward by a high pressure center in the middle Texas, it develops to a cold front when approaching the study area. After the front enters the shelf of the GoM, it becomes a stationary front as the maritime air mass over the Gulf intensifies.

In December 25, the front is further pushed northward to the northern Gulf coast as a warm front. During the same period, the low pressure center, previously located offshore of the Texas coast, gradually moves northeastward to the areas of Appalachian Mountains, which forms the second cold front in December 26. Winds vary quickly from December 22 to 27, so do the near-surface currents (Figure 4.23 and 4.25). The down-coast flow is intensified for about 40 hours from December 22-24, but suddenly switches to strong up-coast flow for the next two days. After that, the down-coast current is re-established by the strong southeasterly winds (Figure 4.24 and 4.26). The cross-shelf flow also reverses with frontal passages and the strong northerly winds drive significant southward current (Figure 4.24 and 4.26). Although river discharge exceeds 20,000 m^3/s after January 4, it is not until January 16 that the buoyancy effects appear obvious at CSI-6 (Figure 4.24). This may suggest that the response of the flow field at CSI-6 lags the river discharge variations. After the passage of the fifth cold front (January 16), northerly or northeasterly winds dominate for nearly 5 days. However, the near-surface currents at CSI-6 do not exactly follow the winds and the westward component seems much stronger than the southward counterpart (Figure 4.24).

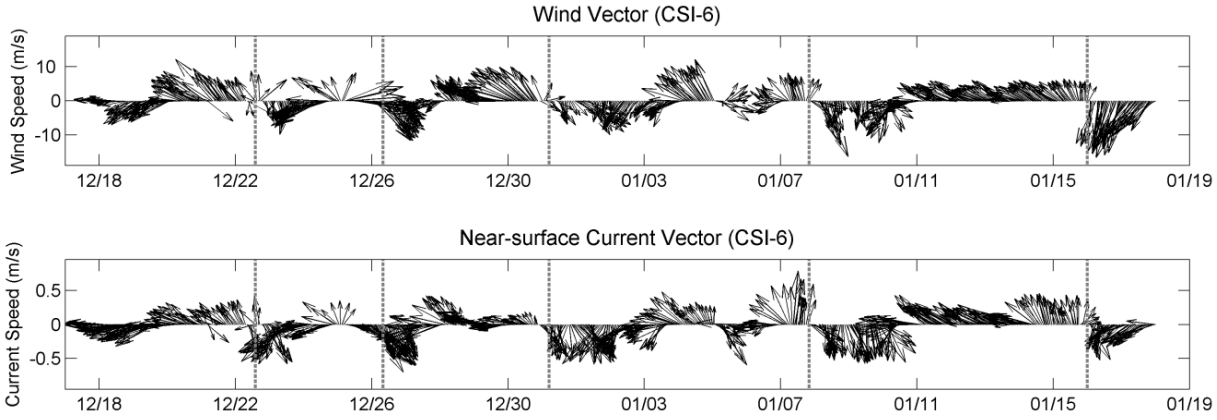

Figure 4.23 Winds and near-surface currents measured at CSI-6 between December 18, 2006 and January 18, 2007.

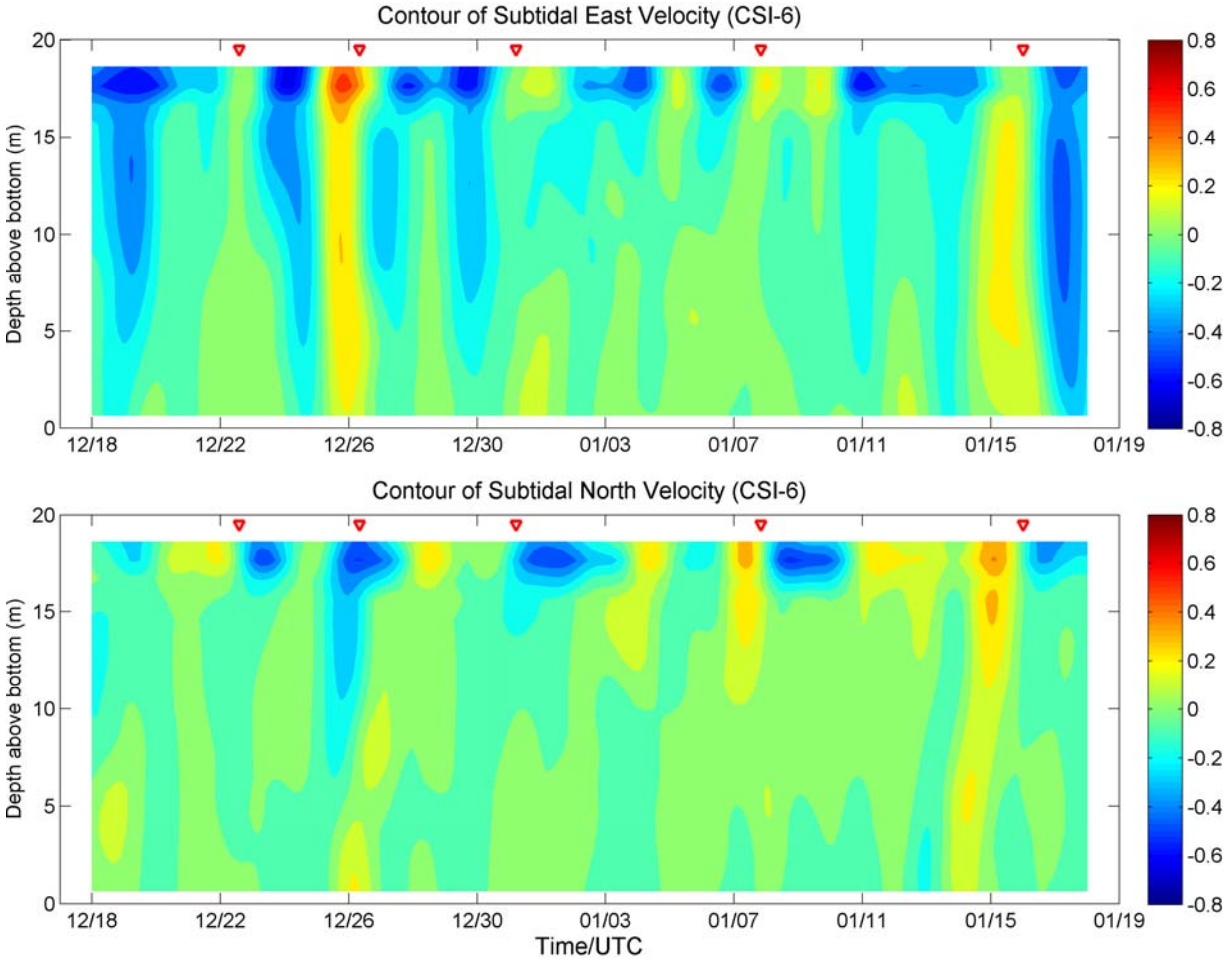

Figure 4.24 Contours of subtidal east/west (east positive) and north/south (north positive) components of current measured by bottom-mounted ADCP at CSI-6 from December 18, 2006 to January 18, 2007. The red triangles indicate cold front passages.

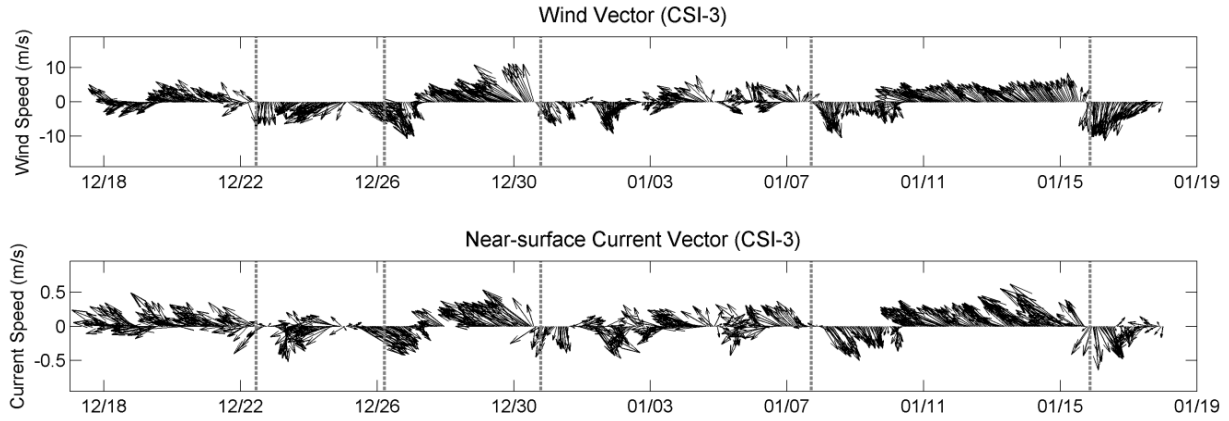

Figure 4.25 Winds and near-surface currents measured at CSI-3 between December 18, 2006 and January 18, 2007.

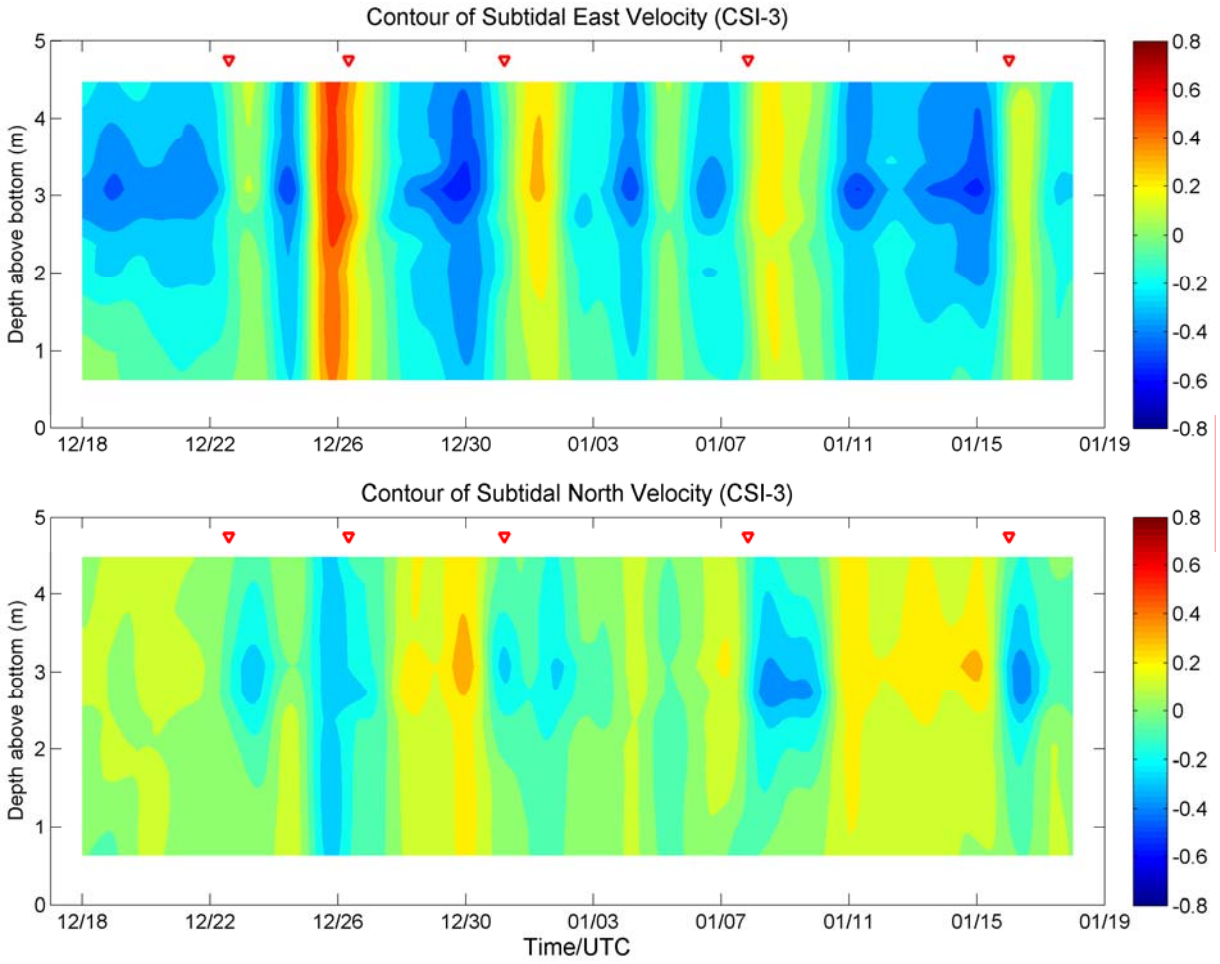

Figure 4.26 Contours of subtidal east/west (east positive) and north/south (north positive) components of current measured by bottom-mounted ADCP at CSI-3 from December 18, 2006 to January 18, 2007. The red triangles indicate cold front passages.

4.5.5 January 19 – February 19, 2007

During January 19 and February 19, 2007, the extratropical cyclones are active and five cold fronts pass through the study area. River discharge remains higher than 30,000 m^3/s from January 22 to February 6, and dramatically decreases after February 7. The large amount of buoyant freshwater advected from the Southwest Pass of the Mississippi River into the continental shelf west of the bird-foot delta has a profound impact on the hydrodynamics. At CSI-6, westward current dominates the near-surface and middle layers from the beginning of this period to February 13 (Figure 4.27). Although the westerly wind component associated with the

first three frontal passages may weaken the down-coast current, it can not drive an up-coast current when river discharge is extremely high (Figure 4.28). This phenomenon indicates that associated with high river discharge, barotropic and baroclinic forcings from buoyant flux reinforce the wind-driven down-coast flow on the inner Louisiana shelf. Previous numerical simulations also indicate that the buoyant low-salinity water is trapped very close to the coast and extends westward in the fall and winter (Morey et al., 2003). After the discharge drops to a normal condition, the fourth cold front can reverse the near-surface current for 14 hours. The discharge continues falling to below the mean level at the end of this period. The up-coast current develops for more than 30 hours with the fifth cold front in February 17 (Figure 4.28).

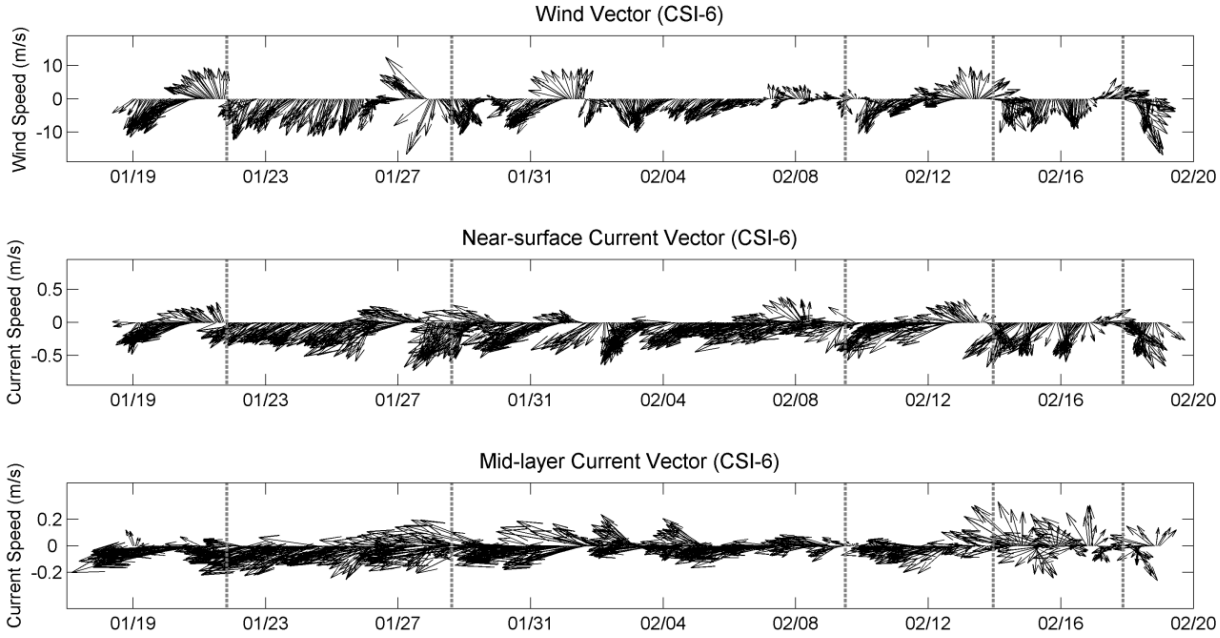

Figure 4.27 Winds and near-surface and mid-layer currents measured at CSI-6 between January 19 and February 19, 2007.

In contrast, currents at CSI-3 still follow the wind closely even when the discharge is high (Figure 4.29), which suggests that the buoyancy-driven current is insignificant due to the local effects of shallow water and coastal boundary. Since the depth of CSI-3 is less than 5 m, the vertical mixing due to strong wind shear and bottom friction becomes very important. The

contours of both east/west and north/south components illustrate quite weak and uniform flow field from sea surface to bottom (Figure 4.30). Although hydrographic data are not available for this period, a well-mixed flow field can still be concluded from the current profiles. The insignificant baroclinic effect may be due to the weak along-shore density gradient, since previous numerical modeling study indicated that salinity gradient, consequently density gradient, was mainly in the cross-shore direction (Cobb et al., 2008b). However, the cross-shore current seems even weaker than alongshore current (Figure 4.30), mainly due to the solid boundary constrain.

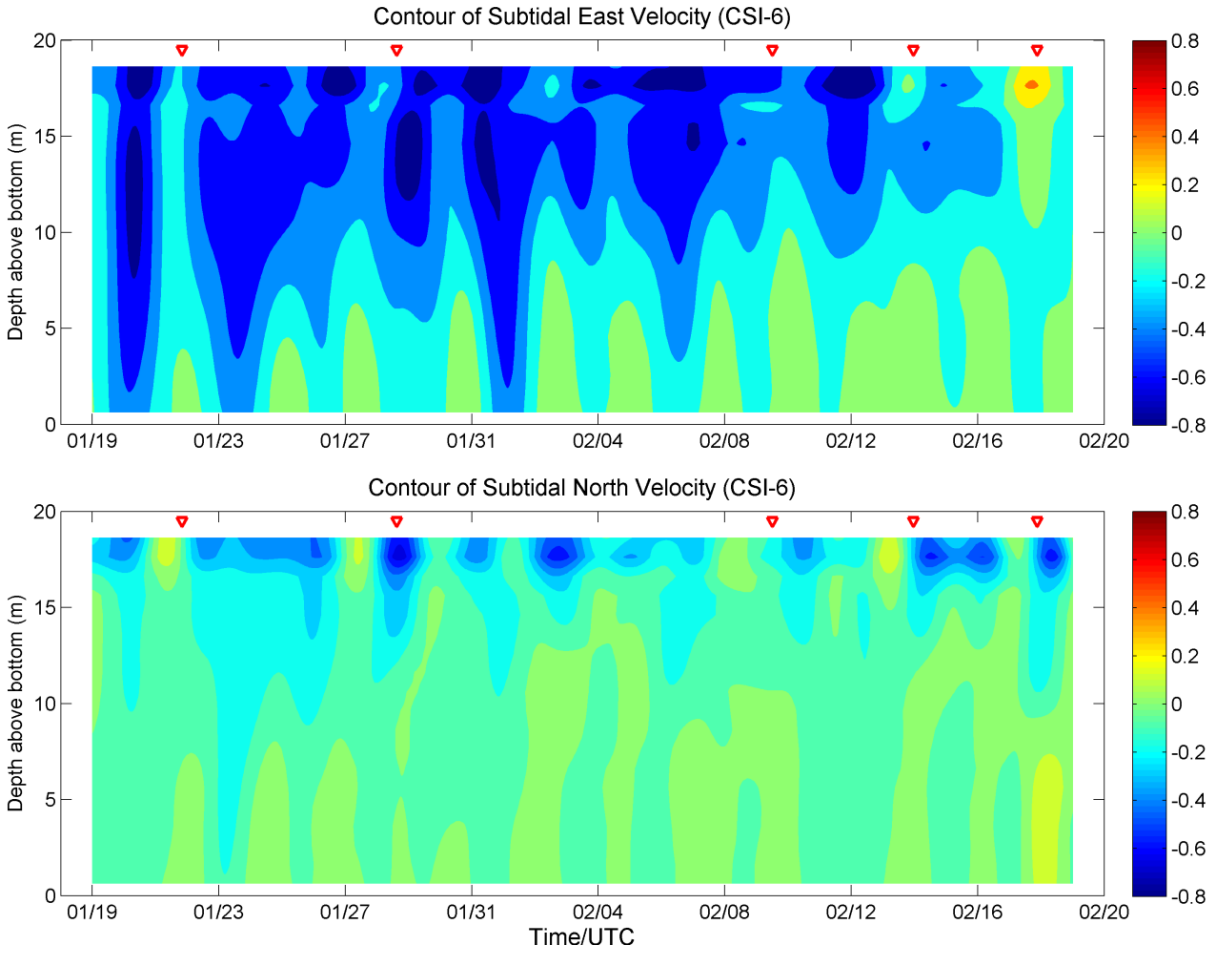

Figure 4.28 Contours of subtidal east/west (east positive) and north/south (north positive) components of current measured by bottom-mounted ADCP at CSI-6 from December 18, 2006 to January 18, 2007. The red triangles indicate cold front passages.

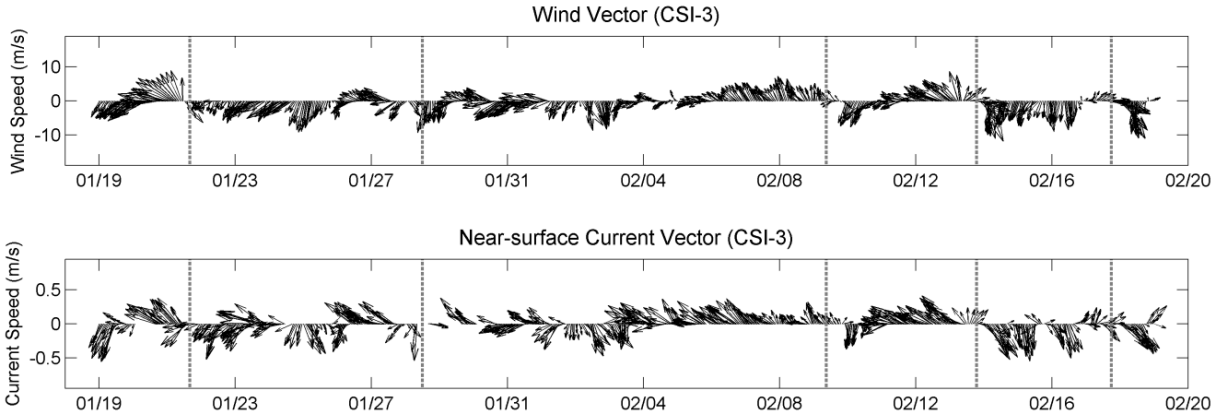

Figure 4.29 Winds and near-surface currents measured at CSI-3 between January 19 and February 19, 2007.

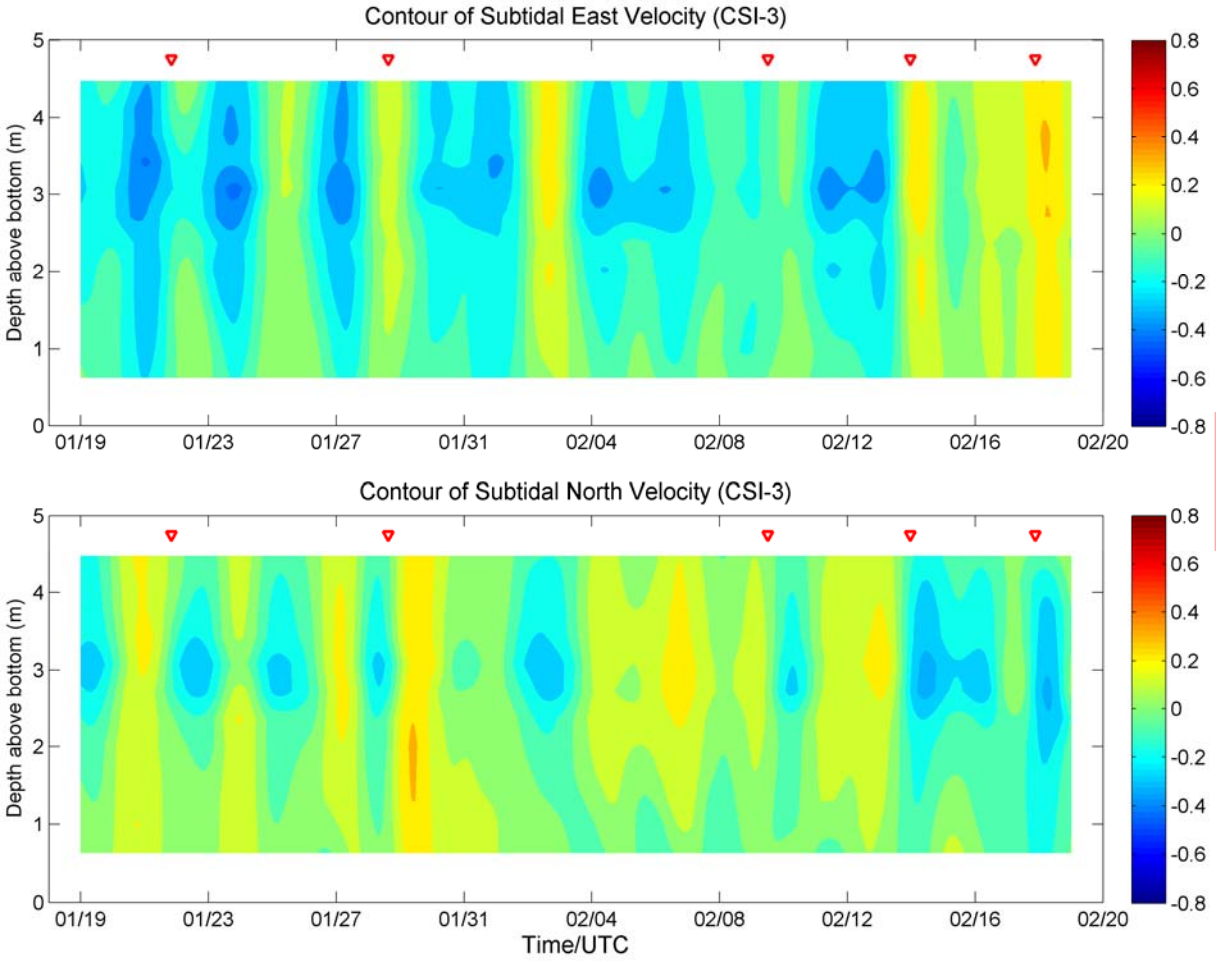

Figure 4.30 Contours of subtidal east/west (east positive) and north/south (north positive) components of current measured by bottom-mounted ADCP at CSI-3 from January 19 to February 19, 2007. The red triangles indicate cold front passages.

4.5.6 April 1 – 30, 2007

There are three cold front events during the month of April 2007. Associated with two low pressure systems (the relatively stronger one is located north of the Great Lakes and weaker one is offshore of Texas), the first cold front is unique with the frontal orientation almost paralleled to the Louisiana coastline. The dominant pre-frontal winds are southerly which then abruptly rotate to northeasterly after the frontal passage, skipping over the transient period of westerly/northwesterly winds (Figure 4.31). The other two cold fronts are migrating cyclones; however, the post-frontal wind of the third events is abnormally weak (~5 m/s). The discharge during this period is slightly higher than the eight-month and long-term means, ranging from 21,323~24,239 m^3/s. At CSI-6, the near-surface current does not exactly follow the wind for some time periods. Before April 4, moderate southerly/southeasterly winds dominate. It seems that the comparatively strong northward near-surface current is not only driven by winds. The first frontal passage reverses the northward current to southwestward (Figure 4.31). In addition, the west component dominates the surface and middle depth for more than a week since April 5, which is believed to be driven by a combined effect from winds and buoyancy flux (Figure 4.32). From April 21 to 24, easterly/southeasterly winds also induce a strong eastward current. The winds measured at CSI-3 in this month are very similar to CSI-6. The current is consistent with the winds (Figure 4.33). The current reversal is the most obvious during the second cold front episode (Figure 4.34), which reverses both the westward and northward current components as well as increasing magnitudes.

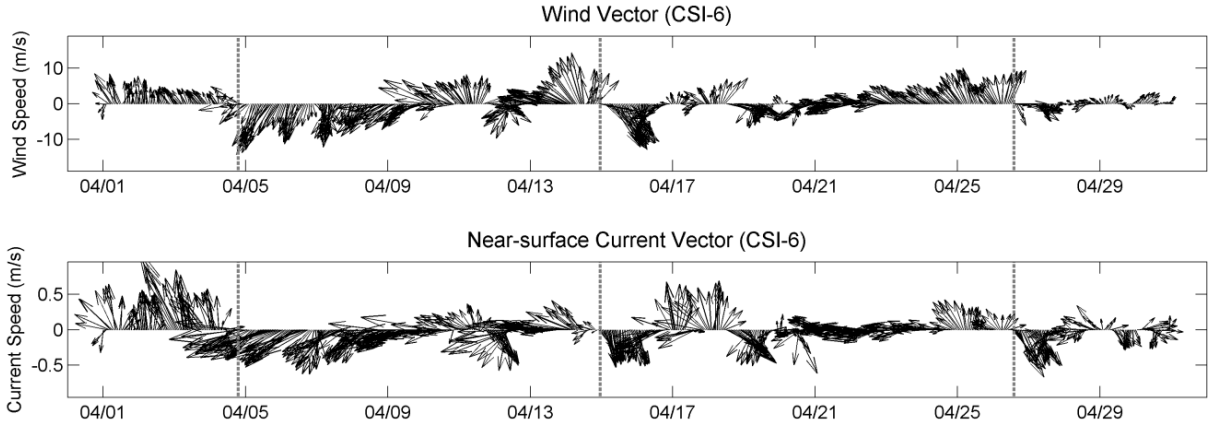

Figure 4.31 Winds and near-surface currents measured at CSI-6 in April, 2007.

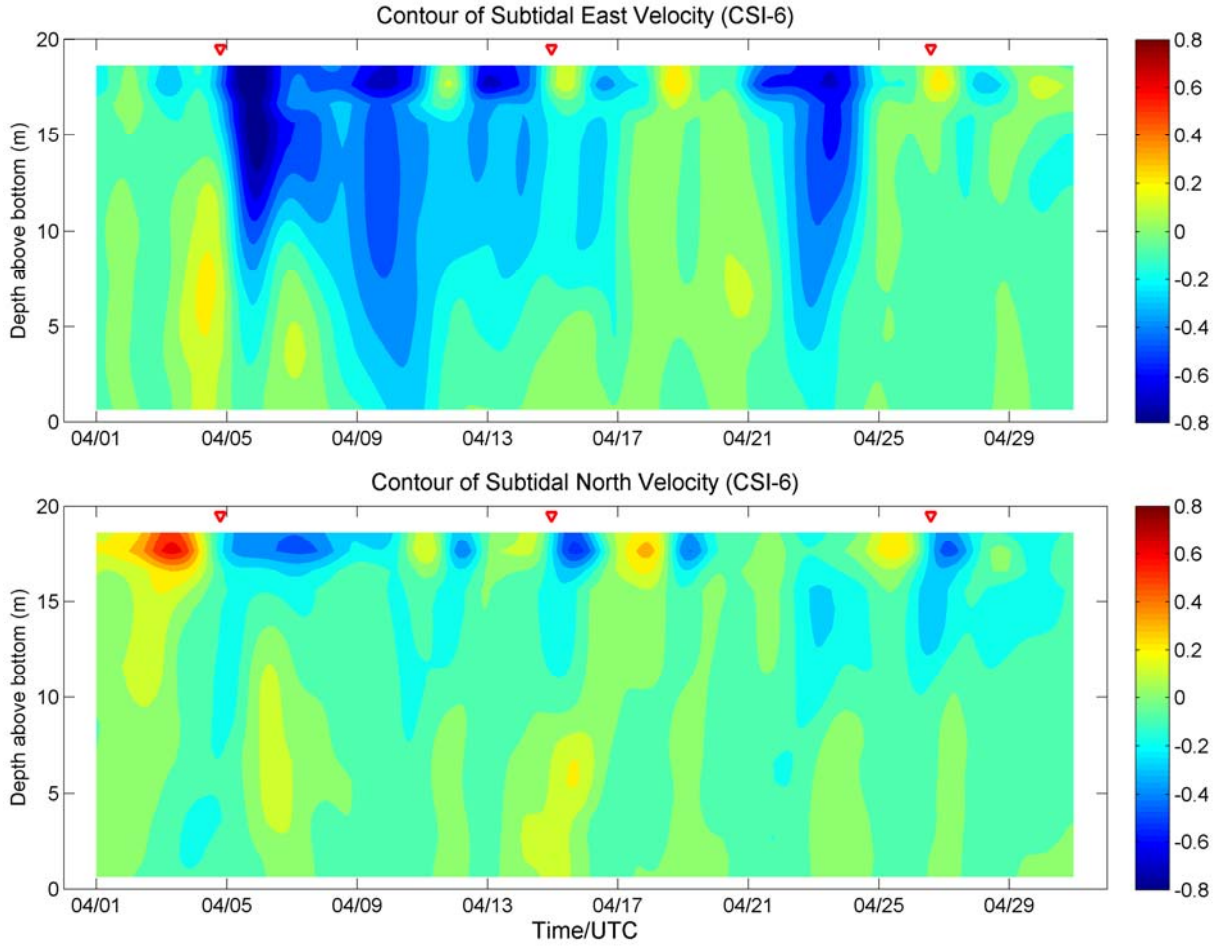

Figure 4.32 Contours of subtidal east/west (east positive) and north/south (north positive) components of current measured by bottom-mounted ADCP at CSI-6 in April, 2007. The red triangles indicate cold front passages.

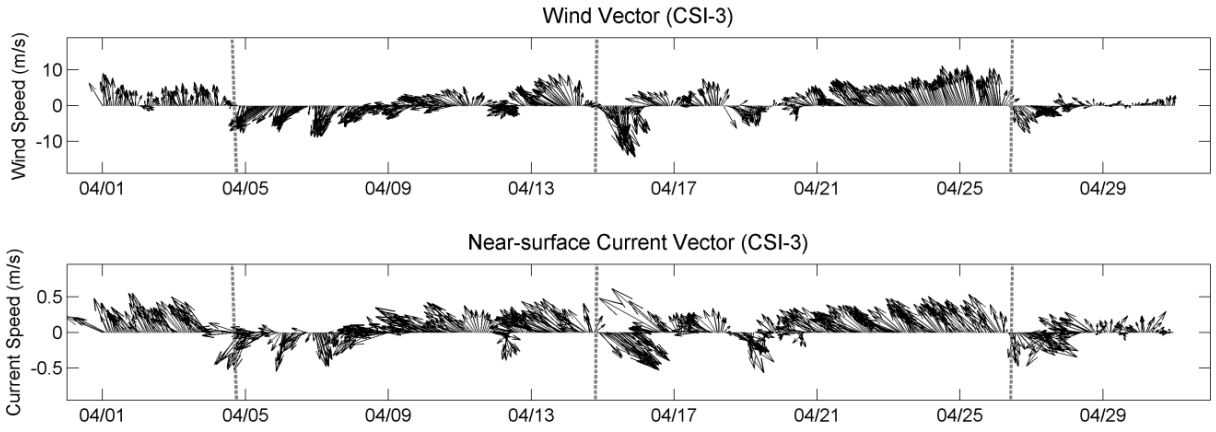

Figure 4.33 Winds and near-surface currents measured at CSI-3 in April, 2007.

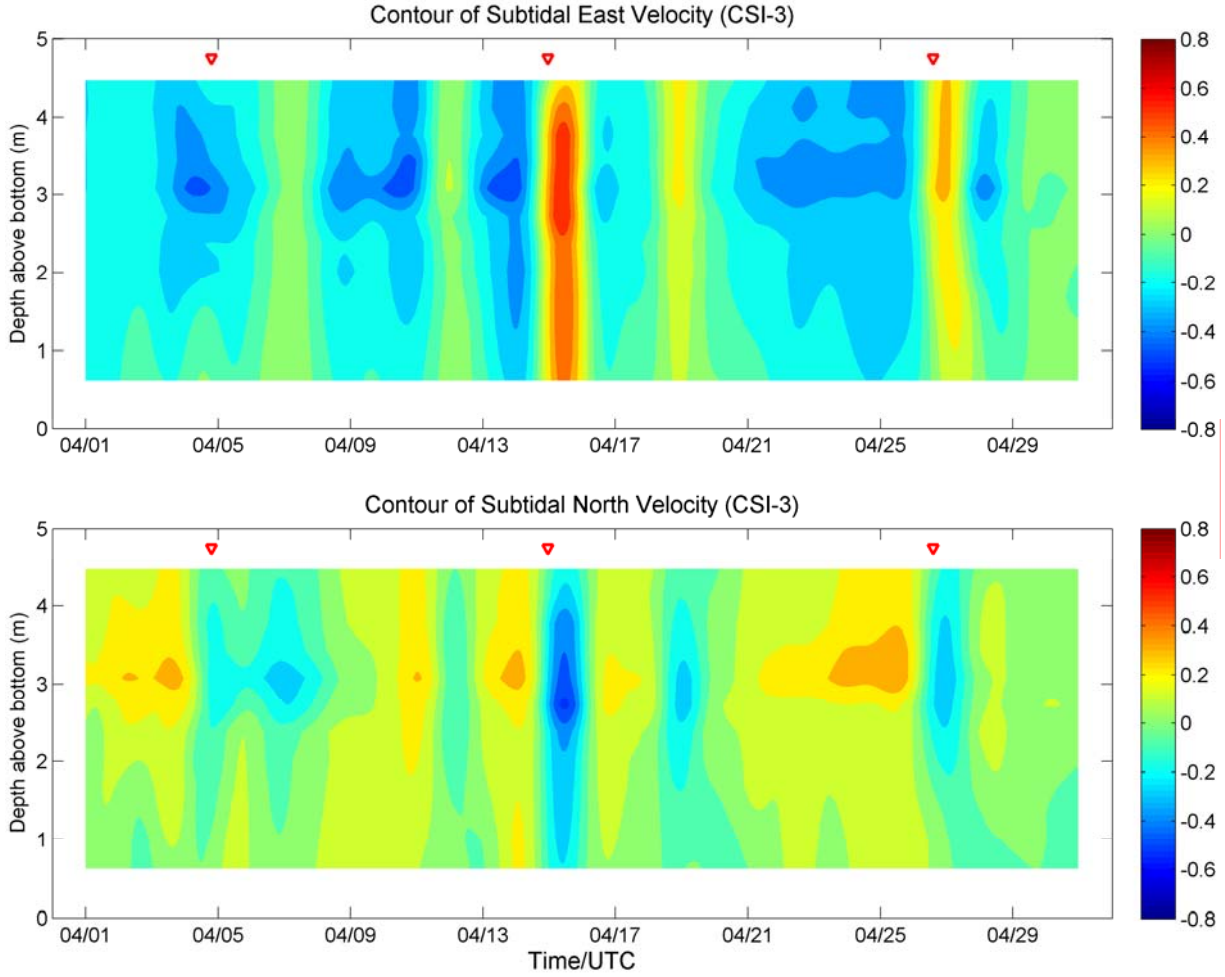

Figure 4.34 Contours of subtidal east/west (east positive) and north/south (north positive) components of current measured by bottom-mounted ADCP at CSI-3 in April, 2007. The red triangles indicate cold front passages.

CHAPTER 5 DISCUSSION

5.1 One-dimensional Analytical Model

5.1.1 Model Development

Garvine (1985) constructed a simple 1-D barotropic model to explain the estuarine subtidal fluctuation forced by local and remote winds in Chesapeake Bay and Delaware Bay. Here, a modified Garvine's model is applied to the Louisiana estuaries. At first, we take Atchafalaya Bay as an example (Figure 5.1).

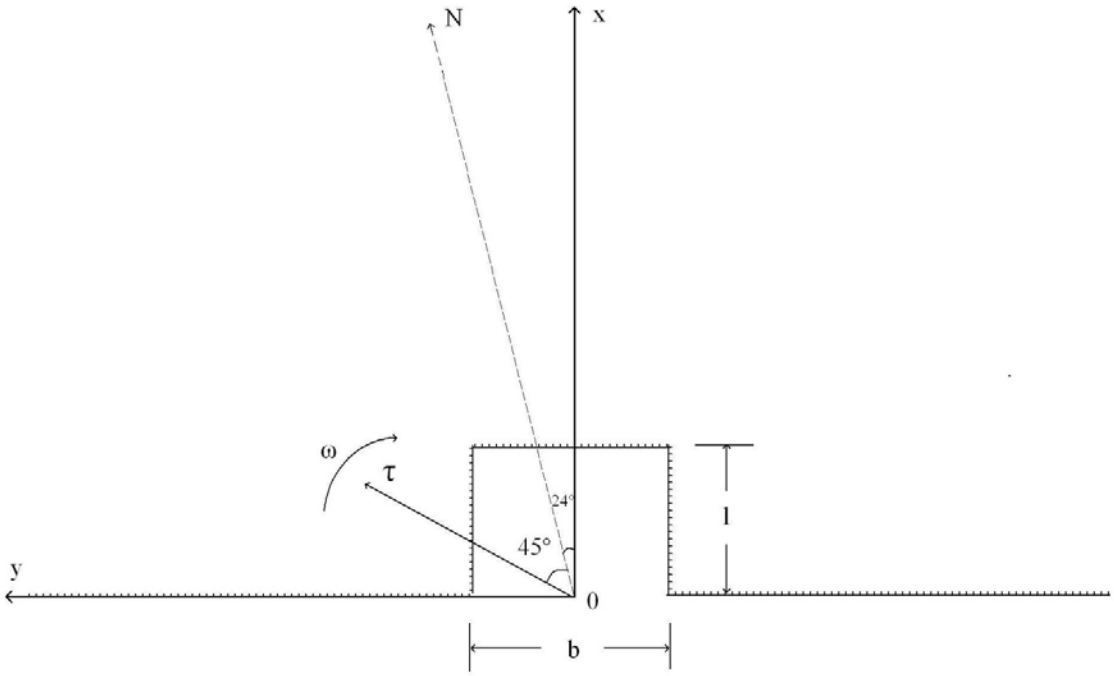

Figure 5.1 The plain view of modified Garvine's model. The Atchafalaya Bay is simplified as a rectangular estuary with a length (l) of 20 km and a width (b) of 50 km. The longitudinal axis (i.e., x-axis) is perpendicular to the coastline, and 24° clockwise rotated from the north direction. The initial wind direction is assumed southeasterly (i.e., the initial phase Θ is -0.383π).

A different wind function is applied to better represent the wind field during a cold front event, instead of the rectilinear and harmonic wind used in Garvine's model (1985). We impose a constant magnitude, spatially uniformed and clockwise rotating wind field with angular velocity of ω and initial phase Θ (Figure 5.1). The cross-shore (or local) and alongshore (or remote)

winds are represented by:

$$\tau_x = \tau e^{i(\omega t+\Theta)} \quad (5\text{-}1a)$$

$$\tau_y = i\tau e^{i(\omega t+\Theta)} \quad (5\text{-}1b)$$

in which i is the imaginary unit. The effects of wind forcing on the subtidal sea level variation can be simplified as two independent mechanisms: (1) direct setup and setdown by local wind stress in the longitudinal direction of the estuary, and (2) remote wind action by producing cross-shelf Ekman transport over the adjacent shelf (Garvine, 1985). The alongshore and cross-shore wind stresses are 90° out of phase with the wind field we used here, while they are in phase in Garvine's model.

Since the model is 1-D, a boundary condition of the subtidal sea level η at the mouth is applied to represent the remote wind effect:

$$\eta(0,t) = \alpha E \quad (5\text{-}2)$$

and $$E = i\left(\frac{\tau}{f}\right)e^{i(\omega t+\Theta)}$$

where E is the cross-shelf component of the Ekman flux, f is the Coriolis parameter, and α is a remote wind coefficient which relates the cross-shelf Ekman flux with subtidal sea level at the estuarine mouth.

The governing equations are:

$$\frac{\partial u}{\partial t} = -g\frac{\partial \eta}{\partial x} + \frac{\tau_x - \tau_b^{(x)}}{\rho h} \quad (5\text{-}3)$$

$$\frac{\partial u}{\partial x} = -\frac{1}{h}\frac{\partial \eta}{\partial t} \quad (5\text{-}4)$$

where u is the subtidal current velocity in x-direction, ρ is sea water density, g is gravitational acceleration, and $\tau_b^{(x)}$ is the bottom friction.

The bottom friction is linearized by:

$$\tau_b^{(x)} = \rho C_D u_T u \quad (5\text{-}5)$$

where C_D is a bottom drag coefficient and u_T is the root mean square subtidal current velocity.

A series of dimensionless parameters are introduced to simplify the governing equations:

$$X \equiv (\omega/c)x \quad (5\text{-}6)$$

$$T \equiv \omega t \quad (5\text{-}7)$$

$$H \equiv \eta/\sigma \quad (5\text{-}8)$$

$$U \equiv hu/(\sigma c) \quad (5\text{-}9)$$

$$W \equiv \tau/(\rho\omega c\sigma) \quad (5\text{-}10)$$

$$\lambda \equiv C_D u_T/(h\omega) \quad (5\text{-}11)$$

Where $c=(gh)^{1/2}$ (i.e., long wave phase speed), σ is the standard deviation of the subtidal sea level, and u_T is root mean square subtidal current.

Now, the dimensionless governing equations can be expressed by the parameters from (5-6)-(5-11):

$$\frac{\partial U}{\partial T} + \frac{\partial \mathrm{H}}{\partial X} + \lambda U = W e^{i(T+\Theta)} \quad (5\text{-}12)$$

$$\frac{\partial U}{\partial X} + \frac{\partial \mathrm{H}}{\partial T} = 0 \quad (5\text{-}13)$$

The boundary conditions become:

$$\mathrm{H}(0,T) = iA(0)e^{i(T+\Theta)} \quad (5\text{-}14)$$

and

$$U(L,T) = 0 \quad (5\text{-}15)$$

where $A(0) \equiv \alpha\tau/(\sigma f)$, the scaled sea level amplitude at the mouth of Atchafalaya Bay. $L \equiv (\omega/c)\, l$, is the scaled length of the estuary.

5.1.2 Model Solution

The equations are solved by introducing the wave-form sea level and velocity terms:

$$\mathrm{H} = iA(x)e^{i(T+\Theta)} \qquad U = B(x)e^{i(T+\Theta)}$$

A second-order ordinary differential equation is derived from the dimensionless governing equations (5-12) and (5-13):

$$B'' + (1 - i\lambda)B = -iW \tag{5-16}$$

The solution of the above equation subject to the boundary conditions (5-14) and (5-15) is:

$$B(X,T) = \frac{-1}{K^2 \cosh(KL)}\{A(0)K \sinh[K(L-X)] - iW[\cosh(KL) - \cosh(KX)]\} \tag{5-17}$$

where K is a complex wave number of order unity given by:

$$K \equiv (-1 + i\lambda)^{1/2} = [(r-1)/2]^{1/2} + i[(r+1)/2]^{1/2}$$

in which $r \equiv (1+\lambda^2)^{1/2}$, a real number.

The analytical solutions of subtidal current and sea level are:

$$U(X,T) = \frac{-1}{K^2 \cosh(KL)}\{A(0)K \sinh[K(L-X)] - iW[\cosh(KL) - \cosh(KX)]\}\, e^{i(T+\Theta)} \tag{5-18}$$

$$\mathrm{H}(X,T) = \frac{i}{K \cosh(KL)}\{A(0)K \cosh[K(L-X)] - iW \sinh(KX)\}\, e^{i(T+\Theta)} \tag{5-19}$$

Or, we may rewrite a complete expression of water level solution:

$$\eta(x,t) = Re\{\frac{i}{K\cosh\left(\frac{K\omega l}{c}\right)}\left[\frac{\alpha\tau K}{f}\cosh\frac{K\omega(l-x)}{c} - \frac{i\tau}{\rho\omega c}\sinh\left(\frac{K\omega}{c}x\right)\right]e^{i(\omega t+\theta)}\} \tag{5-20}$$

For small L and X, we can expand the solutions using Taylor series expansion. After neglecting terms of order higher than L^2 and taking the real part of the waveforms, the simplified current velocity, sea level and sea level gradient are:

$$U(X,T) = (L-X)\left[-A(0)\cos(T+\Theta) - \frac{1}{2}W(L+X)\sin(T+\Theta)\right] \tag{5-21}$$

$$\mathrm{H}(X,T) = -A(0)\sin(T+\Theta) + WX\cos(T+\Theta) \tag{5-22}$$

$$\frac{\partial \mathrm{H}}{\partial X} = -A(0)(\mathrm{L}-\mathrm{X})\,[\sin(T+\Theta) - \lambda\cos(T+\Theta)] + W\cos(T+\Theta) \tag{5-23}$$

5.1.3 Model Coefficients

The average depth of Atchafalaya Bay is assumed to be 2.0 m, based on NOAA's EOS Estuarine Bathymetry data, so the long-wave phase speed c is 4.43m·s^{-1}. We assume that the period of wind event is 80 hours, or an equivalent angular frequency of 2.2×10^{-5} s^{-1}. The wind stress is 0.161 kg·m^{-1}·s^{-2}, assuming the density of air is 1.3 kg·m^{-3}, the constant wind speed is 10 m·s^{-1} and drag coefficient is 1.24×10^{-3}, suggested by Gill (1982). The density of sea water is 1027 kg·m^{-3}. The Coriolis parameter f is 7.18×10^{-5} s^{-1}, considering the mean latitude of the Atchafalaya Bay is 29.5°. We use the bottom drag coefficient of 5.0×10^{-3} (Li, 2003) and root mean square subtidal current of 0.1 m·s^{-1} to estimate the dimensionless bottom friction parameter. The station LAP is 15 km upstream of the mouth, so x in the equation equals 15,000 m. Since east winds have an influx effect, which will increase the sea level in the estuary, the remote wind coefficient α here must be a positive number. In Garvine's paper, he estimated the value of α to be 5×10^{-4} m^2·s·kg^{-1} based on Wang and Garvine's observations (1984). However, the number is not suitable for Atchafalaya Bay, since its bay depth (~2 m) is much smaller than those of the Chesapeake Bay and Delaware Estuary (~10 m). The frictional damping effect on the remote-wind-induced fluctuations becomes dominant, so the expected value should be less than Garvine's estimation.

From the analytical solution of subtidal sea level (5-20), one can determine that it contains two independent parts. The first term in the bracket represents the sea level variations induced by remote winds, which is directly proportional to α through sea level A(0) at the open boundary. The second term in the bracket stands for the sea level fluctuations driven by local winds, which have no relationship with the coefficient α. Here, an experiment is conducted to estimate α by comparing with observed water level records (Figure 5.2). From Section 4.3, we know that the amplitude of subtidal sea level variations measured at station LAP during a typical cold front

event is around 0.25 m. If we use the same α as in Garvine's paper (i.e., 5×10^{-4} $m^2\cdot s\cdot kg^{-1}$), the resultant subtidal sea level amplitude is nearly 5 times of the observation. The coefficient α of 8×10^{-5} $m^2\cdot s\cdot kg^{-1}$ is found to best fit to the observation.

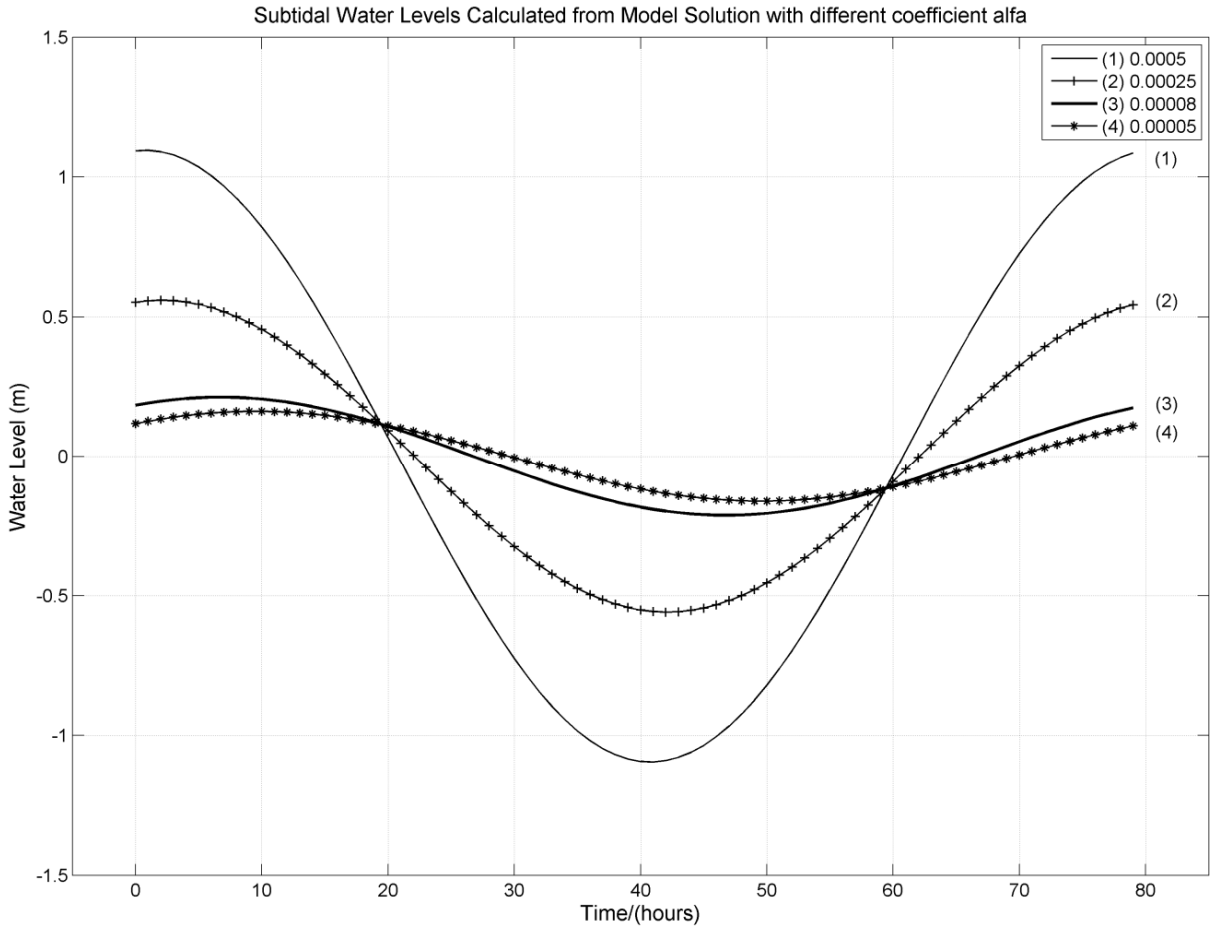

Figure 5.2 Subtidal water levels calculated from the model solution with: (1) α=0.0005 (Garvine's estimation); (2) α=0.00025; (3) α=0.00008; (4) α=0.00005. The thick dash line indicates the observed amplitude of sea level variations at station LAP.

5.1.4 Model Validation and Comparison with Observations

Left panels in Figure 5.3 illustrate a typically observed wind field and subtidal sea level variation during a cold front event and right panels show idealized wind field and model-predicted sea level variation, which is generally consistent with the observed results. From the analytical model, we find that water level fluctuations induced by cross-shore and alongshore winds have the same order of magnitude, although the amplitude of sea level from cross-shore

wind effect (0.12 m) is slightly smaller than that from alongshore wind effect (0.17 m). Furthermore, the model-predicted curve reaches the maximum 3 hours before the north wind component become largest, earlier than subtidal sea level record at station LAP. This suggests that there exists phase lag between subtidal sea level variations and remote wind effect, since it propagates from the adjacent shelf to the estuary. The phase lag may be identified from the coherence squared and phase relationship between subtidal wind stress and sea level record. Also, the observed amplitude of sea level falling is greater than that of rising, which is caused by the asymmetry of wind fields or the strengthening of wind stress in post-frontal phase. For real winds, the magnitudes of pre-frontal winds are less than 10 m/s, while post-frontal winds exceed 10 m/s and also last longer.

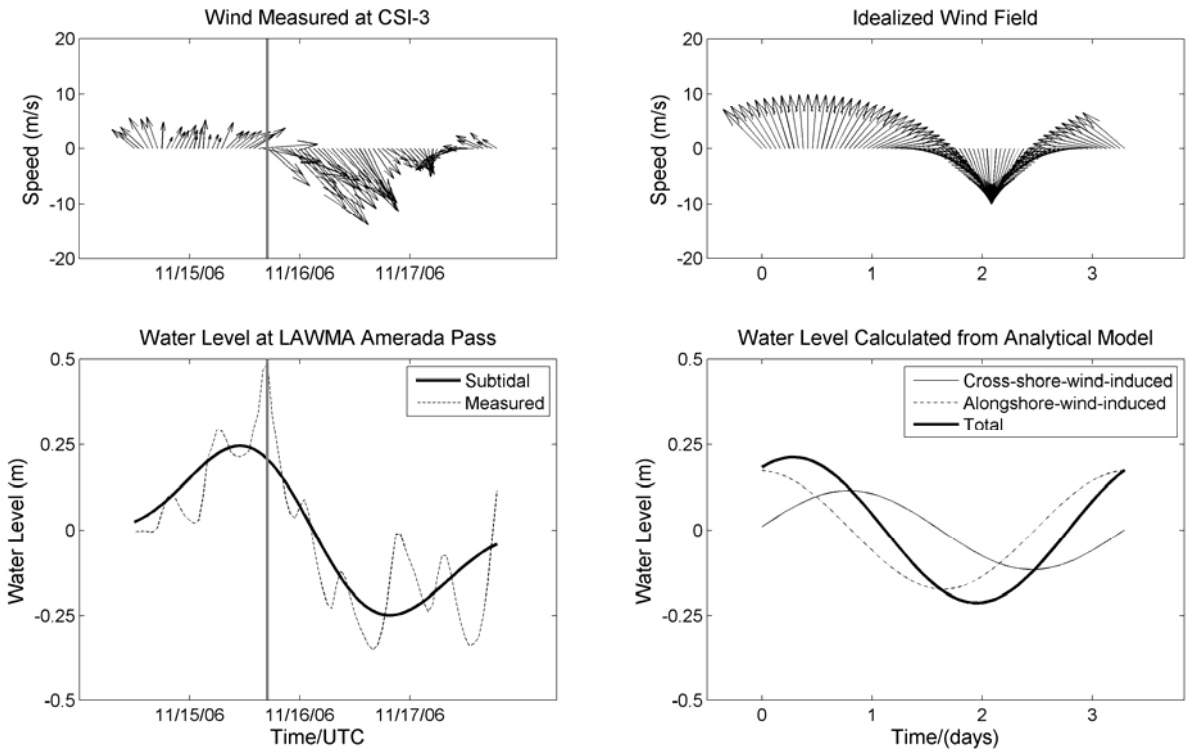

Figure 5.3 (a) Wind field observed at CSI-3. The vertical solid line indicates a cold front passed through the Atchafalaya Bay. (b) Ideal clockwise rotating wind with 80-hour period. (c) Measured and subtidal sea level at LAP. (d) Analytical-model-predicted sea level variations. The thin solid line and dotted line demonstrate the sea level variations induced by cross-shore winds and alongshore winds, respectively and thick solid line is the total sea level variation.

From simplified solution (5-22), one may expect that two oscillations are 90° out of phase. However, the actual phase difference is less than 90°, which indicates that the simplified solution fails to give good approximations on the phase. This can be explained by the large dimensionless bottom drag coefficient (λ) originating from the shallow water depth and frictional damping effect. Figure 5.4 compares the sea level variations calculated from exact and simplified solutions. The sea level variations from simplified solution always lag those from exact solution by 4 hours. In addition, the simplified solution slightly exaggerates both the effects from cross-shore and alongshore winds, and consequently the total sea level variations.

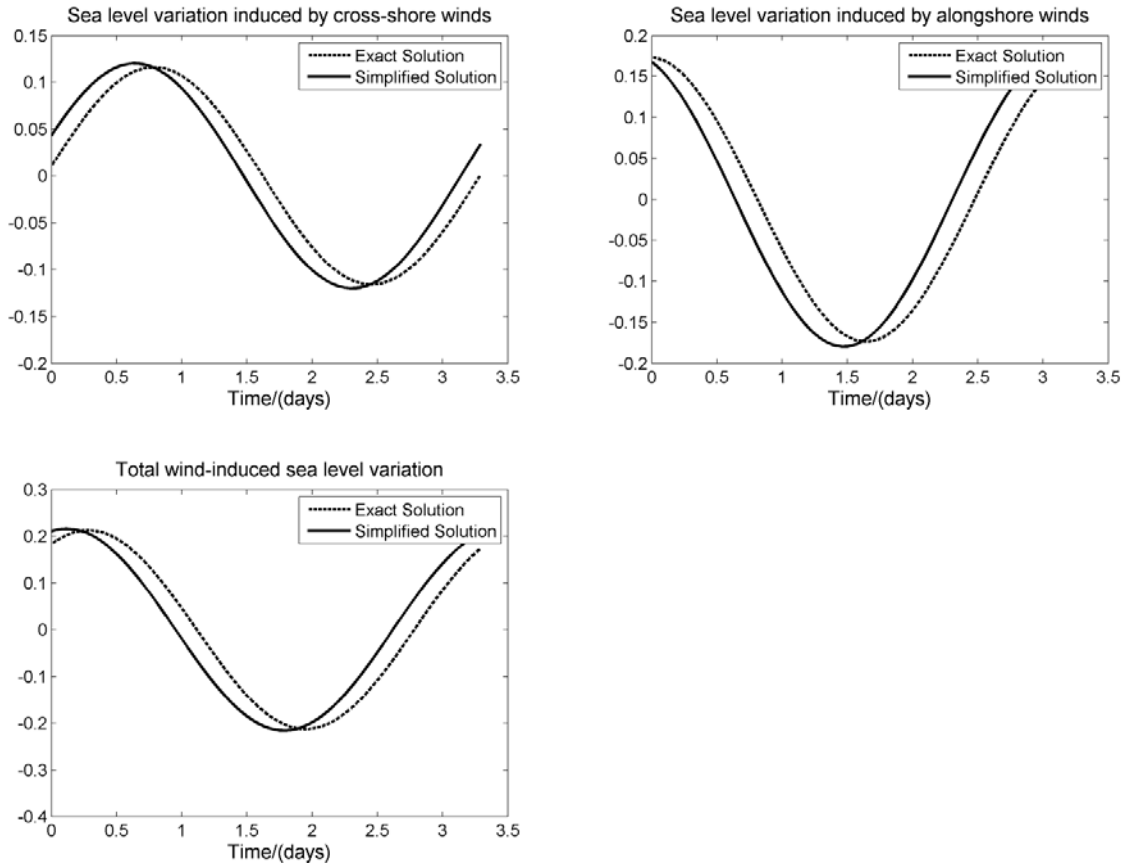

Figure 5.4 Comparison of (a) cross-shore-wind-induced; (b) alongshore-wind-induced; (c) total sea level variations from exact and simplified solutions.

5.1.5 The Relative Importance of Cross-shore and Alongshore Winds

From the previous section, one may know that water levels fluctuations inside the Atchafalaya

Bay induced by cross-shore and alongshore wind stresses are on the same order of magnitude. However, the conclusion is made from only one specific location. Based on the analytical solution, we can study the relative importance of cross-shore and alongshore winds to the entire estuary. Here, same conditions and coefficients as in previous section are used.

Alongshore wind forcing seems more important than cross-shore wind forcing in producing subtidal sea level variation along the entire estuary, since its corresponding sea level amplitudes are always larger (Figure 5.5). Furthermore, distance is the most important factor that determines the amplitudes of cross-shore-wind-induced sea level variation, with the zero amplitude at the mouth and largest amplitude at the head of the estuary. The amplitudes of sea level variation induced by alongshore winds are almost constant along the estuary, only slightly decreasing with distance. Near the bay mouth, sea level variations are produced primarily by alongshore wind forcing, but cross-shore wind forcing becomes significant near the bay head. The lowest amplitude of total sea level variation is found around 5 km to the estuarine mouth, and the highest amplitude is on the head.

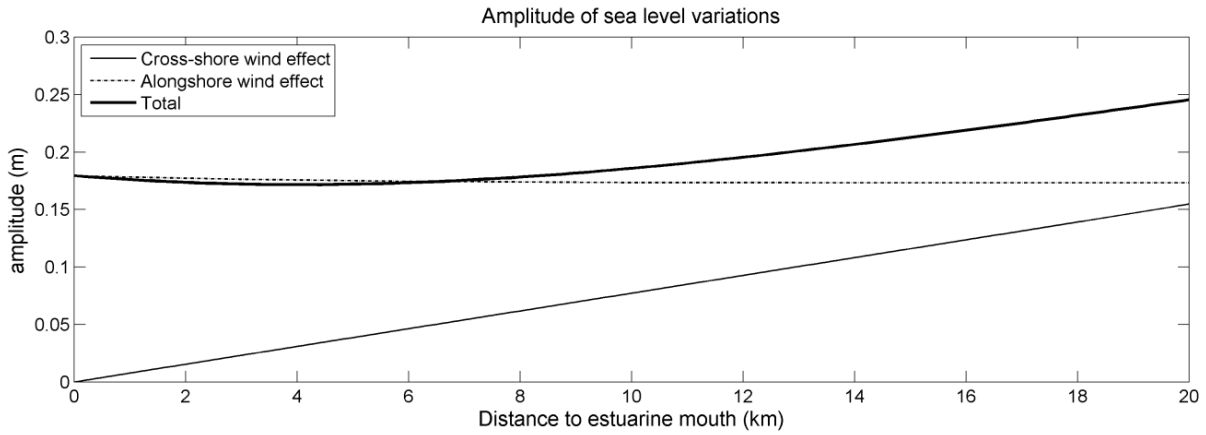

Figure 5.5 Amplitudes of sea level variations from cross-shore and alongshore wind effect and magnitude of total variation for the Atchafalaya Bay.

The highest and lowest total sea level variations are found near the estuarine head where effect of alongshore winds becomes obvious (Figure 5.6). The high subtidal sea level is coherent with

southeasterly/southerly/southwesterly winds near the estuarine head, while the low is also found near the head but coincides with winds from opposite directions. This conclusion is consistent with our previous observations. The highest and lowest sea levels induced by cross-shore wind forcing are on the bay head, but with southwesterly and northeasterly winds, respectively. The alongshore-wind-induced sea level varies with time and has little relationship with location. The highest and lowest sea levels correspond to southeasterly and northwesterly winds, respectively.

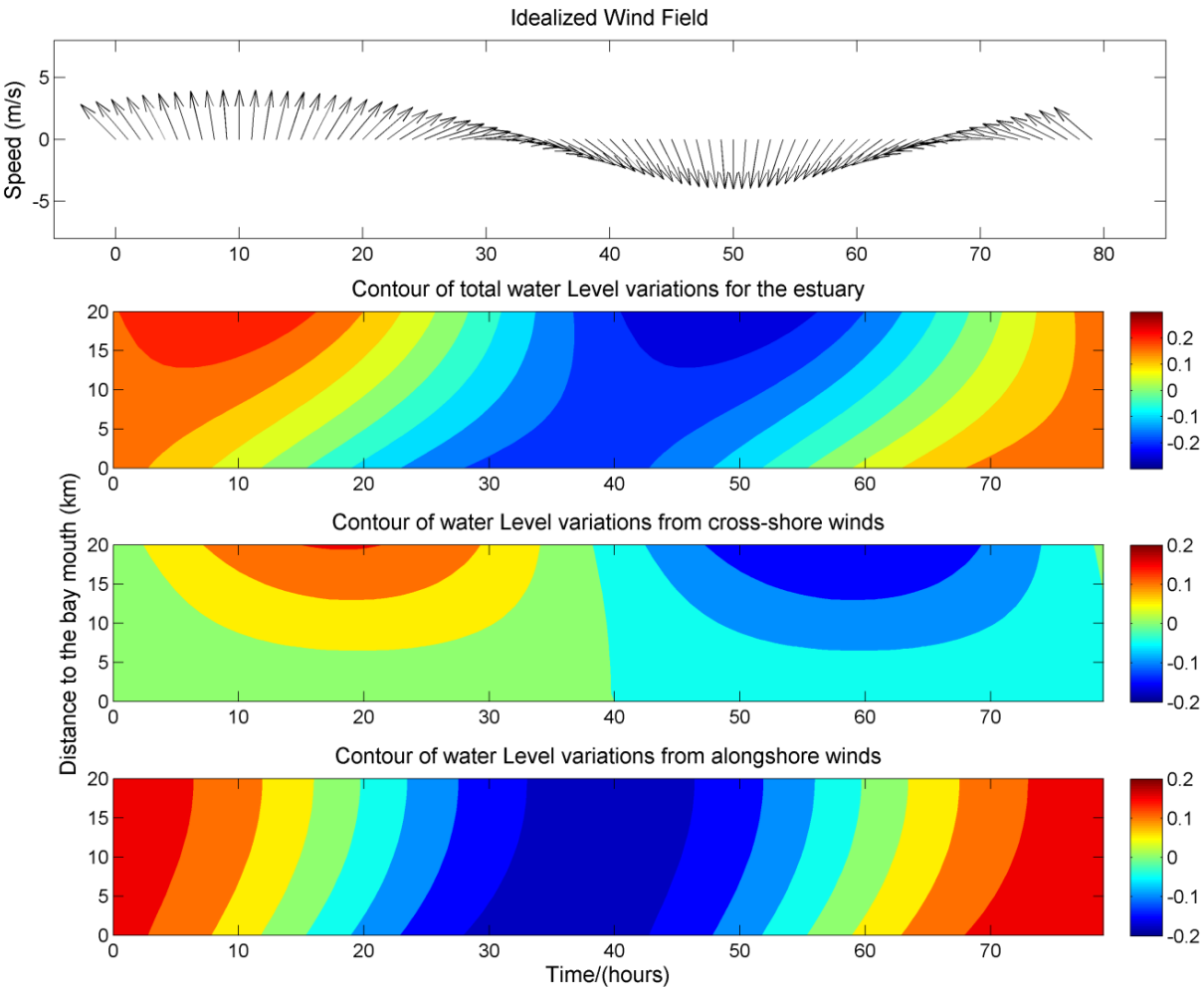

Figure 5.6 (a) idealized wind field, (b) contour of total sea level variations, (c) contour of sea level variations from cross-shore wind forcing and (d) contour of sea level variations from alongshore wind forcing for the Atchafalaya Bay

5.1.6 Implication of the Model to the Other Bays

In order to test the robustness of the analytical model, a question arises whether such model can also be applied to the other estuaries of this area, such as TTB and BB. The major differences of these two bays to Atchafalaya Bay are the barrier islands chains lying at the bay mouths, which may lead to a less significant remote wind effect.

Figure 5.7 shows the plain views of idealized TTB and BB. The longitudinal axes (x-axis) of TTB and BB are in the north direction and rotated counterclockwise 27° from the north direction, respectively. The length of TTB and BB are about 27.3 and 24.6 km. The water depth of TTB and BB is 1.5 m and 1.1 m. The wind fields and other parameters are set the same as used in the Atchafalaya Bay. Water levels from two stations inside the TTB, TAML1 (14.2 km to the bay mouth) and LUML1 (21.6 km to the bay mouth) can be used to verify the analytical solution. For BB, water level data are only available from one station, GISL1, near the bay mouth.

Overall, the model provides good approximations to the subtidal sea level variations for all three stations (Figure 5.8). The model-predicted water level fits the observation well for LUML1. For TAML1, the amplitude of model result seems to be smaller than that of observations. For GISL1, a station in the vicinity of the mouth of BB, the amplitude of model result approximates observation; however, the phase differences between each other are large. The cross-shore-wind-induced water level is nearly zero and the water level is almost totally driven by alongshore winds. This may point out a major limitation of this simple analytical model that it assumes no estuary-shelf interaction from cross-shore wind forcing. The model may not be directly applicable to estimate water levels near the estuarine mouth. A possible way to improve the model is to set the starting point (x=0) at somewhere on the continental shelf and increase the length of estuary.

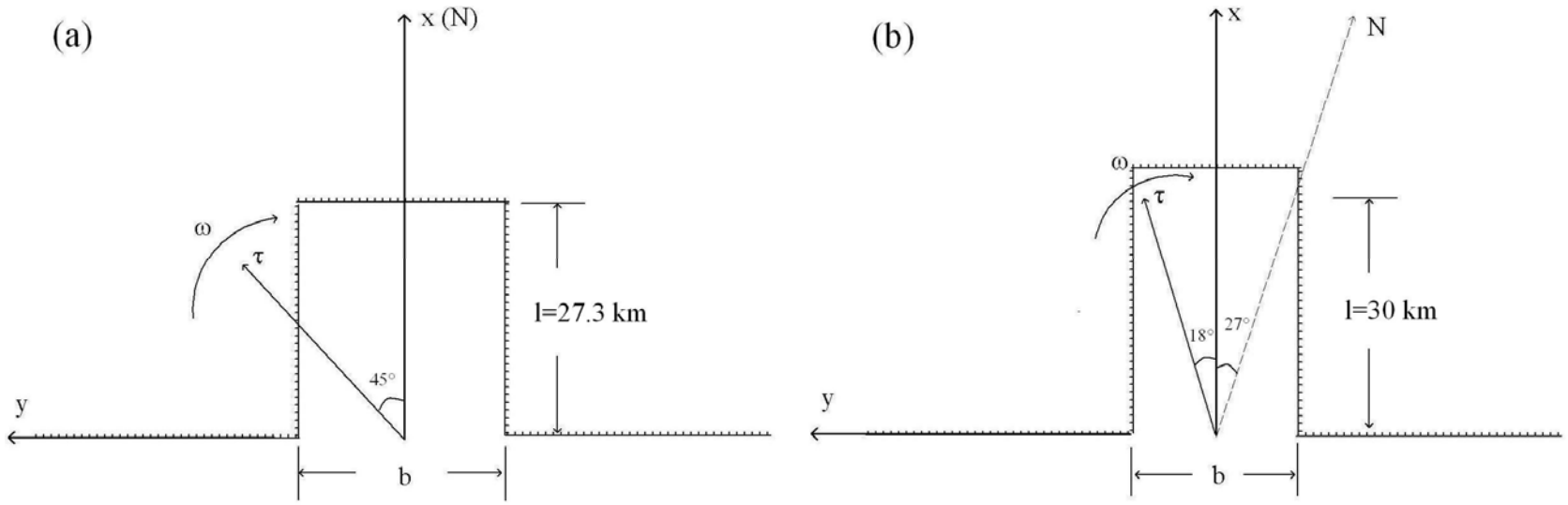

Figure 5.7 The plain view of idealized (a) Terrebonne/Timbalier Bays (TTB) and (b) Barataria Bay (BB). For TTB, the length (l) is 27.3 km and width (b) of 50 km. The longitudinal axis (i.e., x-axis) of the TTB is in north direction. For BB, the length (l) is 30 km and width (b) of 30 km. The longitudinal axis (i.e., x-axis) of the BB and 27° counterclockwise rotated from the north direction. The initial winds for both cases are assumed southeasterly.

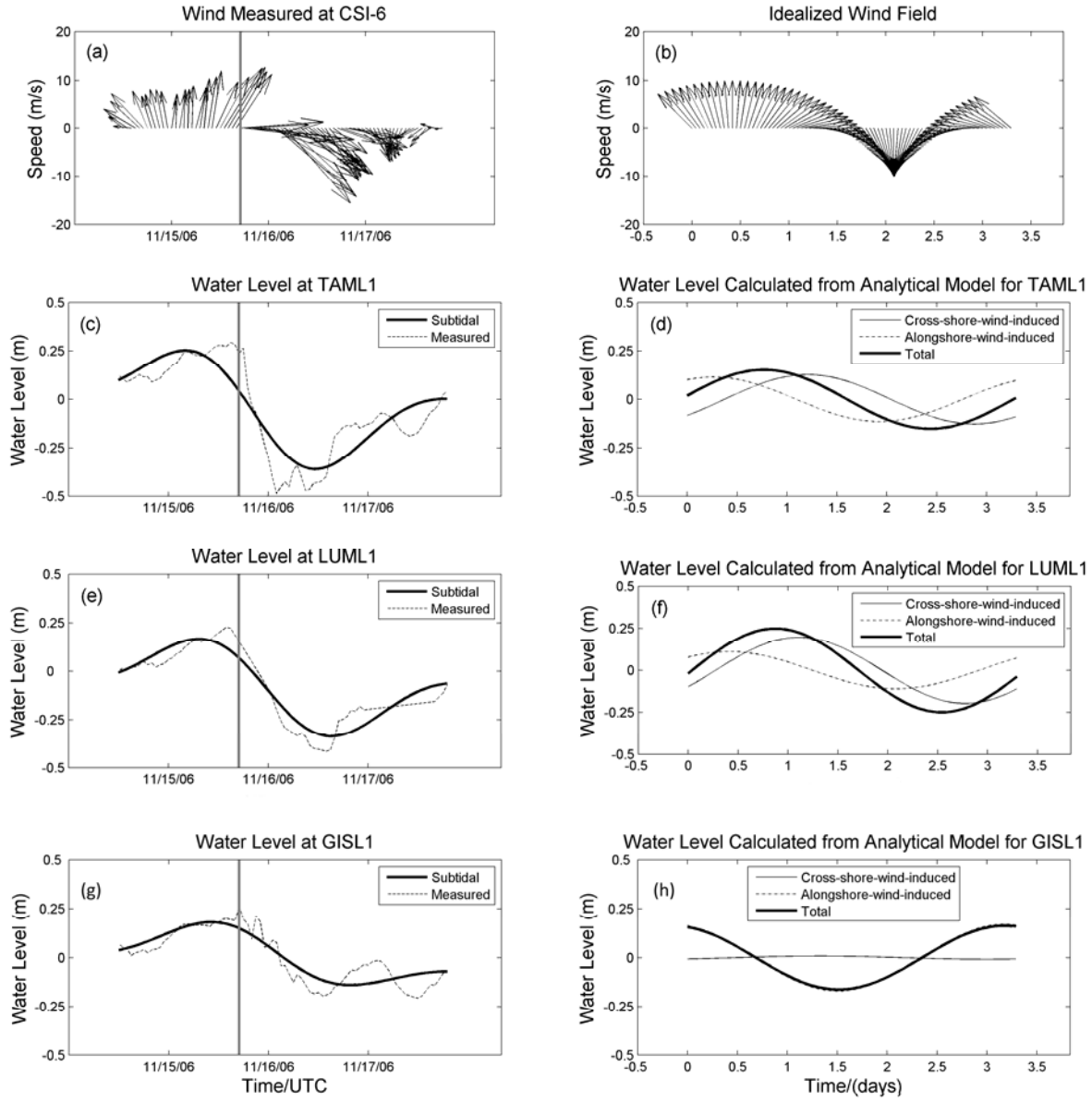

Figure 5.8 (a) Wind field observed at CSI-6. The vertical solid line indicates a cold front passed through the Atchafalaya Bay; (b) ideal clockwise rotating wind with 80-hour period; (c) measured and subtidal sea level at TAML1 (14.2 km to the mouth of TTB); (d) analytical-model-predicted sea level variations at TAML1; (e) measured and subtidal sea level at LUML1 (21.6 km to the mouth of TTB); (f) analytical-model-predicted sea level variations at LUML1; (g) measured and subtidal sea level at GISL1 (near the mouth of BB); (h) analytical-model-predicted sea level variations at GISL1.

CHAPTER 6 SUMMARY AND CONCLUSIONS

In order to better understand the hydrodynamic response to cold fronts along the Louisiana coast, data of water level, current, wind and river discharge from September, 2006 to April, 2007 have been analyzed and an analytical model has been used for the interpretation of the dynamics. This study focuses on the characteristics of cold-front-related hydrodynamics and determines the geographic difference and correlation of hydrodynamic responses to cold fronts in different bays and estuaries and relative importance of wind, tide, and river discharge on water level variability and flow field. The primary conclusions are summarized as follows:

(1) Cold fronts have two end-member types—arctic surge and migrating cyclone. Twenty-nine cold fronts are identified from the eight-month United States surface weather maps, of which only four are arctic surges and the other twenty five are migrating cyclones. Migrating cyclones translate southeastward across the Louisiana, so they first affect Atchafalaya/Vermilion Bays, followed by Terrebonne/Timbalier Bays 3-4 hours later and Barataria Bay after about one more hour. Arctic surges move southward with typical frontal orientations parallel to the coastline, which almost simultaneously influence the Louisiana coastal bays.

(2) The amplitude spectra of water level indicate that diurnal tides are dominant for all stations except West Bank Bayou Gauche in the upper Barataria Basin, which is dominated by wind-induced low-frequency oscillations. The five stations west of 91°W have relatively high semidiurnal tidal signals, the amplitudes of which account for 44% to 70% of those of diurnal signals. The subtidal water level oscillations are mainly wind-driven and consistent with synoptic local weather patterns. Cold front events coincide with major set-up and set-down of water levels, but the variability associated with different events is large, depending on the strength of the weather system and speed,

direction and duration of winds. Only Tesoro Marine Terminal (a station in the channel of Atchafalaya River) shows response to high Mississippi and Atchafalaya River discharge in late January and early February and March 2007, when both the wind-induced and tidal oscillations are overwhelmed by the spring flood. A distinct wind surge event is identified from water level records between two successive cold front passages in the middle of October, which is believed to be driven by strong and sustained south/southwest winds.

(3) Cold fronts play an important role in flushing water out of the Louisiana bays. Different bays have different water exchange rates depending on their water body area and geomorphology. The flux amplitude of the AVB is the largest, which is approximately four time of that of the TTB and an order of magnitude higher than that of the BB. The five largest flushing events correspond to migrating extratropical cyclones when frontal orientation is perpendicular to the coastline, suggesting that wind direction is one of the major controlling factors in determining the flushing rate and amount. Both alongshore and cross-shore winds can effectively induce the bay-shelf water exchange, and northwest to north winds appear to be the most influential events to flush the bays. Two mechanisms can explain the wind-induced barotropic estuary-shelf exchange: direct transport from set-up and set-down of water level by cross-shore wind, and Ekman pumping due to alongshore wind. Those five cold front events can flush 34.4% to 41.9%, 28.5% to 44.9%, and 23.7% to 37.8% of the total bay waters from the AVB, TTB, and BB, respectively. Strong cold fronts can flush more than 40% bay waters onto the continental shelf within 30 to 40 hours. The Atchafalaya River discharge also contributes to the flushing of the AVB, with the total flushed volume from the combined effects of cold front winds and river discharge may account for about half of the bay

volume. The occasionally diverted Mississippi water from the Davis Pond Freshwater Diversion may also influence the BB.

(4) In the eight-month period, east, northeast, southeast, and north winds are four most prevalent winds, occuring about 21%, 20%, 18%, and 15% of the time, respectively. Winds from all other directions occur less than 10% of the time. However, strong winds of speed more than 10.0 m/s are only observed from two directions: northwest (~0.1%) and west (~0.05%), which are mostly associated with cold front passages.

(5) Near-surface current on the Louisiana inner shelf is mainly wind-driven, but tidal forcing becomes more important in the sub-surface layers, or areas adjacent to the coastline. Time-series subtidal current profiles demonstrate a dominant westward down-coast flow along the Louisiana inner shelf, occurring 81% and 70% of the time at CSI-6 and CSI-3, repectively. The Strong cold front events may disturb this down-coast flow system by inducing a 1- to 3-day up-coast flow. At CSI-6, the river discharge from Southwest Pass of the Mississippi River has little influence most of the time with non-flood conditions. Nevertheless, during the period of spring flood, the large amount of freshwater exerts significant barotropic and baroclinic forcings on the current field and reinforces the wind-driven down-coast flow. Currents at CSI-3 during the flood period still follow the winds closely, which may attribute to the local effects of shallow water and coastal boundary.

(6) The 1-D analytical model, modified from Garvine (1985), is successfully applied to the very shallow Louisiana bays to investigate the relationship between subtidal water level variability and cross-shore as well as alongshore winds during cold front episodes. The model results reveal that the amplitudes of water level variations induced by those two independent forcing mechanisms have the same order of magnitude (i.e., 10^{-1} m),

indicating that cross-shore and alongshore winds play almost equally important roles in affecting the subtidal water level variability inside the bays. The amplitudes of cross-shore-wind-induced water level variation increase from zero at the bay mouth to the largest at the bay head, while alongshore winds have almost equal effects along the estuarine longitudinal axis. The high subtidal sea level is coherent with southeasterly/southerly/southwesterly winds and the low coincides with winds from opposite directions, which agree well with observations.

Future study should employ statistical methods (e.g., cross-spectral analysis and multiple coherence analysis) to investigate the complex interactions of wind, river, and tidal influences on water level and current variabilities. The high-resolution Finite Volume Coastal Ocean Model (FVCOM) can be applied to the Louisiana estuaries and inner shelf to simulate cold-front-related hydrodynamics (e.g., water level, current and circulation) and coastal environmental responses (e.g., salinity, temperature and river plume). Future modeling studies will eventually provide us with additional insight on the mechanisms relating meteorological forcing, hydrodynamic processes, and coastal environmental changes.

REFERENCES

Barras, J., Beville, S., Britsch, D., Hartley, S., Hawes, S., Johnston, J., Kemp, P., Kinler, Q., Martucci, A., Porthouse, J., Reed, D., Roy, K., Sapkota, S., and Suhayda, J., 2003. Historical and projected coastal Louisiana land changes: 1978-2050: USGS Open File Report 03-334, 39pp.

Barras, J.S., Hartley, J.S., Johntson, J.B., and Jones, W.R., 2004. 100+ Years of Land Change for Coastal Louisiana.http://www.nwrc.usgs.gov/upload/landloss11X17.pdf

Barras, J.A., 2007, Satellite images and aerial photographs of the effects of Hurricanes Katrina and Rita on coastal Louisiana: U.S. Geological Survey Data Series 281, at http://pubs.usgs.gov/ds/2007/281.

Bass, A.S., and Tuner, E.R., 1997. Relationships between salt marsh loss and dredge canals in three Louisiana estuaries. Journal of Coastal Research, 13 (3), 895-903.

Bellotte, R.T., 2007. Sediment transport on a river-dominated shallow shelf water shelf: Atchafalaya Bay region, Louisiana. Unpublished M.S. Thesis, Louisiana State University, Baton Rouge, LA. 125pp.

Booth, J.G., Miller, R.L., McKee, B.A., and Leathers, R.A., 2000 Wind-induced bottom sediment resuspension in a microtidal coastal environment. Continental Shelf Research, 20, 785-806.

Chesney, E.J., Baltz, D.M., Thomas, G.R., 2000. Louisiana estuarine and coastal fisheries and habitats: perspectives from a fish's eye view. Ecological Applications, 10 (2), 350-366.

Chuang, W.-S. and Wiseman, W.J., Jr., 1983. Coastal sea level response to frontal passages on the Louisiana-Texas Shelf. Journal of Geophysical Research, 88, C4, 2615-2620.

Cho, K., Reid, R.O., Nowlin, W.D. Jr., 1998. Objectively mapped stream function fields on the Texas-Louisiana shelf based on 32 months of moored current meter data. Journal of Geophysical Research, 103, No.C5, 10377-10390.

Cobb, M., keen, T.R., and Walker, N.D., 2008a. Modeling the circulation of the Atchafalaya Bay system during winter cold front events. Part1: model description and validation. Journal of Coastal Research, 24 (4), 1036-1047.

Cobb, M., keen, T.R., and Walker, N.D., 2008b. Modeling the circulation of the Atchafalaya Bay system. Part2: river plume dynamics during cold fronts. Journal of Coastal Research, 24 (4), 1048-1062.

Cochrane, J.D., Kelly, F.J., 1986. Low-frequency circulation on the Texas-Louisiana continental shelf. Journal of Geophysical Research, 91(C9), 10645-10659.

Coleman, J.M., Roberts, H.H., and Stone, G.W., 1998. Mississippi River Delta: an overview. Journal of Coastal Research, 14 (3), 698-716.

Cragg, J., Mitchum G., and Sturges, W., 1983. Wind-induced sea-surface slopes on the West Florida Shelf. Journal of Physical Oceanography, 13, 2201-2212.

Craig, N.J., Turner, R.E., and Day, J.W., Jr., 1979. Land loss in Coastal Louisiana (U.S.A.). Environmental Management, 3 (2), 133-144.

Davidson, K.L., Boyle, P.J., and Guest, P.S., 1992. Atmospheric boundary-layer properties affecting wind forecasting in coastal regions. Journal of Applied Meteorological, 31, 983-994.

Davis, R.A., Jr., 1997. Regional coastal morphodynamics along the United State Gulf of Mexico. Journal of Coastal Research, 13 (3), 595-604.

Day, J.W., Jr., Boech, D.F., Clairain, E.J., Kemp, G.P., Laska, S.B., Mitsch, W.J., Orth, K., Mashriqui, H., Reed, D.J., Shabman, L., Simenstad, C.A., Streever, B.J., Twilley, R.R., Watson, C.C., Wells, J.T., Whigham., D.F., 2007. Restoration of the Mississippi Delta: lessons from Hurricanes Katrina and Rita. Science, 115, 1679-1684.

Del Castillo, C.E., and Miller, R.L., 2008. On the use of ocean color remote sensing to measure the transport of dissolved organic carbon by the Mississippi River Plume. Remote Sensing of Environment, 112, 836-844.

Denes, T.A., Caffrey, J.M., 1988. Changes in seasonal water transport in a Louisiana Estuary, Fourleague Bay, Louisiana. Estuaries, 11(3), 184-191.

DiMarco, S.F., Reid, O.R., 1998. Characterization of the principal tidal current constituents on the Texas-Louisiana shelf. Journal of Geophysical Research, 103, No.C2, 3093-3109.

DiMego, G.J., Bosart, L.F., and Endersen, G.W., 1976 An examination of the frequency and mean conditions surrounding frontal incursions into the Gulf of Mexico and Caribbean Sea. Monthly Wether Review, 104, 709-718.

Dingler, J.R., and Reiss, T.E., 1990. Cold-front driven storm erosion and overwash in the central part of the Isle Dernieres, a Louisiana barrier-island arc. Marine Geology, 91, 195-206.

Dingler, J.R., Hsu, S.A., and Reiss, T.E., 1992. Theoretical and measured aeolian sand transport on a barrier island, Louisiana. Sedimentology, 39, 1031-1043.

Draut, A.E., Kineke, G.C., Huh, O.K., Grymes J.M. III, Westphal, K.A., and Moeller, C.C., 2005. Coastal mudflat accretion under energetic conditions, Louisiana chenier-plain coast, USA. Marine Geology, 214, 27-47.

D'Sa E., and Miller, R.L., 2005 Bio-optical properties of coastal waters. In R.L.Miller et al. (eds), Remote Sensing of Coastal Aquatic Environments, 129-155.

Ellis, J., and G.W. Stone, 2006. Numerical simulation of net longshore sediment transport and granulometry of surficial sediments along Chandeleur Island, Louisiana, USA. Marine Geology, 232, 115-129.

Emery W.J., and Thomson, R.E., 2004. Data Analysis methods in physical oceanography, 2nd

edition. Oxford, UK, Elsevier, 638pp.

Fernandez-Partagas J., and Mooers, C.N.K., 1975. A subsynoptic study of winter cold fronts in Florida, Monthly Weather Review, 103, 742-744.

Garvine, R.W., 1985. A simple model of estuarine subtidal fluctuations forced by local and remote wind stress. Journal of Geophysical Research, 90 (C6), 11945-11948.

Georgiou, I.Y., FitzGerald, D.M., and Stone, G.W., 2005. The impact of physical processes along the Louisiana coast. Journal of Coastal Research, Special issue No.44, 72-89.

Gill, A.E., 1982. Atmosphere-ocean dynamics. Academic Press, San Diego, 662pp.

Goolsby, D.A., Battaglin, W.A., Lawrence, G.B., Artz, R.S., Aulenbach, B.T., Hooper, R.P., 1999. Flux and sources of nitrients in the Mississippi-Atchafalaya Basin: topic 3 report for the integrated assessment on hypoxis in the Gulf of Mexico. Silver Spring (MD): NOAA Coastal Ocean Office. Decision Analysis Series no.17.

Gordon, H.R., O.T., Brown, R.H., Evans, J.W., Brown, R.C., Smith, K.S., Baker, D.K., Clark, 1988. A semianalytic radiance model of ocean color. Journal of Geophysical Research, 93, D9, 10909-10924.

Grenci, L.M., and Nese, J.M., 2006. A world of Weather: fundamentals of meteorology. Kendall/Hunt publishing Co., 780pp.

Henry, W.K., 1979. Some aspects of the fate of cold fronts in the Gulf of Mexico. Monthly Weather Review, 107,1078-1082.

Horton, R.W., 1998. Atmospheric and hydrographic effects on postlarval brown shrimp (Penaeus Aztecus Ives) estuarine recruitment in the northern Gulf of Mexico. Unpublished M.S. Thesis, Louisiana State University. Baton Rouge, LA. 90pp

Hsu, S.A., 1988. Coastal Meteorology. San Diego, California: Academic Press, Inc., 260pp.

Hsu, S.A., 1993. The Gulf of Mexico — a breeding ground for winter storms. Mariners Weather Log, 37 (2), 4-11.

Huh, O.K., Wiseman, W.J., Jr., and Rouse, L.J., Jr., 1978. Winter cycle of sea surface thermal patterns, northeastern Gulf of Mexico. Journal of Geophysical Research, 83(C9), 4523-4529.

Huh, O.K., and Rouse, L.J., Jr., 1984. Cold air outbreaks over the northwest Florida continental shelf: heat flux processes and hydrographic changes. Journal of Geophysical Research, 89(C1), 717-726.

Huh, O.K., Moeller, C.C., Menzel, W.P., Rouse, L.J., Jr., and Roberts, H.H., 1996. Remote sensing of turbid coastal and estuarine waters: a method of multispectral water-type analysis. Journal of Coastal Research, 12 (4), 984-995.

Inoue, M., Wiseman, W.J. Jr., 2000. Transport, mixing and stirring processes in a Louisiana

Estuary: a model study. Estuarine, Coastal and Shelf Science, 50, 449-466.

Johnson, GA., Meindl, E.A., Mortimer, E.B., and Lynch, J.S., 1984. Features associated with repeated strong cyclogenesis in the western Gulf of Mexico during the winter of 1982-83, in post-prints, Third Conference on Meteorology of the Coastal Zone, pp. 110-117, American Meteorological Society, Boston, Mass.

Jose, F., Kobashi, D., and Stone, G.W., 2007. Spectral wave transformation over an elongated sand shoal off south-central Louisiana, U.S.A.. Journal of Coastal Research, Special Issue 50, 757-761.

Keen, T.R., 2002. Waves and currents during a winter cold front in the Mississippi Bight, Gulf of Mexico: Implications for barrier island erosion. Journal of Coastal Research, 18 (4), 622-636.

Kineke, G.C., Higgins E.E., Hart K., and Velasco D., 2006. Fine-sediment transport associated with cold-front passages on the shallow shelf, Gulf of Mexico. Continental Shelf Research, 26, 2073-2091.

Kobashi, D., Jose, F., and Stone G.W., 2007a. Impacts of fluvial sediments and winter storms on a transgressive shoal, off south-central Louisiana, U.S.A.. Journal of Coastal Research, SI 50, 858-862.

Kobashi, D., Jose, F., and Stone G.W., 2007b. Heterogeneity and dynamics on a shoal during spring-winter storm season, south-central Louisiana, USA. Coastal Sediments ’07, Volume 2, 921-934.

Lee, J.M., Wiseman, W.J. Jr., and Kelly, F.J., 1990. Barotropic, subtidal exchange between Calcasieu Lake and the Gulf of Mexico. Estuaries, 13 (3), 258-264.

Lewis, J.K., and Hsu, S.A., 1992. Mesoscale air-sea interactions related to tropical and extratropical storms in the Gulf of Mexico, Journal of Geophysical Research, 97, 2215-2228.

Li C., 2003. Can friction coefficient be estimated from cross stream flow structure in tidal channels? Geophysical Research Letters, 30 (17), 1897, doi:10,1029/ 2003GL018087.

Li, C., Roberts, H.H., Stone, G..W., Weeks, E., and Luo, Y., 2009. Wind surge and saltwater intrusion in Atchafalaya Bay under onshore wind prior to cold front passage. Hyrobiologia (accepted).

List., J.H., Jaffe, B.E., Sallenger, A.H., Jr., and Hansen, M., 1997. Bathymetric comparisons adjacent to the Louisiana barrier islands: processes of large-scale change. Journal of Coastal Research, 13(3), 670-678.

Lohrenz, S.E., Fahnenstiel, G.L., Redalje, D.G., Lang, G.A., Dagg, M.J., Whitledge, T.E., Dortch, Q., 1993. Nutrients, irradiance, and mixing as factors regulating primary production in coastal water impacted by the Mississippi River plume. Continental Shelf Research, 19, 1113-1141.

Marmorino, G.O., 1982. Wind-induced sea level variability along the West Florida Shelf (winter, 1978). Journal of Physical Oceanography, 12, 389-405.

Marmorino, G.O., 1983. Small-scale variations of wind-driven coastal sea-level response in the West Florida Bight. Journal of Physical Oceanography, 93, 93-102.

McBride, R.A., and Byrnes, M.R., 1997. Regional variations in shore response along barrier island systems of the Mississippi River Delta Plain: historical change and future prediction. Journal of Coastal Research, 13 (3), 628-653.

Miller, R.L., and McKee, B.A., 2004. Using MODIS Terra 250 m imagery to map concentrations of total suspended matter in coastal waters. Remote Sensing of Environment, 93, 259-266.

Miller, R.L., McKee, B.A., and D'Sa E., 2005. Monitoring bottom sediment resuspension and suspended sediment in shallow coastal waters. In: Remote Sensing of Coastal Aquatic Environments (R.L., Miller, eds.), pp.259-276. Springer.

Milliman J.D., and Meade, R.H., 1983. World-wide delivery of river sediment to the oceans. The Journal of Geology, 91 (1), 1-21.

Myint S.W., and Walker, N.D., 2002. Quantification of surface suspended sediments along a river dominated coast with NOAA AVHRR and SeaWiFS measurements: Louisiana, USA. International Journal of Remote Sensing, 23 (16), 3229-3249.

Moeller, C.C., Huh, O.K., Roberts, H.H., Gumley, L.E., and Menzel W.P., 1993. Response of Louisiana coastal environments to a cold front passage. Journal of Coastal Research, 9 (2), 434-447.

Morey, S.L., Martin, P.J., O'Brien, J.J., Wallcraft, A.A., and Zavala-Hidalgo, J., 2003. Export pathways for river discharged fresh water in the northern Gulf of Mexico. Journal of Geophysical Research, 108 (C10), 3303, doi:10.1029/2002JC001674.

Mossa J., and Roberts, H.H., 1990. Synergism riverine and winter storm-related sediment transport processes in Louisiana's coastal wetland. Gulf Coast Association of Geological Societies Transactions, 40, 635-642.

Muller-Karger, F.E., Hu, C., Andrefouet, S., Varela, R., and Thunell, R., 2007. The color of the coastal ocean and applications in the solution of research and management problems. In R.L. Miller et al. (eds.), Remote Sensing of Coastal Aquatic Environments, 101-127.

Murray, S.P., 1994. Mississippi River plume hydrography: annual report. OCS study/MMS 94-0028. U.S. Dep. of the Interior, Mineral Mgmt. Service, Gulf of Mexico OCS Regional Office, New Orleans, LA. 229 pp.

Murray, S.P., and Donley, J., 1995. Mississippi River plume hydrography: Second annual report. OCS study/MMS 96-0022. U.S. Dep. of the Interior, Mineral Mgmt. Service, Gulf of Mexico OCS Regional Office, New Orleans, LA. 175 pp.

Murray, S.P., 1998. An observational study of the Mississippi-Atchafalaya coastal plume: Final Report, OCS Study/MMS 98-0040. U.S. Dept. of the Interior, Minerals Mgmt. Service, Gulf of Mexico OCS Regional Office, New Orleans, LA, 513pp.

Noble, M.A., Schroeder, W.W., Wiseman, W.J., Jr., Ryan, H.F., and Gelfenbaum, G., 1996. Subtidal circulation patterns in a shallow, highly stratified estuary: Mobile Bay, Alabama. Journal of Geophysical Research, 101(11), 25689-25703.

Norcross, B.L., and Shaw, R.F., 1984. Oceanic and estuarine transport of fish egg and larvae: a review. Transactions of Americane Fisheries Society, 113, 153-165.

Nowlin, W.D. Jr, Paker, C.A., 1974. Effects of a cold-air outbreak on shelf waters of the Gulf of Mexico. Journal of Physical Oceanography, 4, 467-486.

Nowlin, W.D., Jr., Jochens, A.E., Reid, R.O., and DiMarco, S.F., 1998a. Texas-Louisiana Shelf Circulation and Transport Processes Study: Synthesis Report, Volume I: Technical Report. OCS Study MMS 98-0035. U.S. Dept. of the Interior Minerals Mamt. Service, Gulf of Mexico OCS region, New Orleans, LA. 502pp.

Nowlin, W.D., Jr., Jochens, A.E., Reid, R.O., and DiMarco, S.F., 1998b. Texas-Louisiana Shelf Circulation and Transport Processes Study: Synthesis Report, Volume II: Technical Report. OCS Study MMS 98-0036. U.S. Dept. of the Interior Minerals Mamt. Service, Gulf of Mexico OCS region, New Orleans, LA. 288pp.

Oey, L.Y., 1995. Eddy- and wind-forced shelf circulation. Journal of Geophysical Research, 100, No.C5, 8621-8637.

Ohlmann, J.C., Niiler, P.P., 2005. Circulation over the continental shelf in the northern Gulf of Mexico. Progress in Oceanography, 64, 45-81.

Penland, S., Boyd, R., and Suter J.R., 1988. Transgressive depositional systems of the Mississippi delta plain: a model for Barrier shoreline and shelf sand development. Journal of sedimentary petrology, 58(6), 932-949.

Penland, S., Roberts, H.H., Williams, S.J., Sallenger, A.H. Jr., Cahoon, D.R., Davis, D.W., and Groat, C.G., 1990. Coastal Land Loss in Louisiana. Gulf Coast Association of Geological Societies Transactions, 40, 685-699.

Penland, S., and Ramsey, K.E., 1990. Relative sea level rise in Louisiana and the Gulf of Mexico: 1908-1988. Journal of Coastal Research, 6(2), 323-342.

Pepper, D.A., and Stone, G.W., 2002. Atmospheric forcing of find-sand transport on a low-energy inner shelf: south-central Louisiana, USA. Geo-Mar Lett (2002) 22: 33-41.

Pepper. D.A., and Stone, G.W., 2004. Hydrodynamics and sedimentary responses to two contrasting winter storms on the inner shelf of the northern Gulf of Mexico. Marine Geology, 210, 43-62.

Perez, B.C., Day, J.W., Rouse, L.J., Jr., Shaw, R.F., and Wang, M., 2000. Influence of Atchafalaya River discharge and winter frontal passage on suspended sediment concentration and flux in Fourleague Bay, Louisiana. Estuarine, Coastal and Shelf Science, 50, 271-290.

Pope J., 1997. Responding to coastal erosion and flooding damages. Journal of Coastal Research,

13 (3), 704-710.

Rabalais, N.N., Turner, R.E., and Wiseman, W.J., Jr., 2001. Hypoxia in the Gulf of Mexico. J. Environ. Qual., 30, 320-329.

Rabalais, N.N., Turner, R.E., and Wiseman, W.J., Jr., 2002. Gulf of Mexico hypoxia, A.K.A. "The Dead Zone". Annu. Rev. Ecol. Syst., 33: 235-263, doi:10/1146/annurev.ecolsys.33.010802. 150513.

Reed, D.J., 1989. Patterns of sediment deposition in subsiding coastal salt marshes, Terrebonne Bay, Louisiana: the role of winter storms. Estuaries, 12(4), 222-227.

Rego, J.L., Meselhe, E., Stronachm J., and Habib, E., 2009. Numerical modeling of the Mississippi-Atchafalaya Rivers' sediment transport and fate: considerations for diversion scenarios. Journal of Coastal Research, 25(0), 000-000 (in press).

Roberts, H.H., Adams, R.D., and Cunningham, R.H.W., 1980. Evolution of sand-dominant subaerial phase, Atchafalaya Delta, Louisiana. American Association of Petroleum Geologist Bulletin. 64, 264-279.

Roberts, H.H., Huh, O.K., Hsu, S.A., Rouse, L.J., Jr., and Rickman, D., 1987. Impact of cold-front passages on geomorphic evolution and sediment dynamics of the complex Louisiana coast. Coastal Sediments '87, Proceedings of a Specialty Conference (May 12-14, 1987, New Orleans, Louisiana). American Society of Civil Engineers, New York, pp. 1950-1963.

Roberts, H.H., Huh, O.K., Hsu, S.A., Rouse, L.J., Jr., and Rickman, D.A., 1989. Winter storm impacts on the Chenier Plain coast of southwestern Louisiana, Gulf Coast Association of Geological Societies Transactions, Vol XXXIX, 515-522.

Roberts, H.H., 1997. Dynamic changes of the Holocene Mississippi River Deltaic Plain: the delta cycle. Journal of Coastal Research, 13(3), 605-627.

Roberts, H.H., 1998. Delta switching: early responses to the Atchafalaya River diversion. Journal of Coastal Research, 14 (3), 882-899.

Rogers, B.D., Shaw, R.F., Herke, W.H., and Blanchet, R.H., 1993. Recruitment of postlarval and juvenile brown shrimp (*Penaeus aztecus* Ives) from offshore to estuarine waters of the northwestern Gulf of Mexico. Estuarine, Coastal and Shelf Sciences, 36, 377-394.

Rouse, L. J. Jr., Wiseman, W.J. Jr., Bender, L.C., Guinasso, N.L. Jr., Kelly, F.J., Brooks, D.A., Lo Y-T., She, J. Valle-Levinson, A., 2004. Observational and predictive study of inner shelf currents over the Louisiana-Texas shelf. U.S. Dept of Interior, Mineral Management Service, Gulf of Mexico OCS Region, New Orleans, LA. OCS Study MMS 2004-036. 207pp.

Rouse, L. J. Jr., Wiseman, W.J. Jr., Inoue, M., 2005. Aspects of the Louisiana Coastal Current. U.S. Dept of Interior, Mineral Management Service, Gulf of Mexico OCS Region, New Orleans, LA. COS study MMS 2005-039. 50pp.

Salas-Monreal, D., and Valle-Levinson, A., 2008. Sea-level slope and volume fluxes produced by

atmospheric forcing in estuaries: Chesapeake Bay case study. Journal of Coastal Research, 24 (2B), 208-217.

Schumann, S., Johnson, G.A., Moser, J., Walker, N.D., and Hsu, S.A., 1995. An overview of a strong winter low in the Gulf of Mexico, March 12-13, 1993. National Weather Digest, 20 (1), 11-25.

Shaw, R.F., Wiseman, W.J., Jr., Tuner, E. R., Rouse, L.J., and Condrey, R.E., Kelly, F.J., Jr., 1985. Transport of larval Gulf Menhaden Brevoortia patronus in continental shelf waters of western Louisiana: a hypothesis. Transactions of American Fisheries Soceity, 114, 452-460.

Shaw, R.F., Rogers, B.D., Cowan, J.H., and Herke, W.H., 1988. Ocean-estuary coupling of ichthyoplankton and nekton in the northern Gulf of Mexico. American Fisheries Society Symposium, 3, 77-89.

Smith, S.R., Jacobs, G.A., 2005. Seasonal circulation fields in the northern Gulf of Mexico calculated by assimilating current meter, shipboard ADCP, and drifter data simultaneously with the shallow water equations. Continental Shelf Research, 25, 157-183.

Snedden, G.A., Cable, J.E., and Wiseman, W.J., Jr., 2007. Subtidal sea level variability in a shallow Mississippi River deltaic estuary, Louisiana. Estuaries and Coasts, 30(5), 802-812.

Stone, G.W., Williams, S.J., and Burruss, A.E., 1997a. Louisiana's barrier islands: an evaluation of their geological evolution, morphodynamics and rapid deterioration. Journal of Coastal Research, 13 (3), 591-592.

Stone, G.W., Grymes, J.M., III., Dinger, J.R., and Pepper, D.A., 1997b. Overview and significance of hurricanes on the Louisiana coast, U.S.A.. Journal of Coastal Research, 13 (3), 656-669.

Stone, G.W., and McBride, R., 1998. Louisiana barrier islands and their importance in wetland protection: forecasting shoreline change and subsequent response of wave climate. Journal of Coastal Research, 14 (3), 900-915

Stone, G.W., and Wang, P., 1999. The importance of cyclogenesis on the short-term evolution of gulf coast barriers. Gulf Coast Association of Geological Societies Transactions, Vol XLIX, 478-486.

Stone, G.W., Pepper, D.A., Xu, J. and Zhang, X., 2004. Ship Shoal as a prospective borrow site for barrier island restoration, coastal south-central Louisiana, USA: numerical wave modeling and field measurements of hydrodynamics and sediment transport. Journal of Coastal Research, 20 (1), 70-88.

Stone G.W., and Orford, J.D., 2004. Storms and their significance in coastal morpho-sedimentary dynamics. Marine Geology, 210, 1-5.

Stone G.W., Zhang X., and Sheremet A., 2005. The role of barrier islands, muddy shelf and reefs in mitigating the wave field along coastal Louisiana. Journal of Coastal Research, SI 44, 40-55.

Stone, G.W., Liu, B., and Jose, F., 2007. Winter storm and tropical cyclone impacts on the short-term evolution of beaches and barriers along the northeastern Gulf of Mexico. Coastal Sediments '07, Volume 2, 935-950.

Stumpf R.P., and Tomlinson, M.C., 2005. Remote sensing of harmful algal blooms. In: Remote Sensing of Coastal Aquatic Environments (R.L., Miller, eds.), pp.277-296. Springer.

Suhayda, J.N., 1997. Modeling impacts of Louisiana barrier islands on wetland hydrology. Journal of Coastal Research, 13 (3), 686-693.

The State Wetlands Conservation and Restoration Authority, 2004. State of Louisiana Wetlands Conservation and Restoration Plan-Fiscal Year 2004-2005. http://www. goca.state.la.us/swa-pdf/report20042005stateplan.pdf

USEPA. 1999. Ecological condition of estuaries in the Gulf of Mexico. EPA 620-R-98-004. U.S. Environmental Protection Agency, Office of Research and Development, National Health and Environmental Effects Research Laboratory, Gulf Ecology Division, Gulf Breeze, Florida. 80 pp.USGS, 2005. Depicting coastal Louisiana land loss. http://www.nwrc.usgs.gov/factshts/2005-3101.pdf

Valle-Levinson, A., Wong, K.-C.and Bosley, K.T., 2001. Observations of wind-induced exchange at the entrance to Chesapeake Bay. Journal of Marine Research, 59, 391-416.

Van de Voorde, N.E., and Dinnel S.P., 1998. Observed directional wave spectra during a frontal passage. Journal of Coastal Research, 14 (1), 337-346.

Van Heerden, I.L., and Roberts, H.H., 1980. The Atchafalaya Delta-Louisiana's new prograding coast. Transactions, Gulf Coast Association of Geological Societies, 30, 197-506.

Van Heerden I.L., and DeRouen, K. Jr., 1997. Implementing a barrier island and barrier shoreline restoration program –the state of Louisiana's perspective. Journal of Coastal Research, 13 (3), 679-685.

Walker, N.D., Rouse L.J., and Huh, O.K., 1987. Response of subtropical shallow-water environments to cold-air outbreak events: Satellite radiometry and heath flux modeling. Continental Shelf Research, 7, 735-757.

Walker, N.D., 1993. A preliminary look at cyclogenesis in the Gulf of Mexico during the March 1993 blizzard. Marine Weather Log, 37 (2), 8-9.

Walker, N.D., 1996. Satellite assessment of Mississippi River plume variability: causes and predictability. Remote Sens. Environ., 58, 21-35.

Walker, N.D., Huh, O.K., Rouse, L.J. Jr., and Murray, S.P., 1996. Evolution and structure of a coastal squirt off the Mississippi River delta: Northern Gulf of Mexico. Journal of Geophysical Research, 101 (C9), 20643-20655.

Walker, N.D., and Hammack, A.B., 2000. Impact of winter storms on circulation and sediment transport: Atchafalaya-Vermilion bay Region, Louisiana, U.S.A. Journal of Coastal Research,

16(4), 996-1010.

Walker, N.D., Jarosz, E., Murray, S.P., 2001. An investigation of pressure and pressure gradients along the Louisiana/Texas inner shelf and their relationships to wind forcing and current variability. OCS Study MMS 2001-057. U.S. Dept. of the Interior Minerals Mamt. Service, Gulf of Mexico OCS region, New Orleans, LA. 40pp.

Walker, N.D., 2001a. Tropical storm and hurricane wind effects on water level, salinity, and sediment transport in the river-influenced Atchafalaya-Vermilion Bay system, Louisiana, USA. Estuaries, 24 (4), 498-508.

Walker, N.D., 2001b. Wind and eddy related circulation on the Louisiana/Texas shelf and slope determined from satellite and in-situ measurements: October 1993-August 1994, OCS Study MMS 2001-025. U.S. Dept. of the Interior Minerals Mamt. Service, Gulf of Mexico OCD region, New Orleans, LA. 58pp.

Walker, N.D., Huh, O.K., Babin, A., Haag, A., Cable, J., Snedden, G., Braud, D., Wilensky, D., and Prasad, K., 2003. A Role for Remote Sensing in Managing Mississippi River Diversions. Backscatter, Vol. 1, 25-28, AMRS Association, 2003.

Walker, N.D., 2005. Wind and Eddy-Related Shelf/Slope Circulation Processes and Coastal Upwelling in the Northwestern Gulf of Mexico. Circulation in the Gulf of Mexico: Observations and Models, Wilton Sturges III and Alexis Lugo-Fernandex, Eds. American Geophysical Union Monograph, 295-314.

Walker, N.D., Wiseman, W.J. Jr., Rouse L.J. Jr. and Babin A., 2005a. Effects of river discharge, wind stress, and slope eddies on circulation and the satellite-observed structure of the Mississippi River plume. Journal of Coastal Research, 21 (6), 1228-1244.

Walker N.D., Leben, R.R., and Balasubramanian, S., 2005b. Hurricane-forced upwelling and chlorophyll a enhancement within cold-core cyclones in the Gulf of Mexico. Geophysical Research Letters, 32, L18610, doi:10.1029/2005GL023716.

Walker N.D., and Rabalais, N.N., 2006. Relationships among satellite chlorophyll a, river inputs, and hypoxia on the Louisiana continental shelf, Gulf of Mexico. Estuaries and Coasts, 29 (6B), 1081-1093.

Wang, D.P., 1979. Subtidal sea level variations in the Chesapeake Bay and relations to atmospheric forcing. Journal of Physical Oceanography, 9, 413-421.

Wang K.C., and Garvine, R.W., 1984. Observations of wind-induced, subtidal variability in the Delaware Estuary. Journal of Geophysical Research, 89 (C6), 10589-10597.

Wang, F.C., Lu, T., and Sikora, W.B., 1993. Intertidal marsh suspended sediment transport processes, Terrebonne Bay, Louisiana, U.S.A. Journal of Coastal Research, 9 (1), 209-220.

Williams S.J., Stone, G.W., and Burruss, A.E., 1997. A perspective on the Louisiana wetland loss and coastal erosion problem. Journal of Coastal Research, 13 (3), 593-594.

Wiseman, W.M. Jr., Kelly, F.J., 1994. Salinity variability within the Louisiana coastal current during the 1982 flood season. Estuaries, 17(4), 732-739.

Wiseman, W.M. Jr., Rabalais, N.N., Turner R.E., Dinnel, S.P., MacNaughton, A., 1997. Seasonal and interannual variability within the Louisiana coastal current: stratification and hypoxia. Journal of Marine Systems, 12, 207-248.

Wong, K.-C., and Valle-Levinson, A., 2002. On the relative importance of the remote and local wind effects on the subtidal exchange at the entrance to the Chesapeake Bay. Journal of Marine Research, 60, 477-498.

Zavala-Hidalgo, J., Morey, S.L., O'Brien, J.J., 2003. Seasonal circulation on the western shelf of the Gulf of Mexico using a high-resolution numerical model. Journal of Geophysical Research. 108, No.C12,3389,doi:10.1029/2003JC001879.

APPENDIX: WEATHER MAPS OF COLD FRONTS

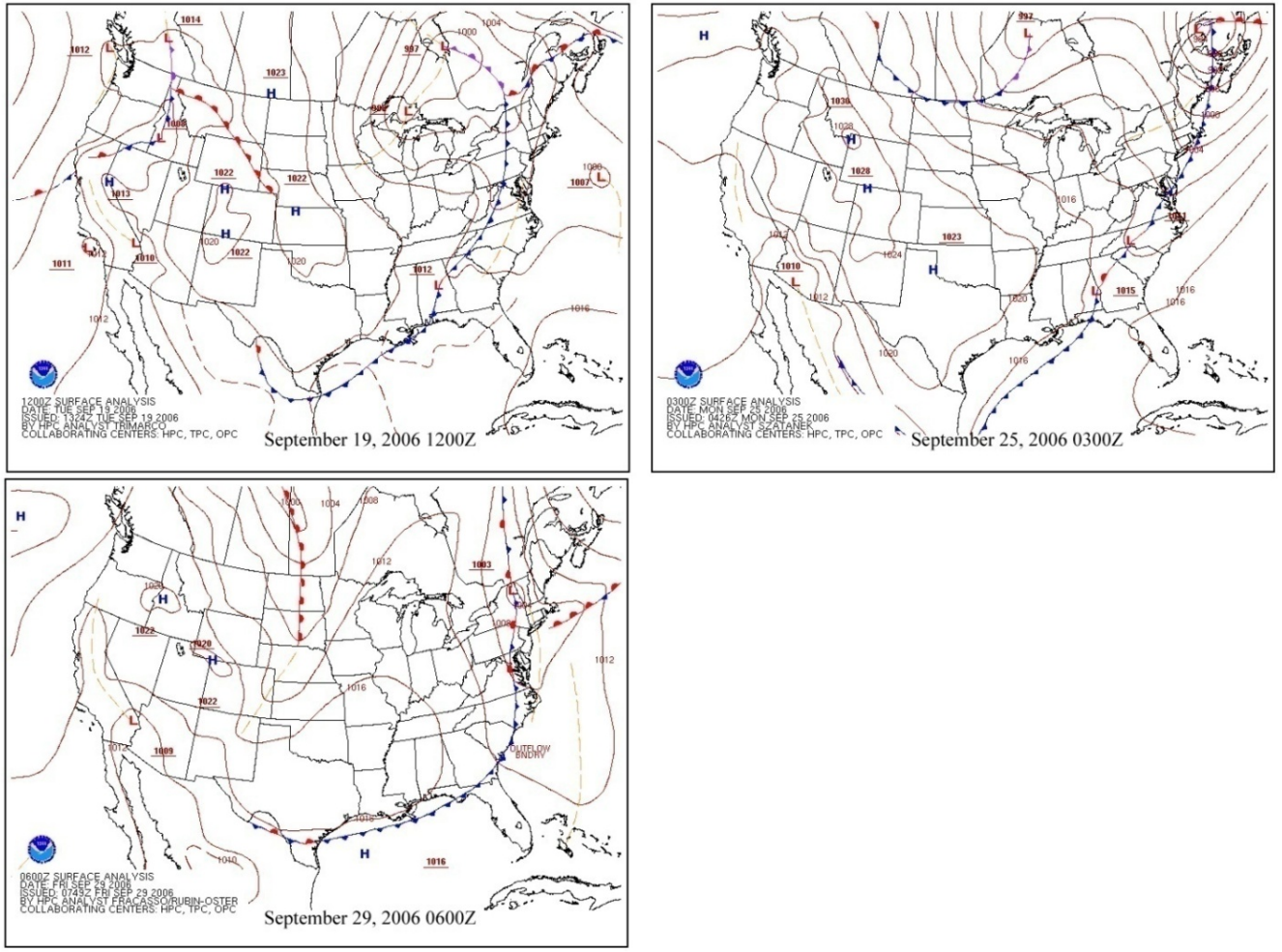

Figure A.1 Weather maps showing cold front passages in September, 2006

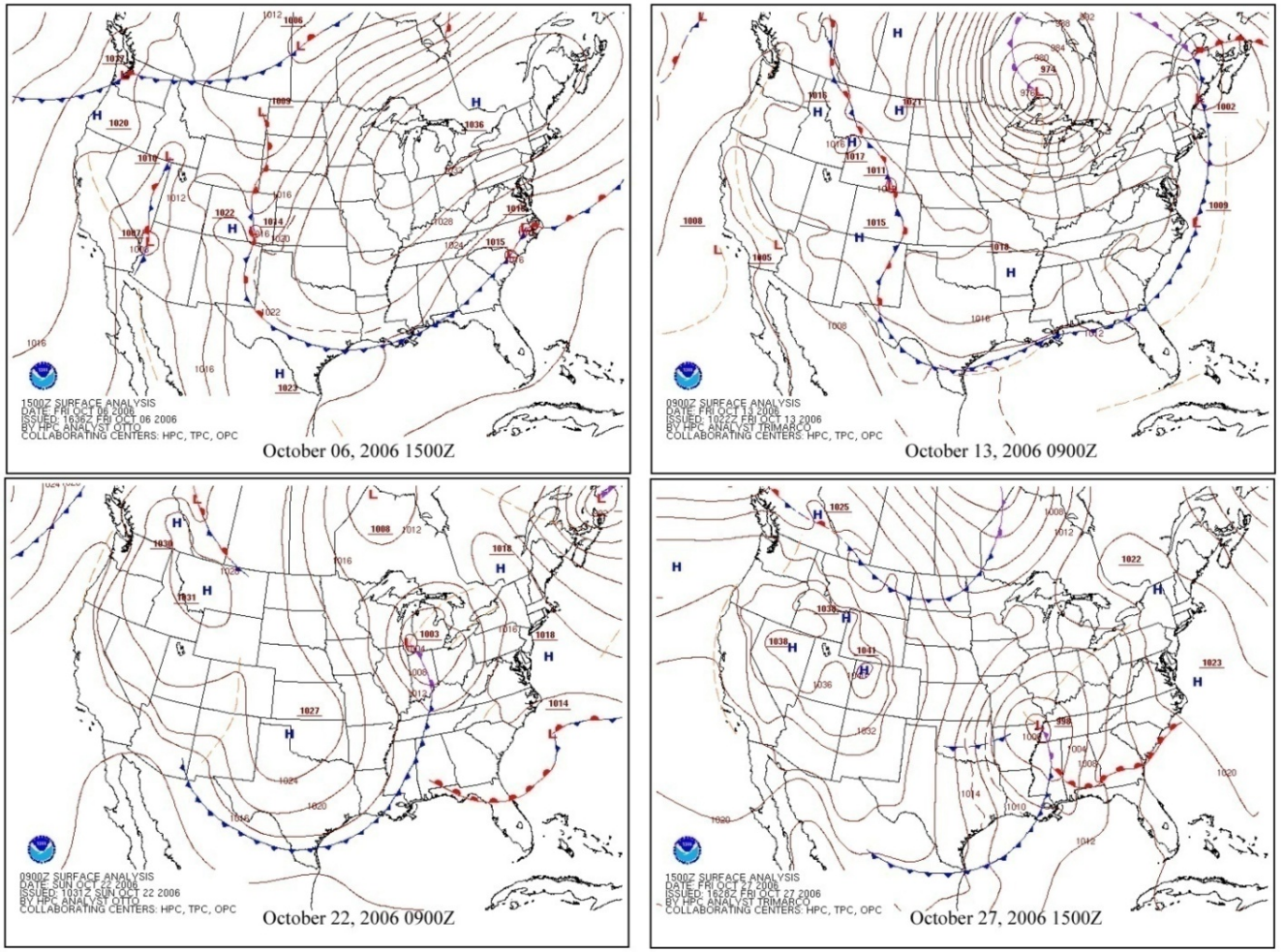

Figure A.2 Weather maps showing cold front passages in October, 2006

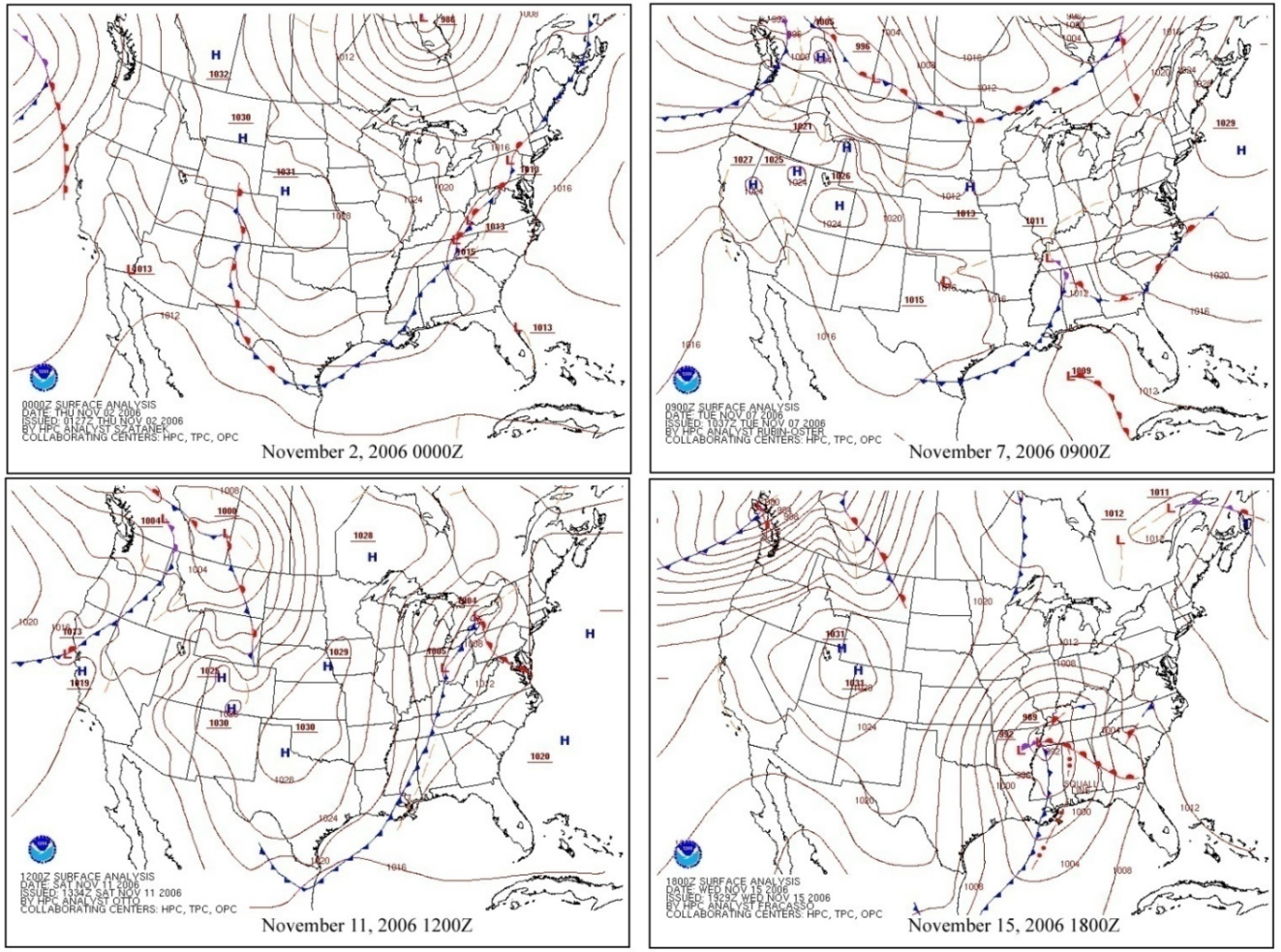

Figure A.3 Weather maps showing cold front passages in November, 2006

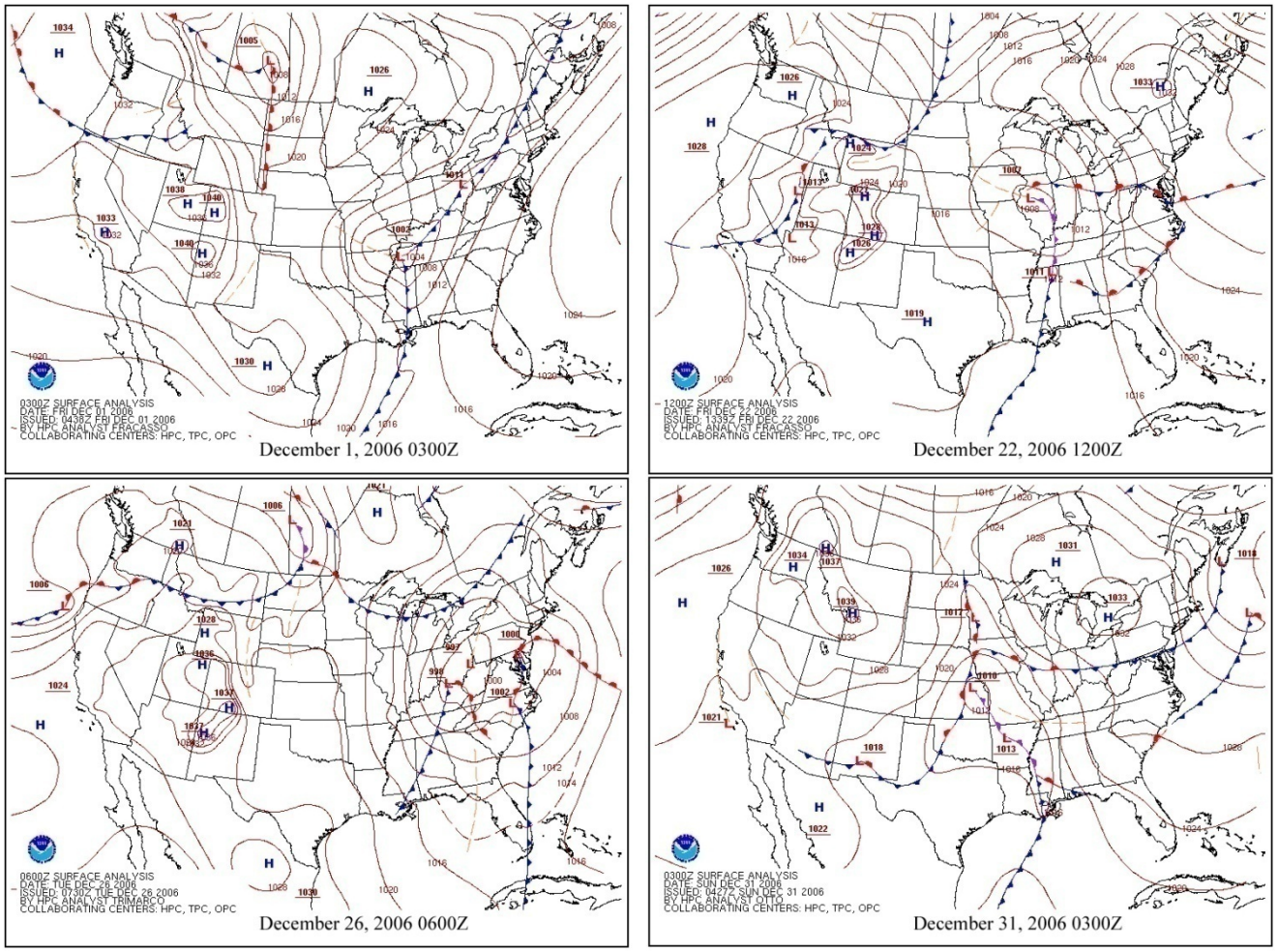

Figure A.4 Weather maps showing cold front passages in December, 2006

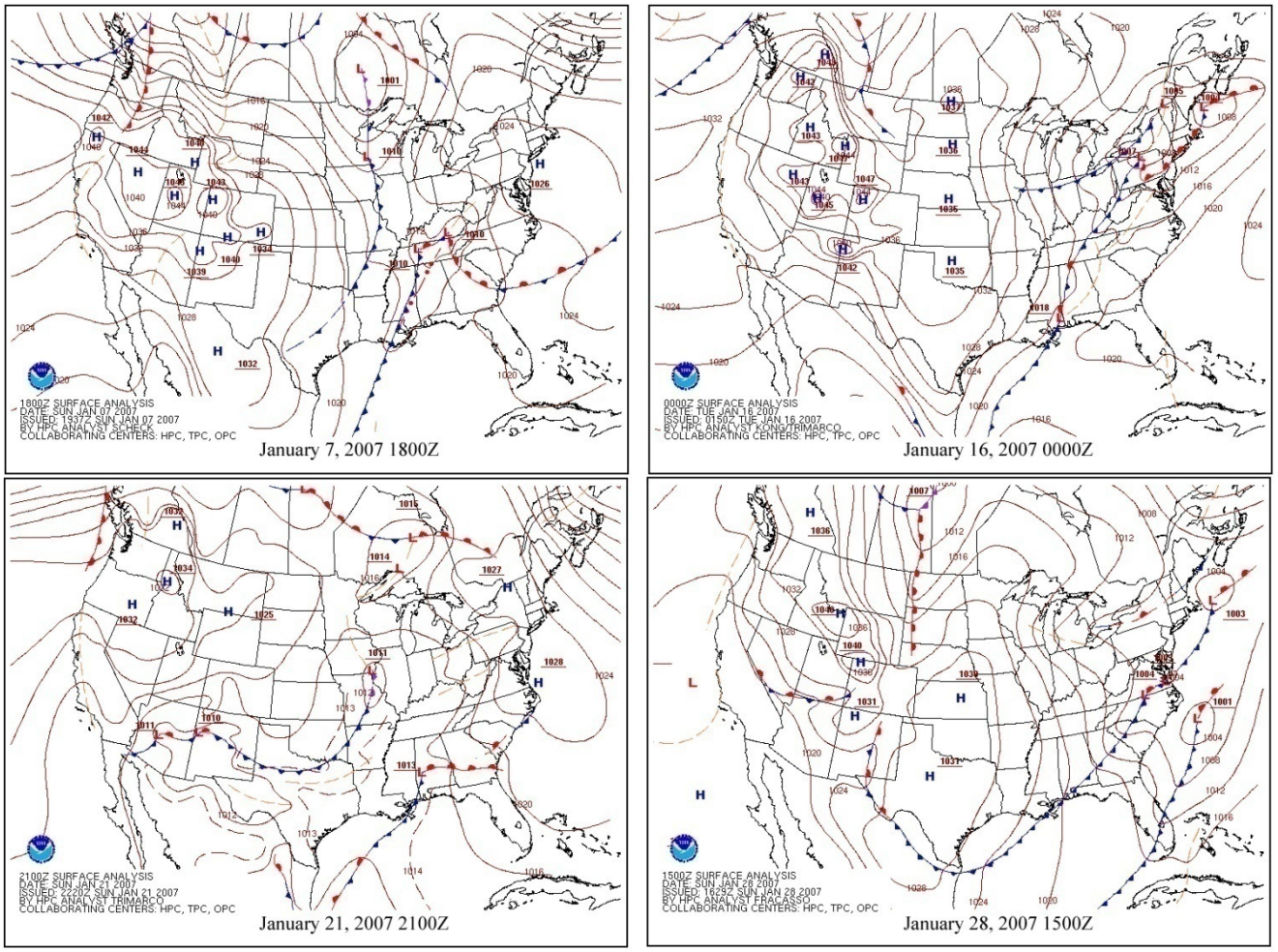

Figure A.5 Weather maps showing cold front passages in January, 2007

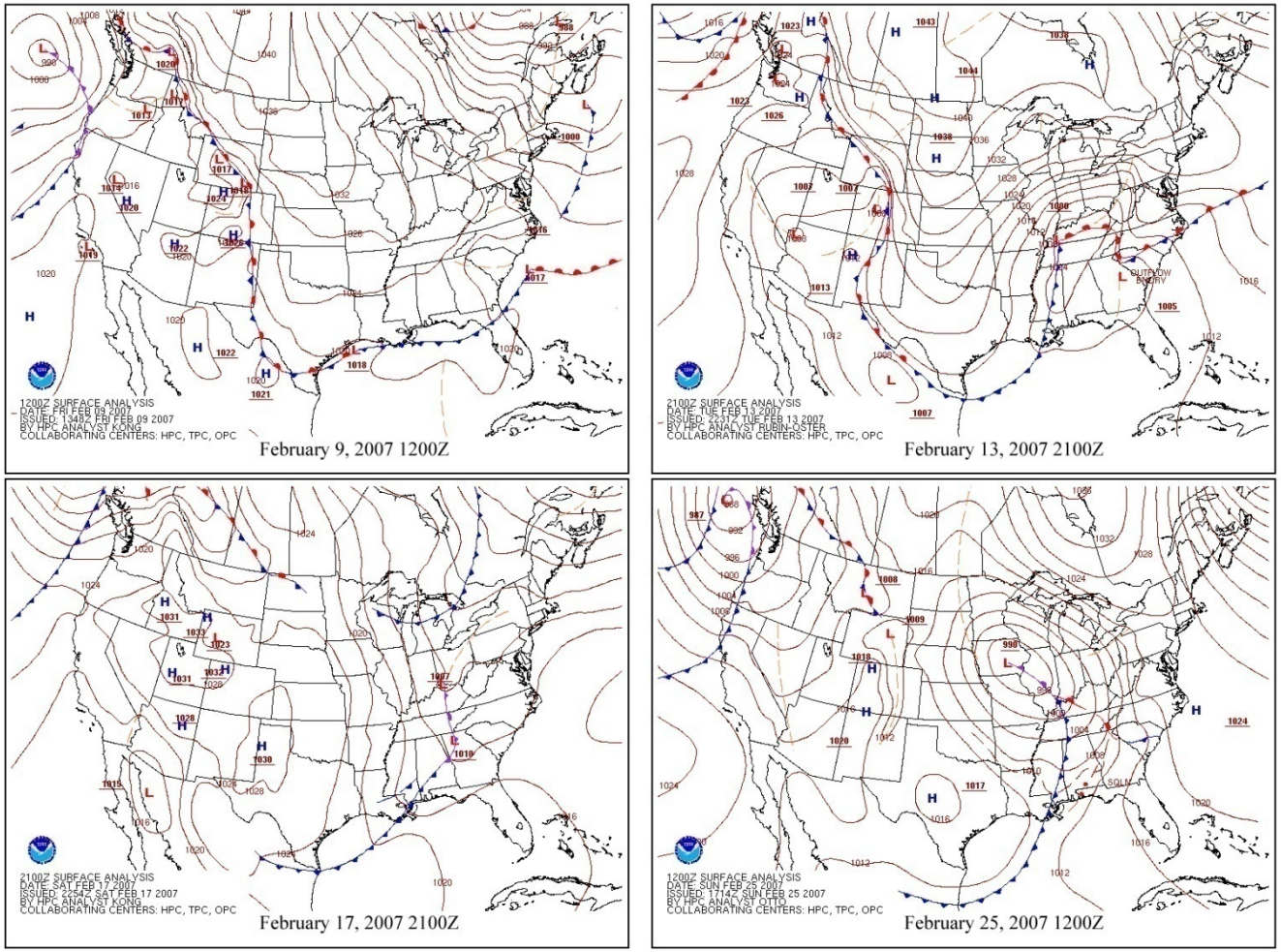

Figure A.6 Weather maps showing cold front passages in February, 2007

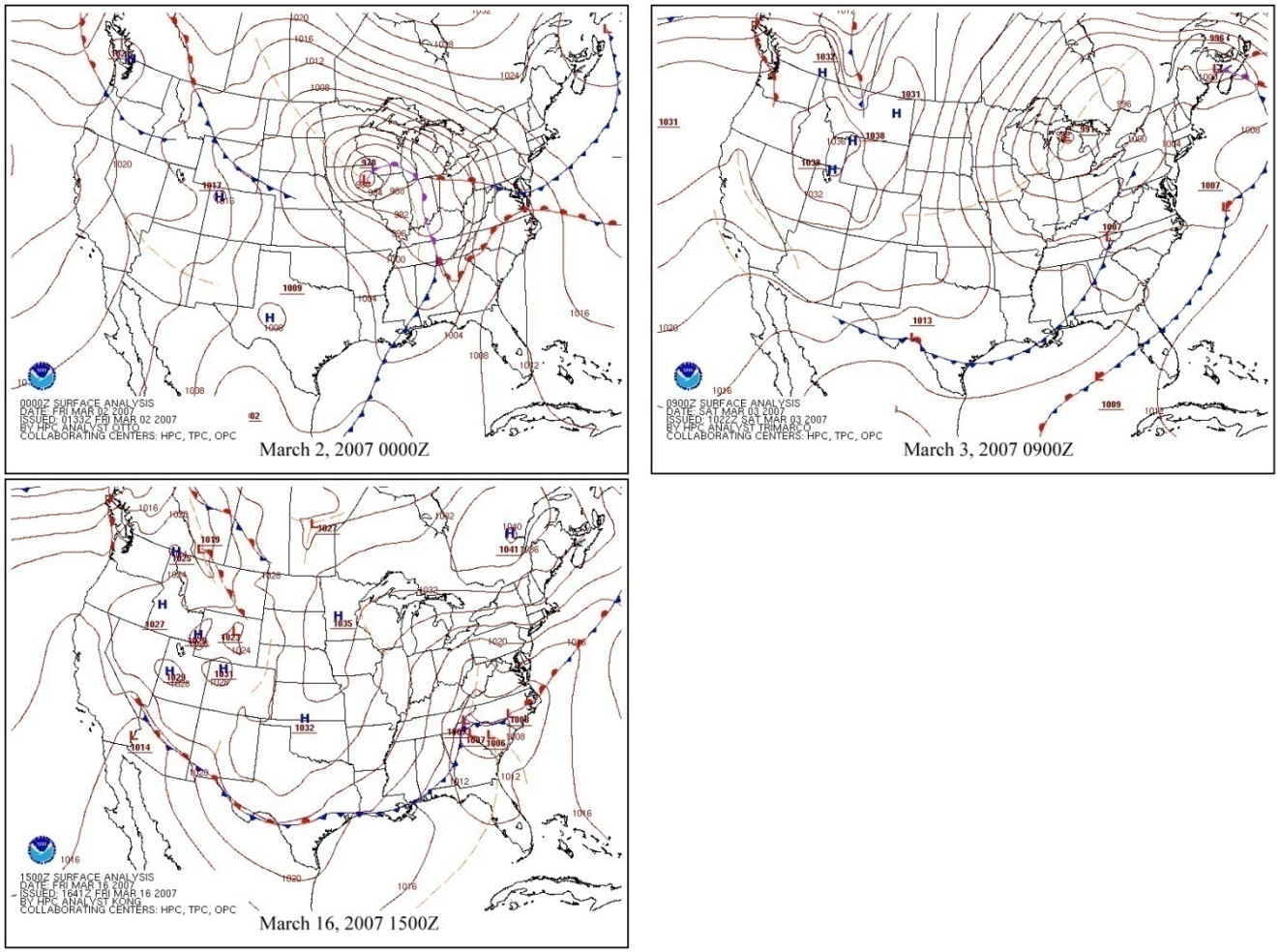

Figure A.7 Weather maps showing cold front passages in March, 2007

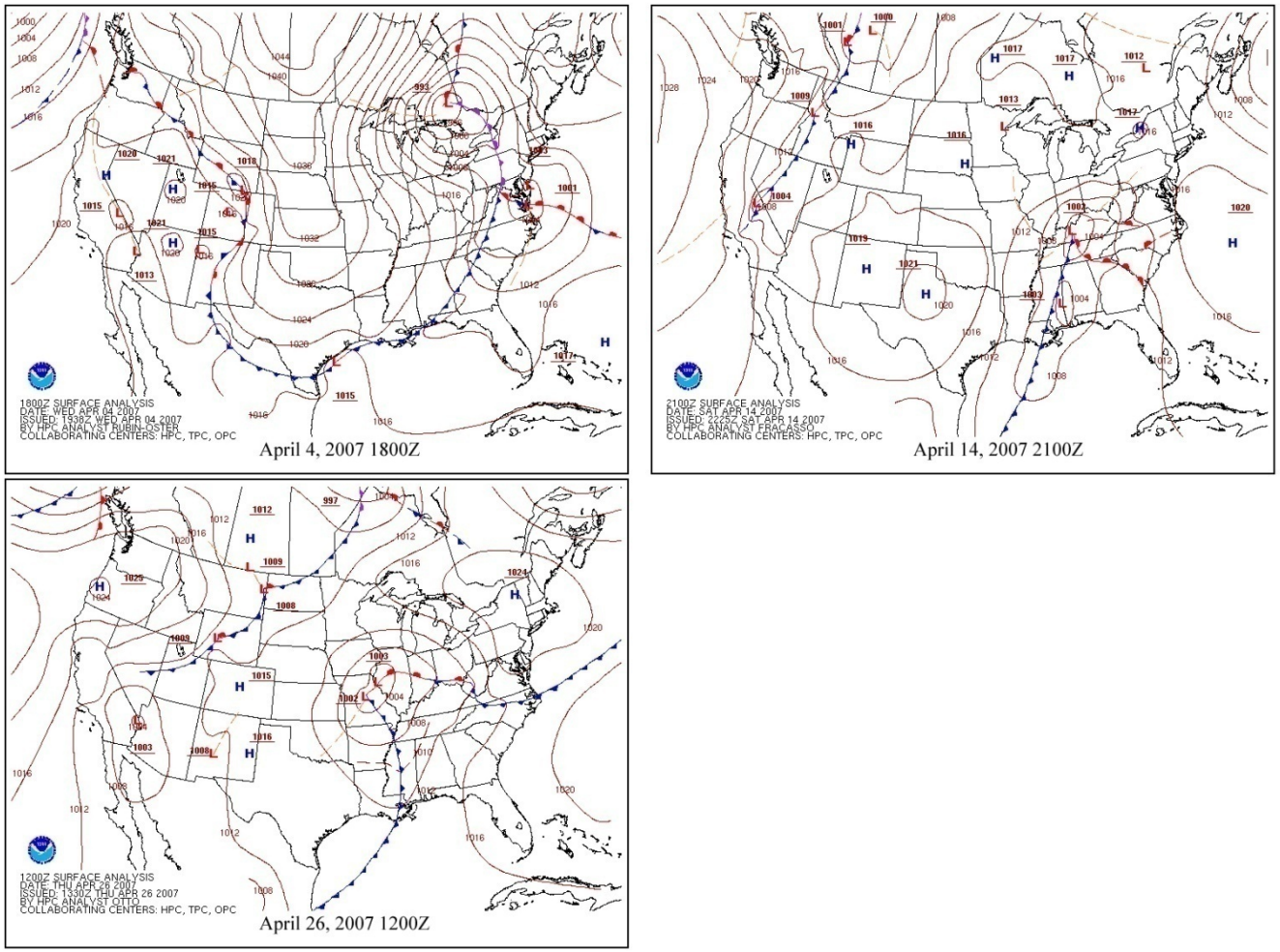

Figure A.8 Weather maps showing cold front passages in April, 2007

VITA

Zhixuan Feng was born in August, 1985, in Baoying County, Jiangsu Province, China. He graduated from Baoying High School in 2003. Zhixuan attended Nanjing University in September, 2003, and obtained a degree of Bachelor of Science in Geography in May, 2007. He was influenced and encouraged by his undergraduate advisor, Dr. Shu Gao, to pursue his interest and career in oceanography and marine sciences.

Zhixuan entered the graduate program and has been working as a research assistant with Dr. Chunyan Li in the Department of Oceanography and Coastal Sciences at Louisiana State University since August, 2007. He plans to pursue a Doctor of Philosophy degree in the Division of Applied Marine Physics, Rosenstiel School of Marine and Atmospheric Sciences, University of Miami, starting from fall, 2009.